Characterization of Fatigue Damage Types in Fibre Reinforced Composites Utilizing Pattern Recognition Techniques Applied to Acoustic Emission Signals

A thesis submitted for the degree of Doctor of Philosophy

by

Jialin Tang

Department of Mechanical, Aerospace and Civil Engineering

College of Engineering, Design and Physical Sciences

Brunel University London, Uxbridge

United Kingdom

October 2018

Abstract

The aim of this work is to develop advanced acoustic emission (AE) techniques to investigate the behaviour and failure of complex composite structures in a fatigue loading environment. The work focuses on using acoustic emission to detect and characterize damage mechanisms within composite structures.

A pattern recognition technique is developed to characterize different acoustic emission activities corresponding to different fracture mechanisms. Pattern recognition techniques are based on the classification between different acoustic emission signal types using signal features. Any parameters that affect the acoustic emission signal features will have an impact on the pattern recognition results.

One of the main parameters that can alter the features of acoustic emission signals is sensor frequency characteristics. This effect is initially investigated using simulated acoustic emission waves and then using acoustic emission signals acquired during lab based experiments carried out on both metal and composite materials with a number of different types of sensors used. Variations in acoustic emission signal features of the signals obtained from different sensors are analysed. A pattern recognition method is developed to identify the characteristics of the acoustic emission signals from plastic deformation.

Another important parameter that influences the acoustic emission signal features is the distance of wave propagation from acoustic emission source to the sensor. Acoustic emission signals lose energy as they propagate within the medium. This effect is called attenuation. An investigation of the effect that attenuation might have to the acoustic emission signals related to monitoring of failures in GFRP laminates used in wind turbine blades is carried out. The developed pattern recognition method is applied for damage characterization.

Finally, based on the knowledge obtained through the work above, a laboratory study is reported regarding fatigue damage growth monitoring in a

complete 45.7 m long wind turbine blade. The damage growth is successfully located and characterized.

Acknowledgements

I would like to express my sincere gratitude to my supervisor Dr. Cristinel Mares and Dr. Slim Soua for the continuous support, insightful comments and consistent encouragement I received through my Ph.D study.

I am grateful to the National Structural Integrity Research Centre (NSIRC) for providing funding for this study.

A very special gratitude goes out to all my colleagues in CSM section at TWI Ltd., who have supported me along the way. Also I thank the technicians in AFM section who helped me conduct the experiments.

I thank my friends for being there for me whenever I need.

Last but not the least, I would like to thank my parents, who encourage and help me at every stage of my life. They are the most important people in my world and I dedicate this thesis to them.

List of publications from this study

Journal Publications

Tang, J., Soua, S., Mares, C., & Gan, T. H. (2017). A pattern recognition approach to acoustic emission data originating from fatigue of wind turbine blades. *Sensors*, 17(11), 2507.

Tang, J., Soua, S., Mares, C., & Gan, T. H. (2016). An experimental study of acoustic emission methodology for in service condition monitoring of wind turbine blades. *Renewable energy*, 99, 170-179.

Conference Publications

Tang, J., Mares, C. and Soua, S. (2017) . Feature variability in pattern recognition on acoustic emission signals from plastic deformation in carbon steel. International Conference on Structural Engineering Dynamics. Ericeira, Portugal. 3 - 5 July.

Tang, J., Lage, Y., Soua, S., Mares, C., & Gan, T. H. (2016). An acoustic emission Pattern Recognition Method for Carbon Steel during Tensile Test. 11th International Conference on Advances in Experimental Mechanics. University of Exeter, UK. 5 - 7 September.

Tang, J., Rafael, S., Mares, C., Soua, S. and Gan, TH. (2015). Analysis of fatigue induced crack propagation in a wind turbine blade using acoustic emission. 7th International Conference on Structural Health Monitoring of Intelligent Infrastructure. Torino, Italy. 1 – 3 July.

Dachev, D., Tang, J., Kanfoud, J., Mares, C., Soua, S. (2018). Destructive testing of open rotor propeller blades for extreme operating conditions. Modern practice in stress and vibration analysis. Clare College, Cambridge, UK. 2 – 4 July.

Table of Contents

Glossary

The following terms relate to acoustic emission are with reference to ASTM E1316-19: Standard Terminology for Non-destructive Examinations.

Acoustic Emission – the class of phenomena whereby transient stress/displacement waves are generated by the rapid release of energy from localized sources within a material, or the transient waves so generated.

Acoustic Emission activity – the presence of acoustic emission during a test.

Acoustic Emission source – one which exhibits increasing cumulative AE activity with increasing or constant stimulus.

Acoustic Emission channel – an assembly of a sensor, preamplifier or impedance matching transformer, filters secondary amplifiers or other instrumentation as needed, connecting cables, and detector or processor.

Hit – the detection and measurement of an acoustic emission signal on a channel.

Event – an occurrence of a local material change or mechanical action resulting in acoustic emission.

Acoustic Emission sensor – a detection device, generally piezoelectric, that transforms the particle motion produced by an elastic wave into an electrical signal.

Acoustic Emission burst signal – a qualitative description of an individual emission event resulting in a discrete signal.

Acoustic Emission continuous signal – a qualitative description of emission producing a sustained signal as a result of time overlapping or successive emission events from one or several sources, or both.

Acoustic Emission broadband/wideband sensor – an acoustic emission sensor which, when calibrated exhibits a displacement or velocity response over serval hundred kHz with a coefficient of variation of the response in V/m or V/m/s that does not exceed 50%.

Acoustic Emission resonant/narrow band sensor – an acoustic emission sensor which, when calibrated, exhibits a displacement or velocity response with one or more dominant frequency peaks such that it does not satisfy the definition of a broadband acoustic emission sensor.

Couplant – a material used at the structure-to-sensor interface to improve the transmission of acoustic energy across the interface during acoustic emission monitoring.

Kaiser effect – the absence of detectable acoustic emission at a fixed sensitivity level, until previously applied stress levels are exceeded.

Felicity effect – the presence of detectable acoustic emission at a fixed predominant sensitivity level at stress levels below those previously applied.

Felicity ratio – the ratio of the stress at which acoustic emission is detected, to the previously applied maximum stress.

Felicity ratio – the ratio of the stress at which acoustic emission is detected, to the previously applied maximum stress.

Attenuation – the gradual loss of acoustic emission wave energy as a function of distance through absorption, scattering, diffraction and geometric spreading.

Dispersion – The phenomenon whereby wave velocity varies with frequency.

Acoustic Emission signal start – the beginning of an acoustic emission signal as recognized by the system, usually defined by an amplitude excursion exceeding threshold.

Acoustic Emission signal end – the recognized termination of an AE signal, usually defined as the last crossing of the threshold by that signal.

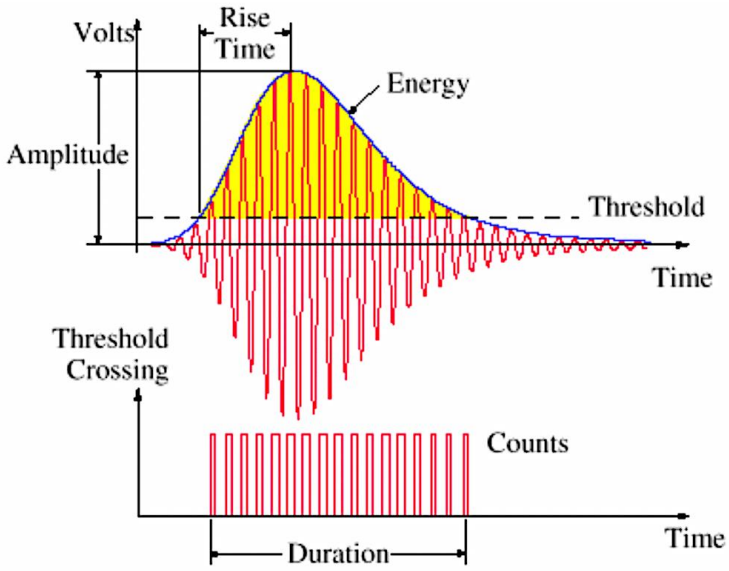

Figure 0-1 The definitions for acoustic emission signal time domain features [44].

Acoustic emission signal features – this refers to the features of an acoustic emission signal such as amplitude, duration, rise time, number of counts, energy and signal strength, see Figure 0-1; representative frequency parameters results after Fast Fourier Transform (FFT), are peak frequency and central frequency, see Figure 0-2.

Acoustic Emission signal peak amplitude (A) – is the greatest measured voltage in a signal and is measured in decibels (dB).

Acoustic Emission signal duration (D) – the rime between signal start and signal end.

Acoustic Emission signal rise time (R) – the time between acoustic emission signal start and the peak amplitude of that signal.

Acoustic Emission signal number of counts (N) – the number of times the acoustic emission signal exceeds a pre-set threshold during any selected portion of a test.

Acoustic Emission signal energy (MARSE) – is the measure of the area under the envelope of the rectified linear voltage time signal from the sensor.

Acoustic Emission signal strength (SS) – is the measure of squared signal envelope.

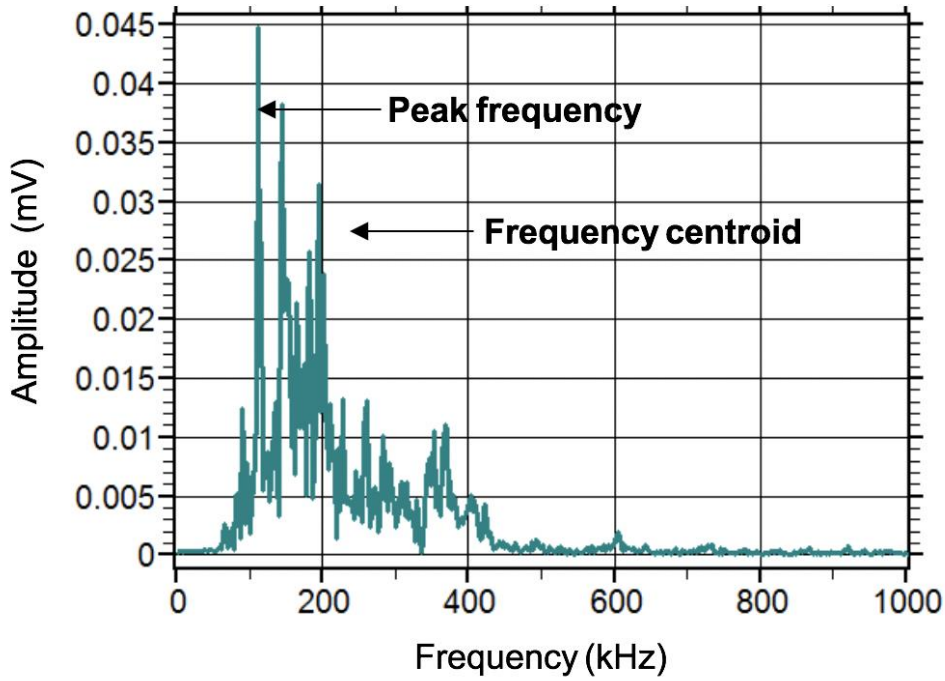

Figure 0-2 The definitions for acoustic emission signal frequency domain features.

Acoustic Emission peak frequency (PF) – is the frequency of the maximum magnitude of the spectrum.

Acoustic Emission frequency centroid (FC) – is the calculated centroid of the spectrum:

$$\text{Frequency Centorid} = \frac{\sum_{n=0}^{N-1}(\text{Magnitude}) \cdot (\text{Frequency})}{\sum_{n=0}^{N-1}(\text{Magnitude})} \qquad (1)$$

Acoustic Emission average frequency (AF) – is the number of counts of the time domain signal over its duration.

Noise: any undesired signal (electrical or acoustic) that tends to interfere with the reception, interpretation, or processing of the desired signal.

List of abbreviations

Abbreviations	Meaning	Page
CFRP/GFRP	Carbon or glass fibre – reinforced plastics	2
CRM	Compact Resonant Masses	127
DAQ	data acquisition system	102
DB	Davies-Bouldin	78
FBG	Fibre bragg grating	3
FCM	Fuzzy C-means	33
FFT	Fast Fourier Transform	48
FRP	fibre-reinforced polymer-matrix composites	27
HDT	Hit definiaiton time	22
LEFM	Linear elastic fracture mechanics	44
MAR	Measured amplitude ratio	38
MARSE	Acoustic Emission signal energy	77
PLB	Pencil lead break	5
PR	Pattern recognition	29
SDDM	Single dominant damage mechanism	35
SFFT	Single-fibre fragmentation test	35
SHM	Structural health monitoring	6
SPR	Supervised pattern recognition	30
TOA	Time of arrival	23
UPR	Unsupervised pattern recognition	30
WT	Wavelet transform	26

List of figures

List of tables

1 Introduction

This chapter begins by outlining the background of the research (Section 1.1), followed by the motivation and research objectives (Section 1.2) and main contributions (Section 1.3). Section 1.4 presents an outline of the remaining chapters of the thesis.

1.1 Background

Wind energy is recognized as a reliable and affordable source of electricity in many countries. Annual wind power installations in Europe have continuously increased over the past 12 years reaching a total of 168.7GW of installed capacity at the end of 2017 and placing wind energy as the second most installed form of power generation, just behind gas installations [1]. The wind turbine technology has advantages amongst other applications of renewable energy technologies due to its technological maturity, good infrastructure and relative cost competitiveness [2]. Success of a wind energy project relies on the reliability of a wind turbine system. A wind turbine's reliability is dependent largely on the particular machine model, how well it is designed, and the quality of manufacture. Reliability also varies with operating environment, as it is the machine's reaction to the environment that determines the loading imposed on the components [3]. Wind turbines can suffer from moisture absorption, thermal stress, wind gusts, ice accretion and sometimes lightning strikes. The variety of potential component failures indicate that the operating conditions and load conditions for a large wind turbine are not completely understood. This results in unscheduled maintenance due to unexpected failures. Consequently, the operation and maintenance (O&M) cost is increased and the wind turbine system lifetime is decreased.

Therefore, researchers, operators, wind farm owners and others within the wind industry agree that increased reliability is desired. One of the effective ways is to identify critical components, characterize failure modes and communicate those in a simple manner to wind farm operators. Identifying the critical components allows the O&M staff to direct their monitoring and

understanding the failure modes of the components allows the staff to focus monitoring efforts and conduct effective maintenance scheduling.

The application of condition monitoring has grown considerably in the last decade in several branches of industry. Condition monitoring provides diagnostic information on the health of the various turbine subsystems and alters the maintenance staff to trends that may be developing into catastrophic failures. Condition monitoring involves in advanced sensing technique with intelligent algorithms to continuously monitor the structure for damage. On wind turbines, condition monitoring is used to monitor the status of critical operating major components such as blades, gearbox, generator, main bearings and tower.

The blade of a wind turbine is generally considered as the most critical component of the wind turbine system, therefore extensive attention has been given to the condition monitoring of blades [4], [5], [6]. Wind turbine blades can be damaged by rain, ice, extreme wind, lightning, bird strikes, and UV rays. Besides they are subject to the cyclic stress loading. In service failure is thus a significant risk and can have catastrophic consequences.

It is usually difficult to predict the remaining life of a blade, but it is possible to determine the condition of the blade and warn of its failure. Wind turbine blades are manufactured from composite materials using fibreglass and polyester or fibre glass and epoxy, sometimes in combination with wood and carbon [7]. The most commonly used types of composite materials in wind turbine industry are carbon or glass fibre – reinforced plastics (CFRP/GFRP). Compared with traditional metallic material, composite materials are deigned to have high strength and stiffness coupled with low density. Their good vibration damping ability ensures composite structures have a low risk of fatigue failures. However, despite the extended range of application of composite materials understanding of their damage and failure mechanisms specifically related to fracture remain challenging. The micro-damage mechanisms in composites can severely affect the performance of composites

therefore correct characterisation of these mechanisms can help avoid catastrophic structural failures.

Condition monitoring techniques used for monitoring wind turbine blades include strain measurements, ultrasonic testing and acoustic emission. For the wind-farm operator, using strain gauges to record the load history in the wind turbine blade has the advantage of understanding loads caused by the damage which enables a better detection of potentially damaging situations, locally.

Fibre Bragg Grating (FBG) based strain gauges offer a variety of advantages over electrical strain gauges. For example, they provide long-term signal stability and system duration, even at high-level vibration loads. Distance and cable length have virtually no impact on measurement accuracy. Optical fibres are much thinner and lighter than copper conductors, so the connection leads are much lighter and a single measuring lead allows connecting many sensors. In addition to strain, FBG-based sensors can be used in transducers to monitor a variety of other parameters such as temperature, tilt, acceleration and pressure. It is predicted that FBG-based sensors will find more application and become an important tool for condition monitoring in the near future [8].

Ultrasonic testing for wind turbine has become an important tool due to its capability to provide information about the state of the composite materials beneath the surface such as exposing the dry glass fibre or delamination. However for this method, a high degree of operator skill is required with spurious indications potentially leading to unnecessary maintenance.

Advances in acoustic emission testing techniques for condition monitoring of wind turbine blades have been reported in the literature [9], [10], [11]. The main advances include the ability to locate and characterize damage in real time. Acoustic emission is defined in ASTM E-1316, Standard Terminology for Non-destructive Examinations, as “the class of phenomena whereby transient elastic waves are generated by the rapid release of energy from localized sources within a material” [12]. Any material or structure that undergoes some

form of movement or displacement will emit energy in the form of mechanical vibration that propagates in waves from the source through the rest of the material or structure.

Once an acoustic emission event is detected, information related to counting the acoustic emission activity, localizing the source position and identifying the classes of acoustic emission signals is gathered. This information helps classify the damage mechanisms and can assist in determining the failure mechanisms for a composite structure.

The main benefit of acoustic emission testing is the fact that specific acoustic emission signal features are closely related to damage mechanisms. In an actual structure a crack that can be detected using acoustic emission will not result in visually detectable deformation. Therefore, in order to detect and identify damage in the early stages, acoustic emission monitoring can be very effective. Acoustic emission monitoring has been used to test metallic structures for many years, and more recently it has become a primary method of testing composite materials [13]. The classification of damage in composite materials using acoustic emission is an emerging field with a few challenges and limitations existing.

In determining damage initiation and identifying failure mechanisms, many acoustic emission analyses focus on the macroscopic level of time-domain and frequency-domain parameter distributions. Single acoustic emission signal features such as peak amplitude or peak frequency can have significant dependency on the type of sensor, the details of the specimen geometry, or the propagation distance between source and sensor. Consequently, source characterization by single acoustic emission feature distributions or two dimensional correlation plots cannot be generalized beyond certain limits. On the other hand, the pattern recognition techniques are adaptive to the problem investigated.

Pattern recognition is the process of recognising and distinguishing the similarities between objects [14]. Pattern recognition techniques for acoustic

emission testing are based on the classification between different acoustic emission signal types using signal features (peak amplitude, rise time, duration etc.). Therefore any parameters that affect the acoustic emission signal features will have an impact on the pattern recognition results.

One of the most important parameters that can affect the features of acoustic emission signals is related to the sensor frequency characteristics that can have significant impact on detected signal amplitudes. This in turn can significantly affect signal features such as peak amplitude and energy among others. The sensor frequency characteristics are introduced during the design of the sensors with most sensors usually designed to be highly sensitive at a certain frequency or with a broad frequency response. In literature, effects of sensor types on acoustic emission signals are studied by carrying out typical pencil lead break (PLB) and ball drop tests [15]. These are widely used as a reproducible source for test signals in acoustic emission applications [16], [17]. In this work, this effect is analysed on simulated acoustic emission signals and compared to recorded acoustic emission signals from lab based experiments carried out on both metal and composite specimens. Acoustic emission signals are recorded using different types of piezoelectric based sensors during the experiments.

Another important parameter that influences the acoustic emission signal features is the distance of wave propagation from acoustic emission source to the sensor. Acoustic emission wave propagation is affected by attenuation. Attenuation is a phenomenon where the acoustic emission signals loses energy as they propagate within the medium. This effect can modify acoustic emission signals by decreasing signal amplitude when considering the varied distance between the source and the sensor. The understanding of this effect is required to analyse acoustic emission signals accurately. In this work, how the position of the sensor relative to the acoustic emission event source may cause a difference and to what extent in the detected time domain features or frequency features of the signals is investigated.

1.2 Aims and Research Objective

The main aim of this work is to develop advanced acoustic emission techniques for classification of damage mechanisms for complex composite structures in a fatigue loading environment.

The main objectives of this thesis are:

- Investigate the effect of the acoustic emission wave propagation in large scale composite structures based on recorded acoustic emission signals.
- Investigate issues related to using different types of sensors in damage characterization.
- Investigate issues related to attenuation in damage characterization.
- Quantify the characteristics of the acoustic emission signals for plastic deformation.
- Classify different composite damage mechanisms with the help of analysing acoustic emission signals.
- Develop a signal processing algorithm for damage detection, localization, and characterization in large complex composite structures.

1.3 Main Contributions of the Present Work

- The sensor's detection frequency influence on the acoustic emission signals are numerically investigated and experimental calibrated. The influences are demonstrated.
- An efficient acoustic emission treatment technique is developed to distinguish the crack generated acoustic emission signals and the background noise generated signals.
- A pattern recognition methodology for damage characterization is successfully applied on the acoustic emission data acquired from a fatigue test on wind turbine blade.
- The overall outcome provided a new reference of the application of acoustic emission technique for Structural Health Monitoring (SHM) to monitor the performance and integrity of complex structures.

1.4 Thesis Organisation

Chapter 2 explains the background theory relevant to this thesis, with a focus on the principles of acoustic emission source mechanics and elastic wave prorogation. Then the commonly used acoustic emission signal detection instrumentation and experimental techniques are explained. Finally in chapter 2, acoustic emission signal processing techniques for determination of source location and signal characterization are reviewed.

Chapter 3 introduces a finite element simulation method to study the acoustic emission responses from different fracture modes. The source model incorporates different crack sizes for each fracture mode. The effect of sensor frequency sensitivity on the simulated acoustic emission signals is investigated by applying different types of frequency filters. Comparison is made between the signals from different types of sensors and the simulated signals under corresponding frequency filters.

Chapter 4 gives details of the investigation performed on variations in acoustic emission signal features of the signals from different sensors during tensile tests on carbon steel and CFRP specimens. A pattern recognition approach is developed to quantify the characteristics of the acoustic emission signals from plastic deformation.

Chapter 5 discusses the effects of attenuation on the signals and source characterization of acoustic emission signals during a three-point bending test on a GFRP panel. Sensors with varied distances from the acoustic emission source are applied on the panel.

Chapter 6 demonstrates a successful application of the developed acoustic emission data processing technique during a fatigue test on 45.7 m long wind turbine blade. During the test, the damage growth is successfully located and characterized through data processing.

Chapter 7 gives conclusions and a short outlook for future investigations.

2 Literature Review

2.1 Theory of Acoustic Emission

Acoustic emission is a phenomenon when the elastic waves generated when a material undergoes inelastic strain or rupture propagate to the surface of the structure. To monitor this process sensors are used to record the elastic waves generated by the acoustic emission process.

One of the main advantages of acoustic emission compared to other non-destructive testing techniques is that damage processes in materials being tested can be observed for the duration of the entire loading history, without any disturbance to the specimen. Acoustic emission studies require, under favourable conditions, only a handful of sensors to capture and monitor the acoustic emission activity of a structure under loading. The sensors can be fixed to the surface of the structure for the duration of the test and do not have to be moved for scanning for example to scan the whole structure point by point [18].

Acoustic emission testing is ideal to identify activity from faults due to the fact that acoustic emission is related to the dynamic processes or sudden changes inside a material. This is a unique feature with active areas highlighted in the acquired signals a fact which makes the localization of the AE event source inside the monitored structure more identifiable compared to other non-destructive techniques [17].

Despite the benefit from the usage of AE to determine the origin of the failure mechanism it would need to be highlighted here the difficulty of this task. First, the sensitivity of an acoustic emission is often limited by the amount of background noise. Noise in acoustic emission testing refers to any undesirable signals detected by the sensors, such as frictional and impact sources. Secondly, wave propagation is affected as the waves propagate through layers of materials with varying properties and signal detection at the surface of the structure is altered by the use of piezoelectric sensors [19].

In this chapter, the background theory relevant to this thesis is reviewed with a focus on the principles of acoustic emission source mechanisms and wave propagation. Then the commonly used acoustic emission signal detection instrumentation and experimental techniques are explained. Finally in this chapter, acoustic emission signal processing techniques for source location and signal characterization are reviewed.

2.1.1 Acoustic Emission Source Mechanics

The elastic waves generated by a mechanical load are of the same nature as those generated by an earthquake and as a result the initial AE source model concept was derived from seismology [20]. Ohstu employed Green's function and moment tensor theory for acoustic emission signal analysis. This generalized theory is proposed to investigate the source characteristics of acoustic emission, in which the moment tensors represent the cracking source, while Green's function yields the transfer function between the acoustic emission event source and the acoustic emission sensor [21], [22]. Crack motion is presented as shown in Figure 2-1.

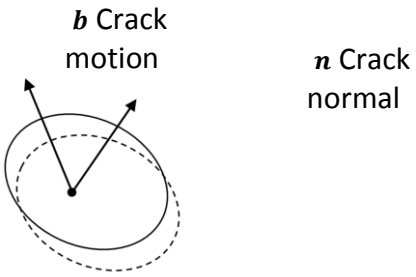

Figure 2-1 A crack model

The dynamic nature of vector b (Burgers vector) generates elastic waves, where b represents the magnitude of crack displacement [19]. The crack kinetics are defined by two direction vectors: the direction of crack displacement and the direction of crack normal n. In isotropic material, the generalized moment tensor components can be expressed as:

$$M_{pq} = C_{pqij} b_i n_j \Delta V = \begin{bmatrix} \lambda b_k n_k + 2\mu b_1 n_1 & \mu(b_1 n_2 + b_2 n_1) & \mu(b_1 n_3 + b_3 n_1) \\ \mu(b_1 n_2 + b_2 n_1) & \lambda b_k n_k + 2\mu b_2 n_2 & \mu(b_2 n_3 + b_3 n_2) \\ \mu(b_1 n_3 + b_3 n_1) & \mu(b_2 n_3 + b_3 n_2) & \lambda b_k n_k + 2\mu b_3 n_3 \end{bmatrix} \Delta V$$

where ΔV is the crack volume, C_{pqij} is the elastic constant tensor.

Irwin proposed three standard conventions for defining relative displacements in elastic materials in order to analyse crack propagation: opening mode (mode I), sliding mode (mode II), and tearing mode (mode III), see Figure 2-2 [23]. For tensile mode cracks, the suddenly-released stress from the crack propagation is in parallel with the crack normal; while for shear cracks, the stress direction is perpendicular to the crack normal. Shear cracks can be in-plane and out-of-plane. In the case that crack displacement vector b is parallel to normal vector n, a tensile crack occurs; a shear crack is created when vector b is vertical to normal vector n. Figure 2-2 showed a schematic of both tensile crack and shear crack. When the shear stress acts parallel to the plane of the crack perpendicular to the crack front the crack opening mode is called the mode II crack (in-plane shear) and when the shear stress acts parallel to the plane of the crack and at the same time parallel to the crack front the crack opening mode is called mode III crack (out-of-plane shear).

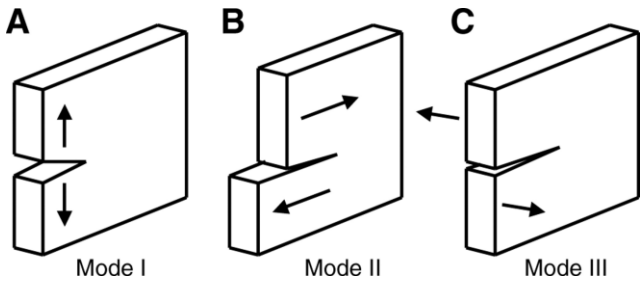

Figure 2-2 Schematic of the basic fracture modes: (A) Tensile crack - Mode I (B) Shear crack - Mode II (Sliding) (C)Shear crack - Mode III (tearing) [24]

Tensile mode crack

For the case of a tensile crack buried inside the material, the crack normal is assumed to be $n = (1, 0, 0)$ and the crack surface displacement, $b = (1, 0, 0)$, accordingly the moment tensor can be written as

$$M_{pq} = \begin{bmatrix} \lambda + 2\mu & 0 & 0 \\ 0 & \lambda & 0 \\ 0 & 0 & \lambda \end{bmatrix} \Delta V$$

Shear mode crack

For the case of a buried shear type crack, the crack normal is assumed to be $n = (1, 0, 0)$, while the crack surface displacement $b = (0, 0, 1)$. The corresponding moment tensor can be expressed as

$$M_{pq} = \begin{bmatrix} 0 & 0 & \mu \\ 0 & 0 & 0 \\ \mu & 0 & 0 \end{bmatrix} \Delta V$$

2.1.2 Elastic Waves

To analyse waves in elastic materials, the equation governing the wave propagation needs to be derived. The basic equations of motion for a linear elastic material are derived by substituting the stress-strain relation into the equation of balance of momentum. The dynamic theory of elasticity, sometimes called elastodynamics, formulates the propagation of mechanical disturbances by considering:

- The exact kinematics of small deformation theory.
- The conservation of linear and angular momentum.
- The general three-dimensional material or constitutive behaviour of linear elastic media.

Balance of linear momentum in terms of stress tensor

The equation of balance of momentum for a material is obtained by assuming that the rate of change of the total linear momentum of the material contained in a material volume V is equal to the total force acting on the material volume. In general, forces on a material volume include body force f_i and surface force:

$$\frac{d}{dt}\int_V \rho v_i \, dV = \int_S \sigma_{ij} \cdot n_j \, dS + \int_V f_i \, dV \qquad (2)$$

where ρ is the material density, v_i is the velocity, σ_{ij} represent the stress tensor. The first term on the right represents the force exerted on the surface S. The second term on the right is the force on the material by the body force. By applying Gauss theorem, we can obtain the equation of linear momentum for a material:

$$\rho a_i = \frac{\partial \sigma_{ij}}{\partial x_j} + f_i \tag{3}$$

a_i is the acceleration.

Stress-strain relation:

The stress-strain relation for an isotropic linear elastic material is given by Hooke's law:

$$\sigma_{ij} = \lambda \varepsilon_{kk} \delta_{ij} + 2\mu \varepsilon_{ij} \tag{4}$$

In here, ε_{ij} is the strain tensor, δ_{ij} is the Kronecker delta function,

$$\varepsilon_{ij} = \frac{1}{2}\left(\frac{\partial u_i}{\partial x_j} + \frac{\partial u_j}{\partial x_i}\right) \tag{5}$$

Equations of motion in terms of displacement:

In the equation of balance of linear momentum of a material,

$$a_i = \frac{\partial^2 u_i}{\partial t^2} \tag{6}$$

The equation of balance of linear momentum of a material becomes:

$$\rho \frac{\partial^2 u_i}{\partial t^2} = \frac{\partial \sigma_{ij}}{\partial x_j} + f_i \tag{7}$$

Substituting this expression into the Hooke's law, we obtain the stress components in terms of the components of the displacement:

$$\sigma_{ij} = \lambda\delta_{ij}\frac{\partial u_k}{\partial x_k} + \mu\left(\frac{\partial u_i}{\partial x_j} + \frac{\partial u_j}{\partial x_i}\right) \tag{8}$$

Combining these equations in terms of displacement $\bar{u}$ yields the equation of momentum for an isotropic linear elastic material:

$$\rho\frac{\partial^2 u_i}{\partial t^2} = (\lambda + \mu)\frac{\partial^2 u_j}{\partial x_j \partial x_i} + \mu\frac{\partial^2 u_i}{\partial {x_j}^2} + f_i \tag{9}$$

In the absence of body forces, equation (9) can be expressed in vector form as:

$$\rho\frac{\partial^2 \bar{u}}{\partial t^2} = (\lambda + \mu)\nabla\nabla\cdot\bar{u} + \mu\nabla^2\bar{u} \tag{10}$$

The above equations express the equation of balance of linear momentum for isotropic linear elasticity in index notation and in vector notation. $\bar{u}$ is the displacement of the material relative to the reference state.

$$\nabla^2\bar{u} = \nabla\nabla\cdot\bar{u} - \nabla\times\nabla\times\bar{u} \tag{11}$$

By substituting equation (11) into equation (9), the equation of motion can alternatively be expressed as

$$\rho\frac{\partial^2 \bar{u}}{\partial t^2} = (\lambda + 2\mu)\nabla\nabla\cdot\bar{u} - \mu\nabla\times\nabla\times\bar{u} \tag{12}$$

The constants λ and μ are the Lame constants which relate to the Young's modulus E and Poisson's ratio ν of the material by:

$$\lambda = \frac{\nu E}{(1+\nu)(1-2\nu)}, \qquad \mu = \frac{E}{2(1+\nu)} \tag{13}$$

The excitation process of an elastic wave as a result of the crack surface movement is represented by the equation of motion of the displacement $\bar{u}$ when the deformation remains elastic.

Longitudinal and transversal wave equations:

The equation of motion can also be expressed in a simplified form. The vector displacement $\bar{u}$ can be expressed via Helmholtz decomposition. In the Helmholtz decomposition, the displacement field $\bar{u}$ of a material can be formulated as the sum of a scalar potential ϕ and the curl of a vector potential $\bar{\psi}$:

$$\bar{u} = \nabla\phi + \nabla \times \bar{\psi} \tag{14}$$

By substituting equation (14) into the equation (10) yields two wave equations:

$$\frac{\partial^2 \phi}{\partial t^2} = \alpha^2 \nabla^2 \phi \tag{15}$$

$$\frac{\partial^2 \bar{\psi}}{\partial t^2} = \beta^2 \nabla^2 \bar{\psi} \tag{16}$$

where the above equations introduced the two basic wave forms, see Figure 2-3, longitudinal wave (which is the wave in which the oscillations occurring in the direction of the wave propagation) and transversal wave (which is the wave in which the oscillations occurring perpendicular to the direction of the wave propagation) propagation velocities α and β:

$$\alpha = \sqrt{\frac{\lambda + 2\mu}{\rho}} = \sqrt{\frac{E(1-\nu)}{\rho(1+\nu)(1-2\nu)}} \tag{17}$$

$$\beta = \sqrt{\frac{\mu}{\rho}} = \sqrt{\frac{E}{2\rho(1+\nu)}} \tag{18}$$

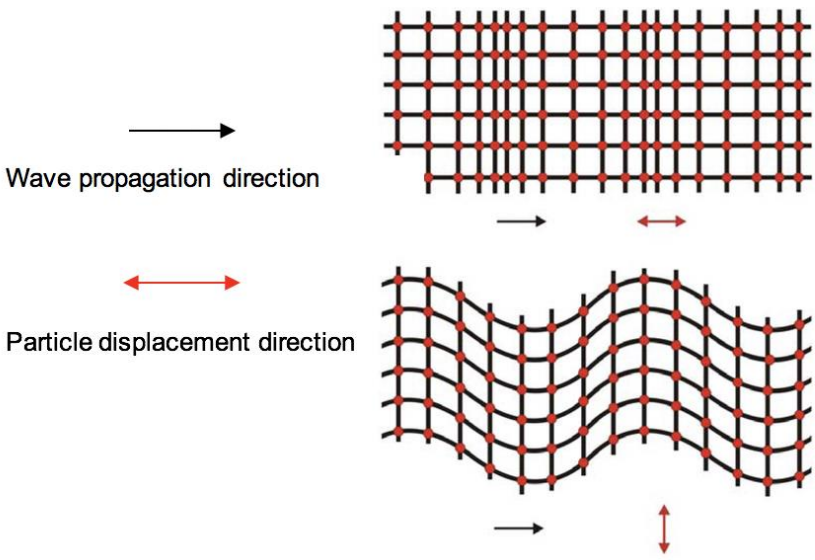

Figure 2-3 Particle displacement of plane acoustic waves propagating in a solid, Top longitudinal wave, Bottom transverse wave [25]**.**

As a result, the equation of motion can be decomposed as two simplified wave equations.

Elastic wave propagation in plate structure:

Typically, the propagation of wave can be categorized into two different types. The longitudinal and transversal waves propagate through the material interior, they are known as body waves. Rayleigh waves propagate primarily at the material's surface and called surface waves [19]. A Rayleigh wave will become a Lamb wave if the thickness of a plate is smaller than the wavelength of a Rayleigh wave.

The combination of longitudinal and transverse waves give rise to two distinct waves, see Figure 2-4: the symmetric (S_0) and anti-symmetric (A_0) Lamb waves for which the characteristic equations are provided as:

S_0 wave:

$$\frac{\tan(\beta h)}{\tan(\alpha h)} = -\frac{4k^2\alpha\beta}{(\beta^2 - k^2)^2} \tag{19}$$

A_0 wave:

$$\frac{\tan(\beta h)}{\tan(\alpha h)} = -\frac{(\beta^2 - k^2)^2}{4k^2\alpha\beta} \tag{20}$$

where, k is the wave number, ω is the circular frequency, h is the half plate thickness, α and β are longitudinal and transverse wave velocities respectively.

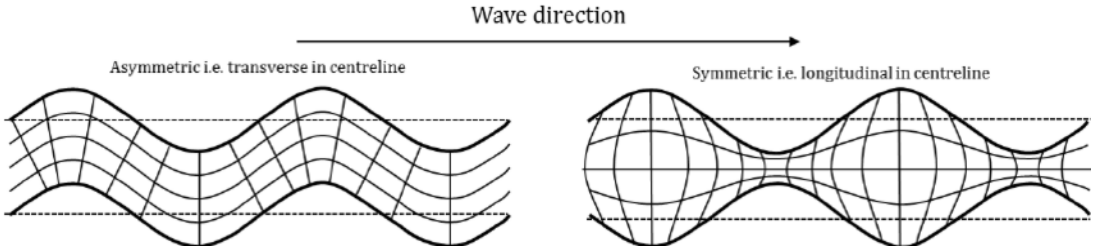

Figure 2-4 A diagrammatic representation of symmetrical and antisymmetric wave modes [26]**.**

As the wave travels, the different modes travel in different velocities due to the dispersion effect. The dispersion effect can be calculated for both S_0 and A_0 waves using equations below:

$$\frac{\tan(qh)}{q} + \frac{4k^2p * \tan(ph)}{(q^2 - k^2)^2} = 0 \tag{21}$$

$$q * \tan(qh) + \frac{(q^2 - k^2)^2 * \tan(ph)}{4k^2p} = 0 \tag{22}$$

Iteratively evaluating the above two equations with different velocities and a specified frequency-thickness product, leads to the calculation of dispersion curves.

$$p^2 = \left(\frac{\omega^2}{\alpha^2} - k^2\right) \tag{23}$$

$$q^2 = \left(\frac{\omega^2}{\beta^2} - k^2\right) \tag{24}$$

Therefore, to determine the dispersion curve for isotropic materials, the longitudinal and transversal wave velocities will be calculated.

For anisotropic materials, such as composite materials, the specific modulus of elasticity and Poisson's ratio in three primary axes including E_{11}, E_{22}, E_{33} and $\nu_{12}, \nu_{13}, \nu_{23}$ should be applied to determine the wave speed in that direction.

Based on the classical plate theory [27], the S_0 and A_0 wave velocity in laminates plates are presented below. The S_0 wave velocity in laminates is dispersion-less:

$$c_{S_0} = \sqrt{\frac{A_{11}}{\rho h}} \tag{25}$$

A_{11} is the in-plane laminate stiffness. The A_0 wave velocity depends on the frequency:

$$c_{A_0} = \left[\frac{D_{11}}{\rho h}\right]^{\frac{1}{4}} \sqrt{\omega} \tag{26}$$

ω is the frequency, and h is the thickness, D_{11} is the bending stiffness.

2.2 Signal Detection

In the last section, the direct wave equations are reviewed. After the stress waves are generated, they propagate from the source to the surface and cause the surface displacements which are measured using sensitive transducers. In this section, commonly used instrumentation, procedures and experimental techniques are discussed.

To perform an acoustic emission detection a number of components are required such as sensors and preamplifiers along with a data acquisition, display and data storage equipment. The acoustic emission sensors respond to the dynamic motion caused by an event such as crack propagation or plastic deformation or external mechanical forces applied to a structure. Sensors and

preamplifiers are designed to help eliminate unwanted signals. First, the preamplifier boosts the voltage to provide gain and cable drive capability. To minimize interference, many transducers today are equipped with integrated preamplifiers [28] .

The acquired signals are then relayed to a bandpass filter to further eliminate low frequency and high frequency components. The acquired signals are then either stored on the data acquisition system or send to a processing unit for further analysis.

Transducers used for acoustic emission detection include non-contact electromagnetic sensors [29], fibre optic sensors [30], capacitive sensors [31] and piezoelectric sensors [32]. The electromagnetic sensors and capacitive sensors are considered less sensitive than piezoelectric sensors [33]. The fibre optic sensors are small in size and light weight and can be embedded in structures. However, the sensitivity of the FBG acoustic emission sensor is different in different directions [34]. The most widespread sensor in acoustic emission detection is piezoelectric sensors. The piezoelectric sensors are made by using a special ceramic called Porous Lead Zirconate Titanite (PZT). Figure 2-5 shows a schematic view of a piezoelectric sensor.

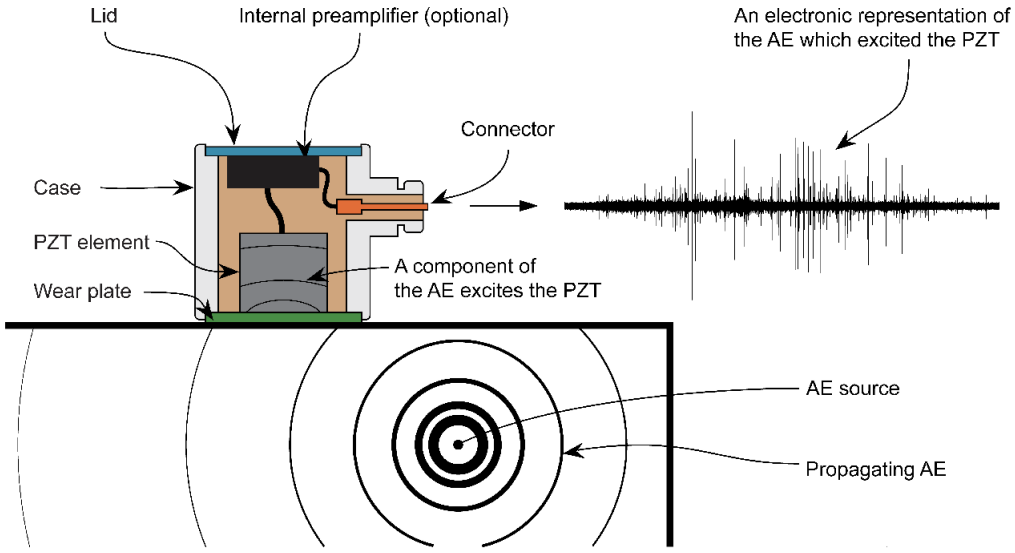

Figure 2-5 A typical resonant acoustic emission transducer and how elastic waves is converted into an electric signal [35]

The piezoelectric sensors can be highly sensitive at a certain frequency (resonant sensors), or with a broad frequency response (broad band sensors). Broadband sensors are often used if the frequency of interest is still unknown or if the different frequencies in one signal should be analysed. Resonant sensors are usually used if the frequency content itself is not if interest but only acoustic emission features such as peak amplitude, duration, energy [36]. The change of the acoustic emission features is a phenomenon that has been widely used to monitor the different stages of the fracture experiment. These features are affected by the peak frequency and frequency range of the AE sensor. Therefore, acoustic emission features can only be compared if recorded with the same sensor type.

The resonance frequency is the decisive factor to select the most appropriate acoustic emission sensor for specific applications. A subsequent measurement system can only process signals which the sensors picked up. If the frequency response of the sensor doesn't suit the application, anything a sensor does not pick up is lost for analysis. Most applications can be classified into one of these three frequency regimes: low (20 kHz – 100 kHz), standard (100 kHz – 400 kHz) and high (≥ 400 kHz) [37]. It has been proven for some specific applications certain frequencies are more suitable: for cases where there is leakage and corrosion defects in terms of acoustic emission signals these usually correspond to low frequency range; for defects in metallic structures and composite structures such as cracks or plastic deformations the generated acoustic emissions are in the standard frequency range of 100 to 400kHz.

Since acoustic emission signals are elastic waves they are subject to attenuation as well as dispersion [38]. Concerning previous studies, the geometries of the specimens used for acoustic emission monitoring were mainly thin plates. In thin plates, propagation is dispersive due to the fact that different frequencies propagate at different velocities. Figure 2-6 gives an

example of the dispersion curves displayed as a function of velocity on the vertical axis and frequency on the horizontal axis.

This affects the generated acoustic emission waveforms in terms of recording as the distance between the event and the location of the different sensors varies. This means that at each sensor location a different acoustic emission waveform will “arrive” a phenomenon that can be amplified if the distance between the source and sensors increases. The above is particularly important when studying for example a large structure where the coverage of the structure with sensors and the distance that these sensors should have between them become extremely important in the effort to not miss any occurring acoustic emission events [39].

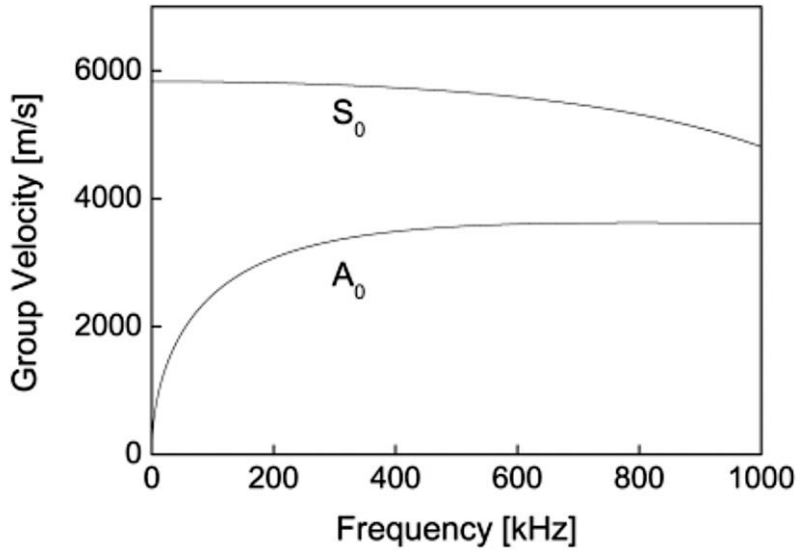

Figure 2-6 Dispersion curves of the S_0 and A_0 Lamb waves for the quasi-CFRP laminate [40]**.**

2.3 Acoustic Emission Signal Processing

2.3.1 Acoustic Emission Signal Features

There are two types of acoustic emission signals: continuous and burst, see Figure 2-7. Continuous is a type of emission that relates to time overlapping and successive emission events from one or several sources that results in sustained signals. It is generally believed that continuous emission signals are mostly unwanted signals such as electrical noise and rubbing [41]. The more useful signals for acoustic emission testing are burst type signals. Burst type

signal is related to individual events that result in discrete acoustic emission signals, they can be generated by fracture of non-metallic inclusions, breakage of corrosion products, crack jumps in brittle or at advance stages in ductile metals [42]. It is important to be able to detect and analyse signals resulting from both emission types. Strong research efforts have been put into understanding the origin of defects through analysing burst type signals [35].

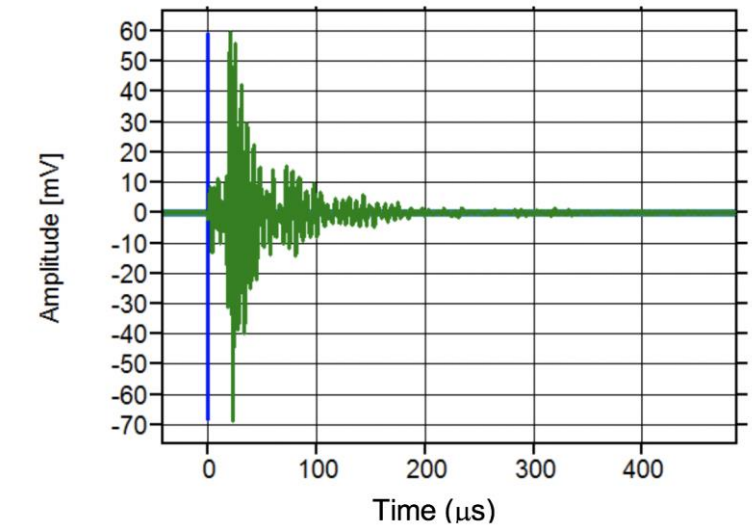

(a)

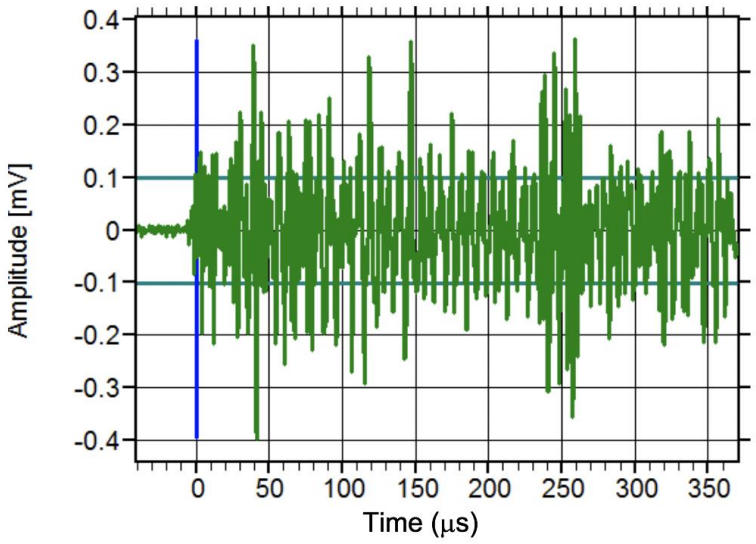

(b)

Figure 2-7 (a) Burst type signal and (b) continuous type signal

The burst type signals, also called hits, are identified based on a detection criterion. The purpose of the detection criterion is to discriminate the hit from

background noise, or continuous acoustic emission. A common detection criterion used for detecting and determining acoustic emission hits is based on threshold and hit definition time (HDT). The threshold is typically set above the background noise level, if the signal surpasses the threshold in either positive or negative direction, a hit is detected. After the hit is detected, HDT is used to determine the end of the hit. HDT specifies the maximum time between threshold crossings, i.e. if no crossing occurs during this time then the hit has ended. If the HDT is set too high then the system may consider two or more hits as one. If the HDT is set too low then the system may not fully capture the acoustic emission hits and possibly treat one hit as multiple ones [35].

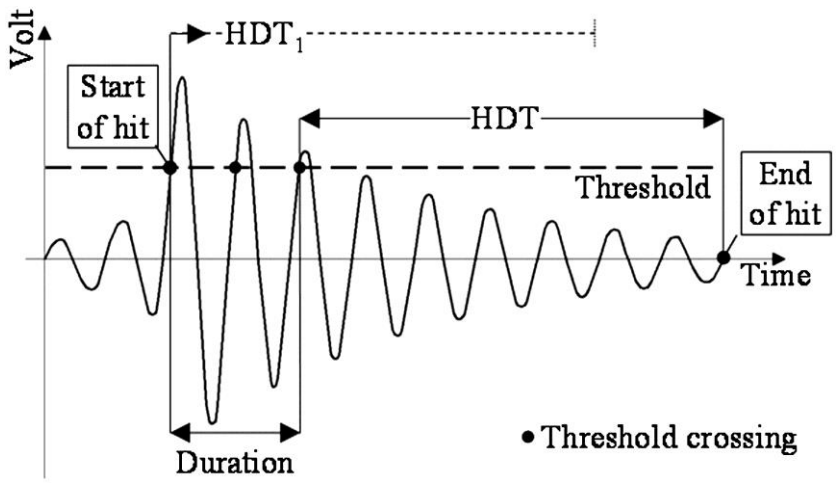

Figure 2-8 Illustration of the threshold based hit detection and hit definition time [43]**.**

In most cases, hundreds or thousands of acoustic emission hits are recorded in one test. It is very important to obtain useful information form these signals. A popular method is to extract features from the identified acoustic emission waveforms. The most commonly used time domain features include Peak amplitude, Rise Time, Duration, Number of counts, MARSE and Signal Strength. The detailed definition is presented in Glossary.

2.3.2 Source Localization

One of the attractive features of acoustic emission technique is the capability of estimating the source location and it is considered of great importance for

the assessment of the integrity of structural components. There are different ways to localize acoustic emission source in practice that can be used in one, two or three dimensions. Source location determination is an inverse problem [18] . The standard approach to one-dimensional and two-dimensional is known as the ‘’time of arrival (TOA)’’ method. For this type of method, signals must be detected in a minimum number of sensors: two for one-dimensional (linear), three for two-dimensional (planar). It is also assumed that acoustic emission waves travel at a constant velocity in a material. The calculations are based on the arrival time differences between two sensors and the know velocity. For a linear structure, the source can be localized through the equations below. The acoustic emission source location can be determined after the measurement of the acoustic emission sensor locations, see Figure 2-9.

$$\mathrm{d} = \frac{1}{2}(\mathrm{D} - \Delta\mathrm{T} \cdot \mathrm{V}) \tag{27}$$

d is the distance from first hit sensor, D is distance between sensors, V is velocity.

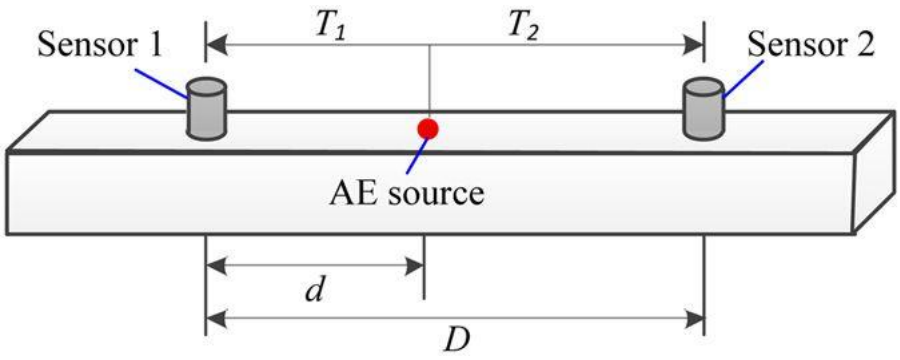

Figure 2-9 The schematic of 1D linear localization [44]

For a planar source localization, it is often assumed that the acoustic emission source $\mathrm{S}(\mathrm{x_s}, \mathrm{y_s})$ is located in a uniform medium. The coordinates of the three sensors are $(\mathrm{x_1}, \mathrm{y_1})$, $(\mathrm{x_2}, \mathrm{y_2})$, $(\mathrm{x_3}, \mathrm{y_3})$ respectively. The acoustic emission source is generated at the $\mathrm{T_0}$, and the time of arrival for these three sensors are $\mathrm{T_1}, \mathrm{T_2}, \mathrm{T_3}$ respectively. The distance between the source and sensors can be obtained as:

$$R_i = \sqrt[2]{(x_i - x_s)^2 + (y_i - y_s)^2} = V(i - T_0), \qquad i = 1, 2, 3 \tag{28}$$

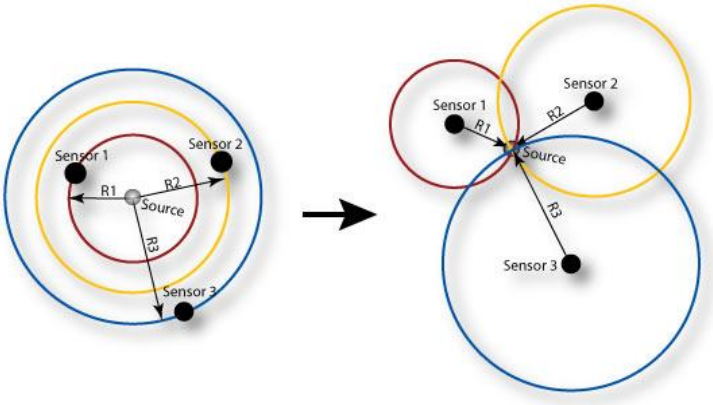

Figure 2-10 The schematic of 2D planar location [45]

There are two main causes of error when using TOA to locate acoustic emission sources, which are signal arrival time measurement and velocity. Arrival time is often set as the time of the first threshold crossing, see Figure 2-11, this method is currently used by commercially available acoustic emission acquisition systems [46]. It can be seen that the time of arrival depends on the value of the threshold. Considering the attenuation effects during wave propagation, if the distance between a sensor and source is far, then there is a possibility that the true arrival time of the signal is within a number of peaks occurring before the signal amplitude crossed the threshold thus will not be detected.

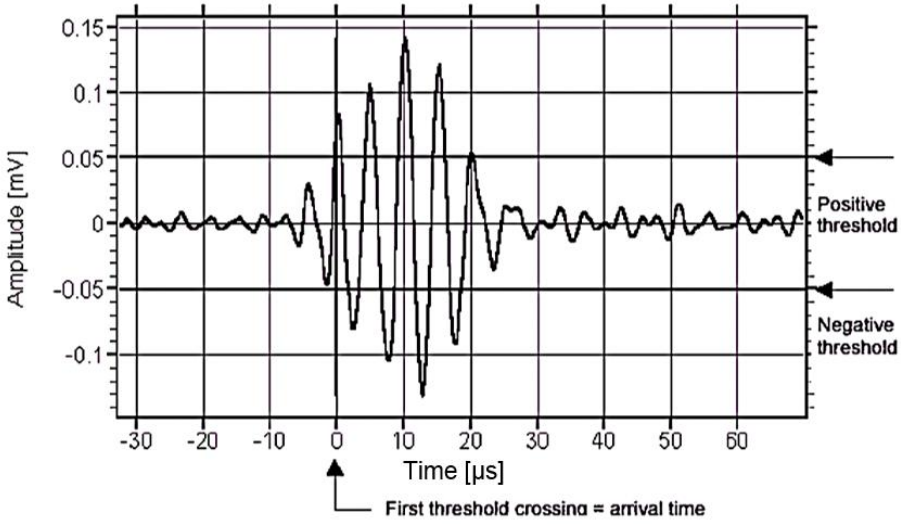

Figure 2-11 Determination of the arrival time [43]

The dispersion behaviour will have an impact on the results in terms of the velocity input to the algorithm. In the plate-like structures for example, two wave modes exist, if the wave mode of the signal phase (with a unique frequency and velocity) that triggers the threshold has a different velocity from the velocity input into the algorithm, then an error will occur. Such triggering errors are particularly obvious in a dispersive media, such as composite structures. Also in composite materials, the wave velocity can vary greatly with the propagation direction due to the anisotropic features of the materials. All these can lead to errors when using the TOA method to locate acoustic emission source [47], [48].

To resolve the issues regarding the signal arrival time estimation, S. Ziola et al. employed a cross-correlation technique to determine the arrival time of a particular frequency in a recorded signal [49]. To achieve this, a short pulse consisting of a single frequency sine wave is modulated by a Gaussian pulse; peaks in the cross-correlation output can be taken as the arrival time of the chosen frequency. In order to guarantee better accuracy in the time-frequency analysis, the Wavelet transforms (WT) is used, allowing to plot waveform spectra as a function of time. Jeong, H. et al. used Gabor WT to identify the relationship between the peaks in magnitude of a time-frequency distribution and the frequency dependent group velocity arrival time s in a carbon fibre laminate [50], [51]. In this case, the arrival times of wave modes, and the corresponding velocities can be used to achieve a more accurate localization result.

However, this method cannot be characterised as real-time processing as the process will produce a big amount of data, which will require the user to select a frequency of interest for each localization process. For plate-like structures, Surgeon M. et al. developed a method to measure the time of arrival for Lamb wave modes (S_0 and A_0) in the signals by considering them as additional sensors. In this way, the source to sensor distances can be estimated using one sensor and to localize the source a secondary sensor will be needed. These two methods have improved the source location accuracy albeit when

the sensors are placed close to the edges as multiple reflections from the boundaries can increase the complexity of the recorded signals.

Since the amplitudes of the WTs of the signal generated by the background noise at the times of mode arrivals would be a random and unpredictable condition, a statistical study of background noise effects on arrival times has been proposed to estimate the arrival time of signals. Shehadeh et al. used a sliding window energy technique in which the ratio of high frequency energy and low frequency energy is calculated for a shot time window which is shifted along a signal. Changes in this parameter is used to identify the wave modes and their arrival times [52]. Lokajicek and Klima take the derivative of the 6th order statistical moment of data within a sliding window, the normal distribution of noise data is skewed with the inclusion of a few signal points in the window, thus affecting a change in the 6th order moment. It is found that more than 95% events that are analysed are within an accuracy of ±2 sampling points [53]. These limitations have a direct effect on the performance of the acoustic emission localization technique.

2.3.3 Source Characterization

Apart from source localization, the main advantage of acoustic emission technique over other condition monitoring techniques is that detected acoustic emission signals are sensitive to various damage mechanisms and as a result acoustic emission is very useful for real-time damage evolution. In general, damage characterization is achieved by correlating the acoustic emission waveform features with a particular damage mechanism.

2.3.3.1 Using Time Domain Feature Distribution

Continuous fibre-reinforced polymer-matrix composites (FRP) are anisotropic or orthotropic materials with at least two constituents, which are fibres and the matrix polymer into which the fibres are embedded. Main failure modes in composite materials include fibre failure, matrix cracking, fibre-matrix debonding and delamination [54]. Matrix cracks can cover a wide range of scales, from sub-micrometre to several millimetres. Matrix cracks may

continue growing under load, which will lead to larger areas of separation in the matrix polymers and can cause delamination between fibre plies. Debonding occurs along the fibre-matrix interface, together with fibre breakage and may lead to fibre pull-out [55], [56].

The identification of a particular type of damage in composite materials is an emerging research field in terms of acoustic emission. To date, most studies focus on the macroscopic time-domain waveform feature distributions to determine damage initiation and failure mechanisms. Several of the above mentioned acoustic emission features have been correlated with fracture mechanisms in the composite material. J.M. Berthelot. investigated the relationship between amplitudes and rupture mechanisms in laminates of epoxy matrix with carbon fibres, the fibre breakage showed the highest amplitude [57]. Woo, S.C. et al. reviewed the established different amplitude classifications for the damage mechanisms of composites–fibre breakage (i.e., 70 dB–100 dB), fibre/matrix debonding (i.e., 50 dB–70 dB), and matrix cracking (i.e., 30 dB–50 dB), respectively [58]. On the other hand, P. Nimdumn and J. Renard carried out a series of tensile and buckling tests on specimens with different stacking sequences, and found the fibre breakage showed low amplitude (< 60 dB), while delamination showed high amplitude (>80dB), and fibre/matrix debonding showed intermediate amplitude [59]. De Rosa, I.M. et al. summarized previous work to conclude that the acoustic emission events of higher energy and frequency can be ascribed to fibre breakages, while events of lower energy and frequency can be ascribed to matrix cracking [60]. Joung-Man Park et al. also concluded that the acoustic emission energy released by the fibre breakage is generally larger than that of the matrix cracking and debonding [61]. H. Suzuky et al. studied various types of failure in a model polyester-matrix composite with one layer of quartz and concluded that compared with debonding, fibre breakage exhibited acoustic emission signals with shorter rise time [57]. Although a lot of work has been carried out, it is pointed out that using the time-domain parameters to characterize failure modes is not always reliable and can even be inaccurate. The main reasons for this include the difficult separation of the signals generated from the noise

from the signals generated from real damage, the dispersion and attenuation effects on waveform features.

2.3.3.2 Using Frequency Domain Feature Distribution

Apart from the time domain features, acoustic emission signals can also be well characterized by frequency domain analysis. Qing-Qing Ni et al. concluded that the frequency analysis is an effective way to process acoustic emission signals in composite materials [62]. This approach is based on the assumptions that different damage mechanisms will produce signals with different frequency contents. In this regard, the identification of the different damage mechanisms through frequency-based methodologies in acoustic emission data analysis from loaded carbon/epoxy material has also been studied. C.R Ramirez-Jimenez et al. carried out tensile tests on glass/polypropylene specimens with different fibre orientations, it is concluded that the event frequency range occurring around 100 kHz is due to fibre/matrix debonding; the one from 200 and 300 kHz are due to the fibre slippage and fibre pull out [63]. R. Gutkin et al. investigated failure in CFRP using acoustic emission, the classification of the damage mechanisms follows patterns in acoustic emission signal peak frequency: the peak frequency band from 0 – 50 kHz corresponds to matrix cracking, the band from 50 – 150 kHz is due to delamination, fibre/matrix debonding occurred in the frequency range in between 200 – 300 kHz, while the fibre failure and fibre pull out showed a high frequency range from 400 – 500 kHz, and 500 – 600 kHz respectively [64]. M. Eaton et al. used peak frequency content to examine signals resulting from the different damage modes identified in tensile and buckling tests on carbon fibre composite materials, and demonstrates that the matrix damage relates to the signals with low frequency content and fibre failure to the signals with high frequency content [65]. The correlation between damage types and the corresponding frequency is not always the same in all studies, this is because the signal frequencies not only depend on the source mechanism but also sensor response and wave propagation effect in the material. The approach of using parameter distribution has the advantage of real-time damage

detection, but has many limitations and is not always reliable to provide reliable damage characterization.

2.3.3.3 Pattern Recognition

In order to overcome limited resolution inherent when using single acoustic emission feature distributions for damage classification, the use of pattern recognition (PR) techniques for the analysis of acoustic emission data has been proposed in this study. PR is the process to recognise and distinguish the similarities between objects [14]. PR technique for acoustic emission is based on the classification between different acoustic emission signal types using signal features (peak amplitude, rise time and duration among others.). PR process can be performed by two main methodologies [66]:

Unsupervised Pattern Recognition (UPR) is the process by which the acoustic emission signals are classified in general groups by comparing their features. In such cases, no previous knowledge or database is needed.

Supervised Pattern Recognition (SPR) usually involves in a learning process and each new set of data is processed and classified into one of the previously recognized groups by comparing its features to a database.

Unsupervised pattern recognition technique has been successfully applied to discriminate between the acoustic emission signals generated from the noise and real damages[67], [68]. For a structure, UPR is often used to focus on detection of characteristic similarities of the recorded signals since it is often not possible to provide a set of training patterns.

The first step of developing an unsupervised pattern recognition process is to classify signals into groups based on similarities. This process involves in statistical effects and the key point of successful feature selection to construct fine classification accuracy. Following this initial step and based on the selected features, data partition is performed using clustering analysis. This step aims to separate the acoustic emission signals into a limited number of

groups. The final step involves assigning the clustering results to the fracture mechanism.

Feature selection

Feature selection is a process which selects an optimal subset of the extracted features based on an evaluation criterion. By removing the irrelevant and redundant features the database dimensions are reduced resulting in reduced data processing time and more importantly increased classification accuracy. T. Warren Liao reviewed the previous feature selection methodologies and categorized them in three types [69]:

Complete (brute-force) search that guarantees to find the optimal result. Sequential search that adds or removes features one (or more) at a time. Finally, a random search that starts with a randomly selected subset. It then proceeds to generate the next subset in a completely random manner or via a sequential search.

For the first type of method, common methods include data variance, which protects the data points along the dimensions of the maximum variance, finding the useful features to represent the data. Laplacian Score has been proved to be an effective and efficient feature selection method, which seeks features that best reflect the underlying manifold structure [70], [71].

M.G.R. Sause presented a feature selection procedure using exhaustive search to investigate the failure modes in CFRP specimens [72]. During this procedure, all possible feature combinations with a given minimum number of features to be used for clustering are used. Each combination is evaluated by investigating the classification performance using several clustering algorithm evaluating metrics (details will be discussed in clustering analysis). Then the rating of each clustering algorithm evaluation metric is cumulated based on a voting scheme and finally the best signal features and number of clusters can be decided. This method can identify the natural clusters of acoustic emission signal without previous knowledge about the cluster structure. A complete

search can also ensure a high-quality feature subset but is computationally expensive.

In contrast, the sequential search technique is comparatively faster and provides a good trade-off between computational complexity and quality of selected optimal features [73]. The sequential search technique, such as sequential forward selection method starts with empty subset with incrementally features added to the subset with the evaluation of the subset as the last step. Sequential forward floating selection is an improvement of sequential forward selection with reverse feature dependency check. This process repeats until the all feature added or no better feature is found. D. D. Doan et al. applied a sequential search technique to reduce high dimensional fatigue dataset during a tensile fatigue test carried out on CFRP specimen. The results demonstrate that the proposed feature selection methodology together with the clustering analysis allow to identify some relevant clusters of different levels of energy which can correspond to the damage mechanisms in the materials [74].

The third type - randomized approach, such as genetic algorithm, used a large number of generations to find an optimal subset form randomly generated subset. Md. Rashedul Islam et al. investigates the feature selection approaches including sequential forward selection, sequential floating forward selection and generic algorithm for identifying the most discriminant subset. The effectiveness of this discriminant features subset is verified with a low-speed bearing fault diagnosis application. The results showed that after embedding the feature selection in fault diagnosis process, the diagnosis performance is increased to 100%. General algorithm showed a better accuracy than sequential approaches [75]. However, the randomized search can provide a good trade-off between the efficiency and computational complexity [76]. Besides, the genetic algorithm with fixed length chromosomes and stationary searching space of gene bases cannot be directly employed to find the optimal feature subset [77].

Depending on the feature evaluation method, the feature selection method can also be categorized as “wrapper” or “filter” from another perspective. The “filter” method is totally independent of any learning algorithm and evaluates the feature subsets by adapting statistical measures to rank available features with the scores falling below a predetermined threshold getting rejected. On the contrary, the “wrapper” method is the process which needs a predetermined learning algorithm to evaluate the features. The performance of a feature subset can be evaluated and lead to a better solution, see Figure 2-12. The “wrapper” method can be carried out in complete search, sequential search and randomized search.

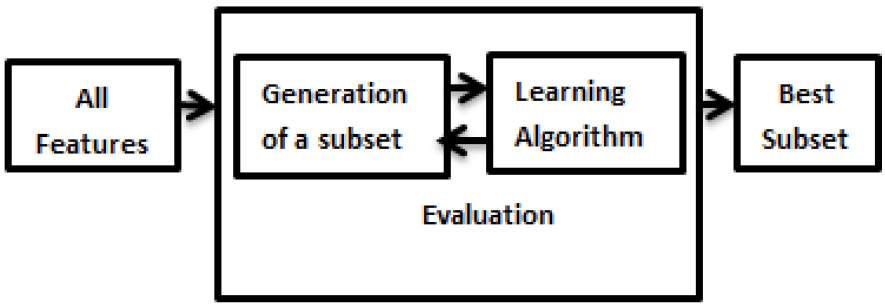

Figure 2-12 Wrapper feature selection method [78]

Clustering analysis methods

After the successful feature collection and selection, the next step for unsupervised pattern recognition is clustering analysis. Clustering analysis is to separate a set of acoustic emission signals into several groups based on their similarities. Several data clustering techniques have been proved effective for different applications. Clustering can be classified as exclusive clustering also named as partitional clustering, overlapping clustering and fuzzy clustering. Through exclusive clustering, each object can only be assigned to one cluster. However for overlapping clustering one object can be assigned to one or more groups simultaneously. In a fuzzy clustering, every object belongs to a group with a membership weight that is between 0 (absolutely doesn’t belong) and 1 (absolutely belongs) [79].

For clustering algorithms, most frequently used methods are Fuzzy C-means (FCM), k-means, self-organized map combination with k-means and neural networks. S. N. Omkar et al. used FCM clustering to classify the acoustic

emission signals to different sources of signals including PLB and spark signals, noise and pulse signals. FCM has the ability to classify the data in the boundaries which can be challenging in terms of acoustic emission signal analysis due to the superficial similarities in acoustic emission signals from damage and from the environment. Results showed that the Fuzzy C-means method classifies the signals generated by PLB and sparks with a higher degree of accuracy than the signals generated by noise and pulse [80].

T. P. Philippidis et al. employed artificial neural system methods for clustering of similar acoustic emission signals, enabling a phenomenological correlation with the actual failure modes in carbon/carbon composite material [68]. Apart from the failure modes distinction, artificial neural network is also used to predict the strength of GFRP beams, pre-fatigued in flexure up to different portions of their fatigue life. Acoustic emission signals, the residual strength measurement and the associated stress are the inputs for the method. The results show that that the artificial neural network provided reliable predictions, performing better than the theoretical model based on fracture mechanics [81].

The exclusive clustering (partitional clustering) process divides the data into partitions based on some evaluation criteria. K-means is a very popular partitional clustering algorithm and has been proved successful in AE signal clustering. A. A. Anastassopoulos et al. used k-means method to characterize the damage evolution in 2-D carbon/carbon composite materials. The results proved the effectiveness of cluster analysis in correlating patterns and associated damage mechanisms [82]. V Kostopoulos et al. applied k-means method to correlate the resulted clusters to the damage mechanisms in oxide/oxide composites based on the acquired acoustic emission signals [83]. M. Moevus et al. investigated the damage mechanisms in two SiCf/[Si-B-C] composites which exhibiting different mechanical behaviours under tensile testing, the different types of matrix cracking in the composite are successfully distinguished using clustering based acoustic emission analysis [84].

The k-means clustering method aims at minimizing the sum of the squared distances between all the points of a cluster and its centre. It requires the user

to define number of partitions k and divides a set of n signals into k clusters. The first step is to find k centroids and take each data point belonging to a given dataset and associate it to the nearest centroid according to the distance between the considered point and the centroids. This distance calculation plays a vital role in the clustering algorithm. The distance measurement techniques include “City Block”, “Euclidean”, “Cosine” and “Correlation”. Dibya Jyoti Bora et al. applied the clustering algorithm with all the above different distance measurement techniques and evaluated the performance. The results show that the city block distance has the best performance in terms of the computation time while the cosine has the worst. The correlation distance measurement show a better interpretation of the clustered data[85].

Since the number of partitions is not known a priori, the algorithms have to be executed with different number of k with the optimal number of clusters k determined using a few clustering indices. The most common ones are “Davies-Bouldin”[86] , “Calinski-Harabasz”, “Silhouette” and “Gap” indices [87]. Researchers always used more than one index in order to select the best clustering solution [88].

In summary, there are quite a few clustering methods that have been successfully applied in acoustic emission signals analysis, k-means clustering has been proved to be a reliable clustering method, however the distance measurement method and the optimal number of clusters needs to be carefully evaluated during the process.

Damage classification

After the acoustic emission signals are classified into groups by comparing their features and deciding upon their similarity through clustering analysis, the clustering results need to be assigned to the fracture mechanisms.

The identification of the acoustic emission signal source mechanisms can be achieved by experimental techniques. The difficulty of this method is that even the simplest conceivable FRP composites yield several damage mechanisms

under the simplest type of loading. For example, in the single-fibre fragmentation test (SFFT), fibre breakage is always accompanied by some fibre-matrix debonding. Therefore, R.A. Nordstrom [89] developed the theory called Single Dominant Damage Mechanism (SDDM). The theory demonstrates that during a test, there is always one specific type of damage mechanism being more active than all the others. As a result, acquired acoustic emission signals from the PR can be assigned to one specific fracture mechanism.

The theory of SDDM applies in a defined volume during a specific time interval as well as the whole volume of the specimen for the total duration of the test. Based on this theory, A.J. Brunner used laboratory-scale specimens to study acoustic emission signals originating from matrix cracking, delamination and pin pull-out damage mechanisms separately. This study allows an independent validation of the assignment of damage mechanisms to the PR signal clusters [56]. However, to determine the damage state of a large-scale FRP structure, such as a wind turbine blade, would require a suitable SDDM design of the test specimen. Due to the attenuation effect in FRP structures, the maximum detection distance between sensor and acoustic emission source is less than one metre, which is not too far from the typical laboratory-scale specimen size, therefore whether the SDDM theory can be applied in large-scale specimens is not clear at this stage.

M. G. Sause applied finite element simulations to interpret the signals acquired during the experiments on CFRP samples. Various failure mechanisms are modelled including matrix cracking, fibre breakage, and interface failure. Simulations results have shown the frequency contents of the signals can be very useful to correlate to different damage mechanisms, this agrees with the experimental results [90]. This is a very successful example of using finite element simulation to interpret the damage mechanisms. The influence of the attenuation effect as well as the specimen geometry on the acquired signals is also investigated. However, this application is also limited to the laboratory-scale specimens, as the input for the simulation needs to be accurate to obtain reliable results.

In summary, most of the previous studies on signal discrimination have been performed on small-scale specimens. It is important to investigate an effective way to analyse the propagation effects on the classification results on large complex composite structures.

2.3.3.4 Modal Analysis of Acoustic Emission Signals

Another attempt at providing a better theoretical background for acoustic emission testing is known as modal acoustic emission analysis. Modal acoustic emission analysis starts from the general theory of wave propagation in solids which can be summarised as the propagation of acoustic emission waves in a variety of wave modes. The separation of these modes at the sensor could make it possible to extract information about the source event that produced the wave [91].

Due to the laminate nature of composite materials, they are commonly manufactured as thin walled and plate like structures. In plate like structures, the propagation behaviour of the two wave modes S_0 and A_0 follow dispersion curves as discussed in section 2.2. Modal analysis of acoustic emission signals considers the wave modes in digitised and stored representations of the transient elastic waves [92].

Studies have been carried out using Hsu-Nielesen PLB test [93] to create an acoustic emission source in both aluminium and composite plates. Pressing and breaking the pencil lead against the structure surface creates an elastic wave containing both S_0 and A_0 wave modes, but the amplitude of the S_0 mode reduces and the amplitude of A_0 mode increases as the PLB source orientation changes from 0° to 30°, 60° and 90°, with respect to the plane of the plate [94]. In-plane displacements (breaking the pencil lead 0° against the plane of the plate) cause larger amplitude S_0 modes, out-of-plane

displacements (breaking the pencil lead 90° against the plane of the plate) causes larger amplitude flexural modes.

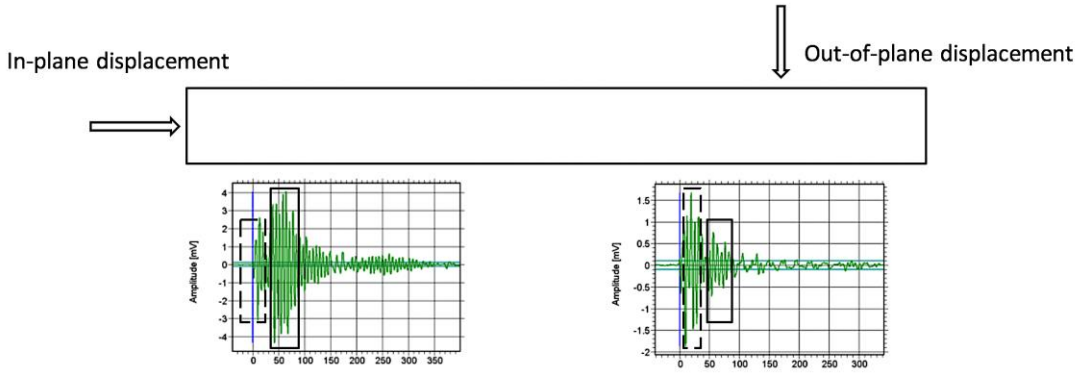

Figure 2-13 Example of signals from PLB source measured at in-plane displacement (left) and out-of-plane displacement (right)

John P. McCrory et al. utilized the ratio of the S_0 to A_0 mode amplitude to provide a measure of source orientation, the ratio is defined as measured amplitude ratio (MAR) [95]:

$$\mathrm{MAR} = \frac{S_0 \text{ mode amplitude}}{A_0 \text{ mode ampltidue}}$$

The modal analysis method utilises the MAR and works on the bases that damage which causes an out-of-plane displacement, for example the delamination in composite materials, will generate a larger amplitude A_0 mode signal, see Figure 2-14.

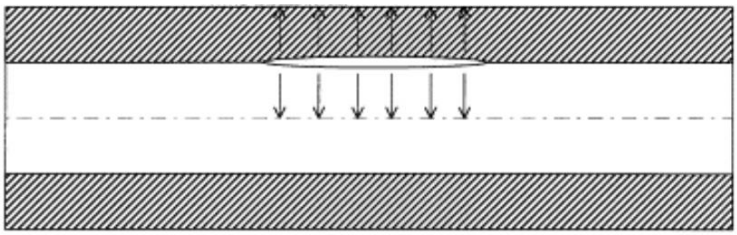

Figure 2-14 Schematic illustration of out-of-plane motion caused by delamination growth [91]

Conversely, an in-plane displacement such as matrix cracking, fibre breakage in composite materials will generate a larger amplitude S_0 mode signal. Matrix

cracks often initiate at one of the outer piles, which results in a particle motion which in plane, see Figure 2-15.

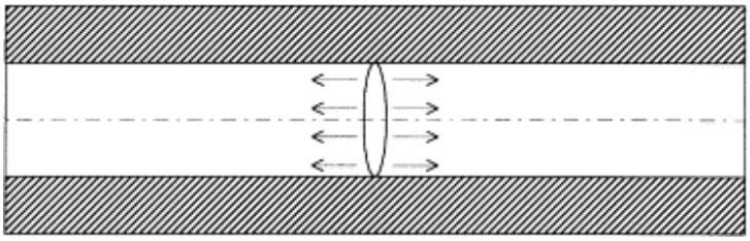

Figure 2-15 Schematic illustration of in plane motion caused by matrix cracking [91]

In this regards, M. Eaton et al. used the MAR analysis on the acoustic emission signals obtained during tensile testing of carbon fibre composite specimen. Results have proven that in-plane matrix cracking generated acoustic emission signals with higher values of MAR; and signals with lower MAR values are considered from out-of-plane sources [92]. A novel form of MAR analysis is proposed by J. McCrory. The modified MAR analysis takes the attenuation effect into account before making the calculation. The amplitude correction process comprises of comparing the maximum amplitude of a particular wave mode to the amplitude of that mode's attenuation curve for the same propagation distance. The result will then input to the equation for the attenuation curve, which is assumed to be able to predict the amplitude of that wave mode at any propagation distance. This process can be carried out for both S_0 and A_0 modes. The amplitude of each mode at the source of the event will be calculated, then the values will be used to calculate the MAR of that acoustic emission event [96].

2.4 Summary

In this chapter, a variety of methods by using acoustic emission signal features to characterize damage mechanisms are reviewed. It has been proved that the PR approach has a distinct advantage over the time/frequency domain features analysis in damage characterization. Micro-fractures generate numerous acoustic emission signals, the characteristics of these acoustic emission signals can be classified by PR approach. However, these acoustic emission signal features are affected by the type of the sensor and the

distance between the source and the sensor. The literature reviewed in this chapter has shown that the above mentioned effects on the PR approach is yet to be analysed.

This work aims to study the above two effects on the acoustic emission signal features, then more importantly on the PR analysis results. The investigation is carried out on laboratory-level studies. Once solve, the challenge is in implementing the PR approach on acoustic emission signals acquired during a large-scale experiment.

3 Finite Element Modelling of Acoustic Emission Signals

3.1 Introduction

Acoustic emission signal features are affected by several parameters including sensor frequency characteristics and the distance of wave propagation from acoustic emission source to the sensor. Therefore in order to interpret the acoustic emission signals' relevance to failure mechanism, the above two challenges need to be carefully investigated separately. In this chapter, the effect of signal detection process by the use of different types of sensors is investigated on the direct acoustic emission waves. In this case, the wave propagation effect can be neglected on the simulated acoustic emission signals.

The direct acoustic emission waves are reproduced using finite element modelling as the results of the interaction of elastic waves radiated by the different fracture modes cracks using commercial software *ABAQUS.* Two fracture modes are taken into account: the opening one (mode I) and the in-plane sliding one (mode II). The source model incorporate different crack sizes for each fracture mode.

The effect of sensor frequency sensitivity on the simulated acoustic emission signals is investigated by applying different types of frequency filters. Comparison is made between the signals from different types of sensors and the simulated signals under corresponding frequency filters.

3.2 Mode I Fracture Simulation

3.2.1 Model setup

Finite element simulation is performed to provide information on the behaviour of the waves emitted from various crack sizes. The basic procedure is shown in Figure 3-1.

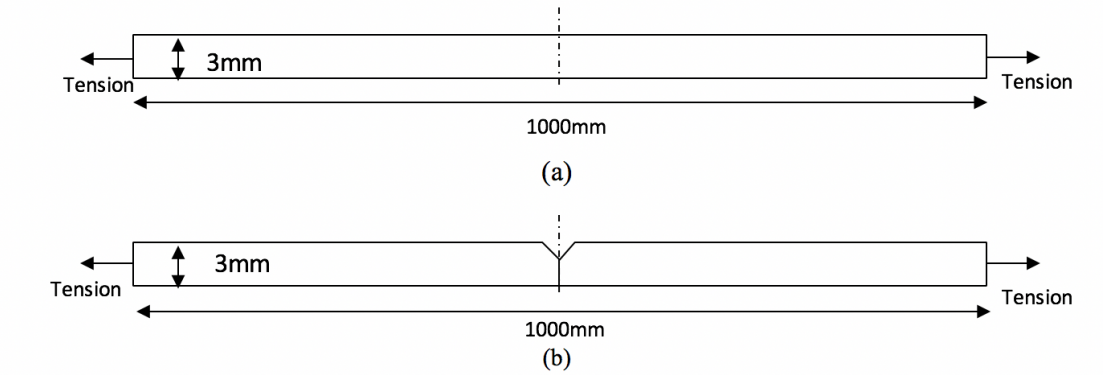

Figure 3-1 Crack through the thickness of the plate (a) before and (b) after the crack growth

The dimension of the plate is 1000mm × 1200 mm × 3mm. The model is based on a steel plate, the material properties are as follows:

$$\mathrm{E} = 200\ \mathrm{Gpa};\ \nu = 0.3;\ \rho = 8000\ \mathrm{kg/m^2}$$

The cracked plate is modelled using linear plane strain elements, with a symmetry at crack location. Due to the symmetry about the crack face, only half of the plate needs to be modelled. A fine mesh is required to capture acoustic emission. The size of one element respects the following criterion:

$$\mathrm{l_e} = \frac{\lambda_{\min}}{\mathrm{R}} \tag{29}$$

$$\lambda_{\min} = \frac{\mathrm{V_{min}}}{\mathrm{f_{max}}} \tag{30}$$

where, $\mathrm{f_{max}}$ is the maximum frequency, which is set as 1MHz, $\lambda_{\min}$ is the minimum wavelength and $\mathrm{l_e}$ is the size of one element, R is the resolution parameter (number of elements per wavelength). The longitudinal wave velocity and shear wave velocity are calculated based on equation (17) and (18):

$$\alpha = \sqrt{\frac{E(1-\nu)}{\rho(1+\nu)(1-2\nu)}} = 5801\ \mathrm{m/s}$$

$$\beta = \sqrt{\frac{E}{2\rho(1+\nu)}} = 3101\ \mathrm{m/s}$$

In order to determine the minimum element size, the smallest velocity ($3101\ \mathrm{m}/s$) and the largest frequency (1MHz) should be used. The number of elements per wavelength, R, is set as 8, which results in the smallest element size needs to be 0.387 mm. Therefore, an element size of 0.1 mm is used. Four crack sizes are investigated:

$$\mathrm{a}_1 = 0.375\ \mathrm{mm};\ \mathrm{a}_2 = 0.75\ \mathrm{mm};\ \mathrm{a}_3 = 1.125\ \mathrm{mm};\ \mathrm{a}_4 = 1.5\ \mathrm{mm}$$

A dynamic model with the crack growth is carried out to measure the acoustic emission. The ABAQUS manual recommends a time increment of less than the minimum element size divided by the longitudinal wave velocity:

$$\Delta t \leq \frac{l_e}{\alpha} \tag{31}$$

The equation above gives a time increment of 66ns, in this work, a time increment of 10 ns is used.

Prior to the dynamic analysis, a static analysis where a tensile load of 150 kN is applied to the un-cracked plate to generate the stress distribution. Then the dynamic analysis is carried out. The reason for the requirement of both static and dynamic models is due to the time increment of the dynamic analysis is limited by the element size, it would take a long time for the stresses to settle to a steady state. Therefore instead, the stress field is calculated using a static analysis, and then imported as a predefined filed in the dynamic analysis. The boundary condition of the crack surface is defined as symmetry in the static analysis. In the dynamic analysis, the boundary condition of the crack surface is deleted. This sudden release of nodes resulted in high frequency components in wave signals.

3.2.2 Simulated Acoustic Emission

The above describe process is accompanied by the radiation of elastic waves, which is known as acoustic emission. The output of acoustic emission is represented in terms of vertical displacement (U2), see Figure 3-2.

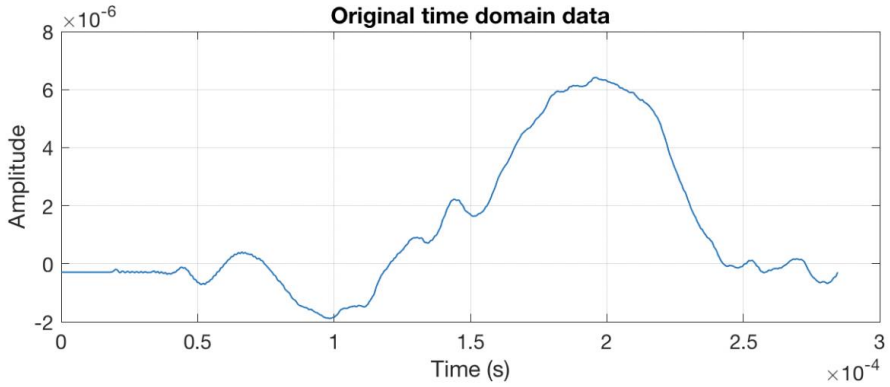

Figure 3-2 Simulated acoustic emission response from crack size 1.5 mm

The crack growth criterion can also be based on the stress state at the crack tip. The stresses in the vicinity of an elastic crack tip are controlled by the stress intensity factor, which depends on the geometry, shape and size of a component, size and location of the flaw and the type of loading. Assumption of linear elastic material behaviour leads to infinite stresses at the crack tip, where non-elastic effects are significant. However, in reality plastic deformation will occur in the crack tip region. The crack tip plastic zone can be determined using yield criteria. When this zone is small enough, Linear Elastic Fracture Mechanics (LEFM) concepts can be used. In these circumstances, the onset of fracture is controlled by the magnitude of the stress intensity factors $\mathrm{K_I}, \mathrm{K_{II}}$ and $\mathrm{K_{III}}$ relating to three different loading modes. In this work, the opening mode $\mathrm{K_I}$ solution is referred to BS7910 - edge flaws in plates solutions:

$$\mathrm{K_I} = (\mathrm{Y}\sigma)\sqrt{\pi \mathrm{a}} \tag{32}$$

where σ is the nominal stress remote from crack, a is half crack length for through-thickness flaw; and Y is the stress intensity correction factor. The details of the formula is detailed in Appendix A. A further static model is built

to calculate the value of stress intensity factor (K_I) from the models using the contour integral. K_I calculated for different crack sizes from modelling and the BS7910 solution is shown in Table 3-1. The results of modelling are consistent with the results calculated according to the BS7910 standard. It is shown that the K_I aggress well with the analytical solution given in BS7910.

Table 3-1 Stress intensity factor vs crack size

Crack Size (mm)	K_I (Modelling)	K_I (BS7910)	% Difference
0.375	1.7469	1.7475	0.03%
0.75	3.0063	3.0432	1.21%
1.125	4.8186	4.9076	1.81%
1.5	7.7934	8.1303	4.14%

3.2.3 Comparison to Experimental Results

3.2.3.1 Experimental Set Up

The experimental work is constructed to allow the mode I crack propagation as acoustic emission sources. A tensile test is carried out on a S355 low carbon steel specimen. Prior to the test a 2 mm depth notch is created in the middle of the specimen, test specimens are manufactured according to the ASTM E8/E8M09 with a length of 450 mm. The dimensions of the dog bone specimen and the manufactured specimens are shown in Figure 3-3.

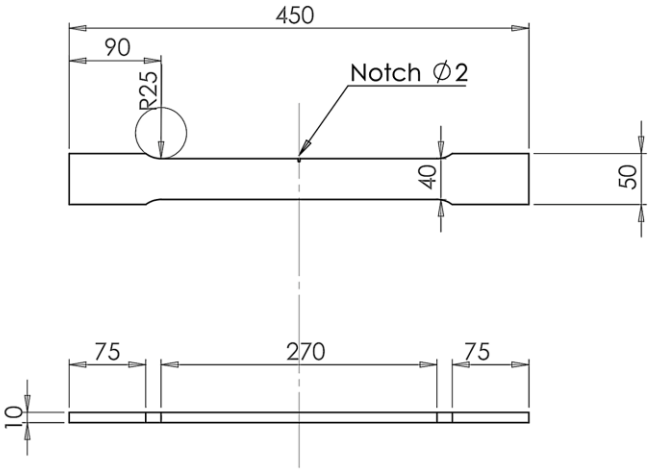

(a)

(b)

Figure 3-3 Tensile test specimens: (a) Specimen dimension details (b) Manufactured specimens

Prior to the test, a 2 mm deep notch is created in the middle of the specimen boundary in order to control the crack initiation and propagation position, see Figure 3-4.

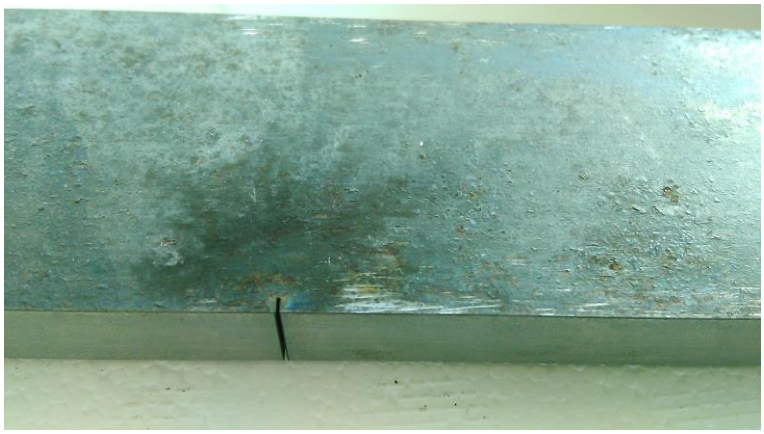

Figure 3-4 Notch in the tensile test specimen

During the test a Vallen AMSY-6 data acquisition system is used to measure the acoustic emission signals. A constant displacement speed of 1mm/min is used throughout the test. The tests are carried out using an Instron machine, see Figure 3-5.

(a)

(b)

Figure 3-5 Tensile test setup (a) Tensile test machine and Vallen system (b) acoustic emission sensors on the specimen

Three different types of acoustic emission sensors are used to compare the signals detected by sensors with different resonant frequencies. The details of the frequency range of the sensors are in Table 3-2.

Table 3-2 The frequency range of acoustic emission sensors

Sensor	Frequency Range
VS900-RIC	100-900 kHz (broad band)
VS150-RIC	100-450 kHz (resonant frequency 150 kHz)
VS375-WIC-01	250-700 kHz (resonant frequency 375 kHz)

VS900-RIC is able to pick up both low frequency and high frequency range signals due to its broad band sensitivity. VS150-RIC and VS375-RIC are resonance type sensors, they are most sensitive at resonant frequencies, the calibration sheet of the sensors can be found in Appendix B. The sensors have built-in preamplifiers, the gain is 34dB, they are mounted on the specimen using magnetic holders with grease applied in between used as couplant. During the test, a digital filter of 95 kHz to 850 kHz is used to filter out the extraneous background noise. The detection parameter is shown in Table 3-3.

Table 3-3 Detection parameter for data acquisition

Detection parameter	Value
Threshold	40 dB
Sampling Rate	5 MHz
HDT	400 μs

3.2.3.2 Results

The comparison is made between the results from the numerical modelling and the corresponding experimental signals. During the experiment, different types of sensors are applied. Since they all have different frequency responses, in order to compare modelling results and experiment results, different filters are applied to the signal resulted from modelling.

The release of nodes result in high frequency components, these high frequency components cannot be modelled accurately due to the number of elements per wavelength is not high enough. Therefore, the high frequency components in the modelled wave signals are filtered by post-processing of the received time-domain signals. First the time domain signal is converted to frequency domain using Fast Fourier Transform (FFT), which is a commonly used tool for obtaining frequency contents of a signal. Then a filter is applied to modify the signal's spectrum, in the end the data is converted back to the time domain. The filter process is shown in Figure 3-6.

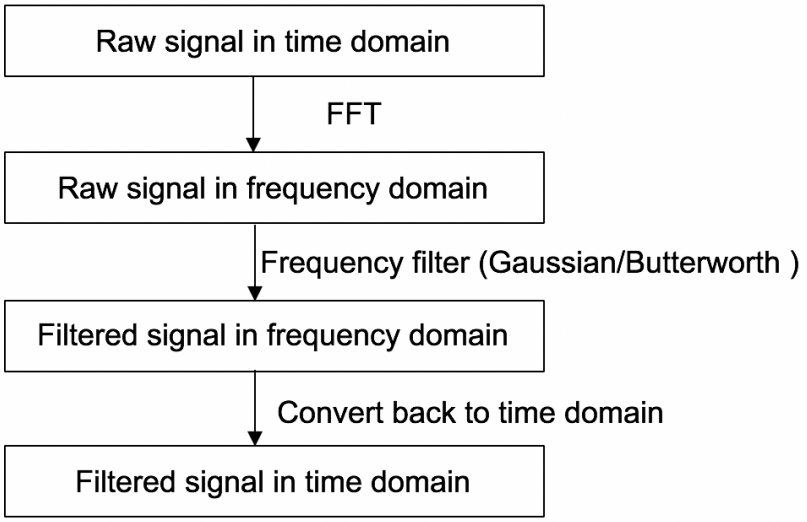

Figure 3-6 Data filtering process

In order to investigate on the effect of sensor frequency sensitivity on the simulated acoustic emission signals, different types of filters are applied on the signal resulted from modelling. Three different filters are applied on the signals from modelling:

1. The applied Gaussian filter is with a centre frequency of 150 kHz and a bandwidth of 250 kHz. The signal resulted from modelling with the above filter applied is compared with the signal acquired by VS150-RIC (100 kHz – 400 kHz).

   Figure 3-7 (a) shows the resulted time domain signal with the Gaussian filter applied on the original acoustic emission response from crack size 1.5 mm. Figure 3-7 (b) shows a typical recorded signal from VS150-RIC sensor.

   Figure 3-8 shows the spectrums of the filtered simulated signal and signal acquired by VS150-RIC. It can be observed that the spectrum of the signal acquired by VS150-RIC has a dominant frequency of 150 kHz. While for the spectrum of the filtered simulated signal, there isn't a clear dominant frequency. By applying a centre frequency of 150 kHz and a bandwidth of 250 kHz, the resulted frequency spectrum is

essentially limited to the centre frequency 150 kHz plus and minus bandwidth. Therefore for the filtered simulated signal, the frequency responses from 0 kHz to 400 kHz. The domain frequency has a range from 50 kHz to 150 kHz. Whereas for the signal acquired by VS150-RIC, according to the datasheet (see Appendix A), the frequency range of VS150-RIC is from 100 kHz to 450 kHz, the low frequency components are not acquired.

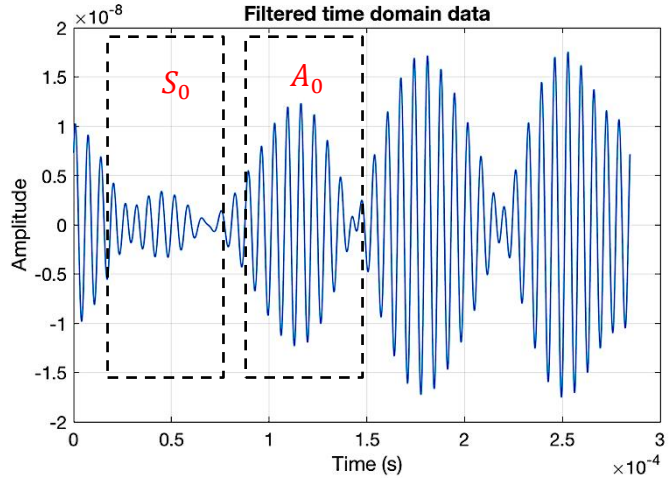

(a)

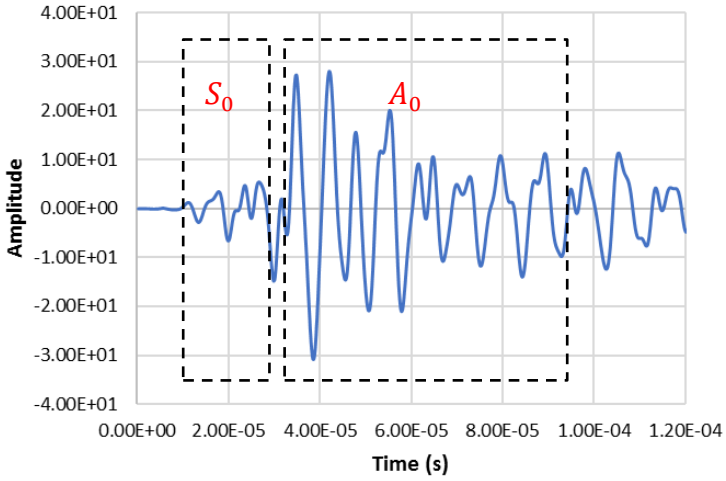

(b)

Figure 3-7 Time domain (a) simulated filtered acoustic emission signal showing distinct S_0 and A_0 wave modes (b) experimental acoustic emission signal recorded from VS150-RIC

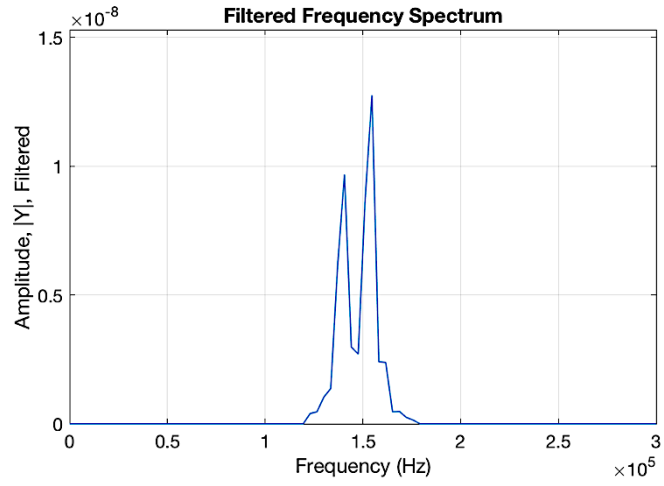

(a)

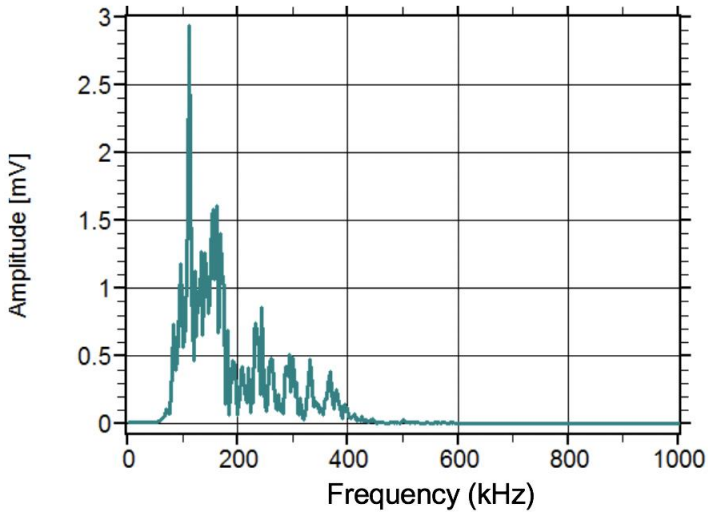

(b)

Figure 3-8 Frequency domain (a) applied with Gaussian window (central frequency 150 kHz, bandwidth 250 kHz) on the simulated signal (b) experimental signal recorded from VS150-RIC

2. A Gaussian filter with a centre frequency of 375 kHz and a bandwidth of 325 kHz is applied, the signal from modelling with this filter applied is compared with the signal acquired by VS375-WIC (50 kHz – 700 kHz).

   Figure 3-9 (a) shows the resulted time domain signal with the above Gaussian window applied on the original acoustic emission response from crack size 1.5 mm. Figure 3-9 (b) shows a typical recorded signal from VS375-WIC sensor.

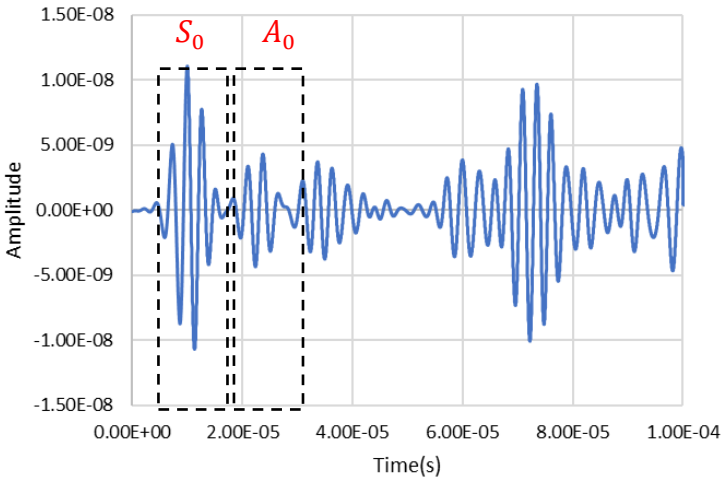

(a)

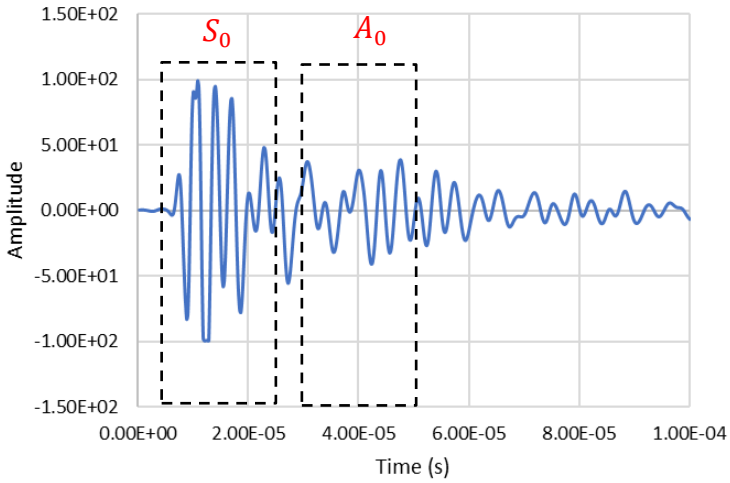

(b)

Figure 3-9 Time domain (a) simulated filtered time domain signal with Gaussian filter (central frequency 375 kHz, bandwidth 325 kHz) (b) experimental acoustic emission signal recorded from VS375-WIC

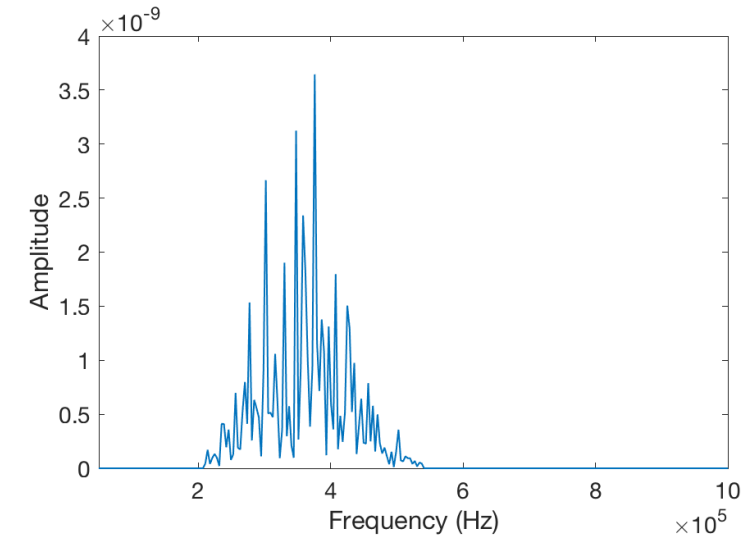

(a)

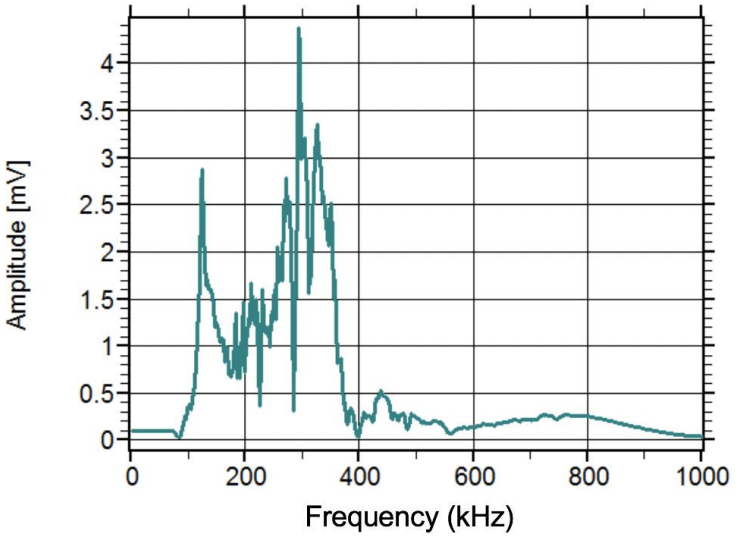

(b)

Figure 3-10 Frequency domain (a) applied with Gaussian window (central frequency 375 kHz, bandwidth 325 kHz) on simulated signal (b) experimental signal recorded from VS375-WIC

3. A Butterworth band pass filter range from 100 kHz to 900 kHz is applied, the signal resulted from modelling with this filter applied is compared with the signal acquired by VS900-RIC (100 kHz – 900 kHz).

   Figure 3-11 (a) shows the resulted time domain signal with the above Butterworth applied on the original acoustic emission response from crack size 1.5 mm. Figure 3-11 (b) shows a typical recorded signal from VS900-RIC sensor.

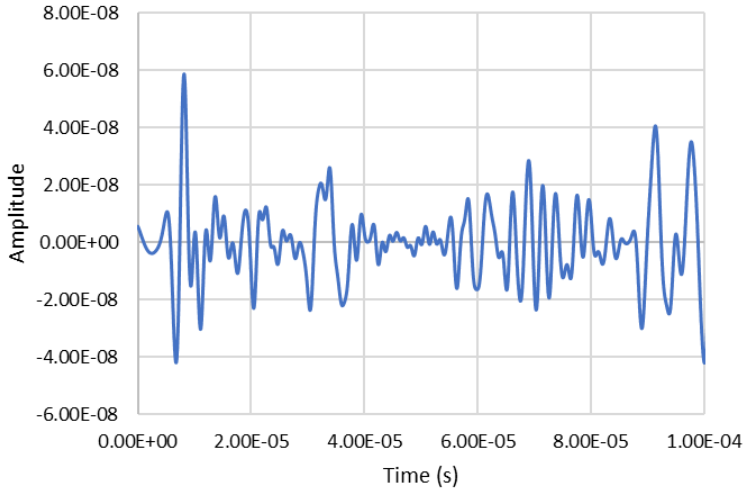

(a)

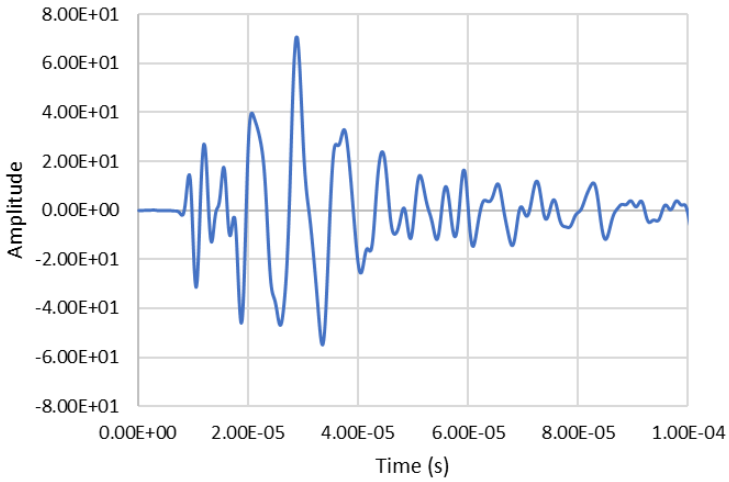

(b)

Figure 3-11 Time domain signal (a) simulated filtered time domain signal with Butterworth filter (100 – 900 kHz) (b)experimental acoustic emission signal recorded from VS900-RIC

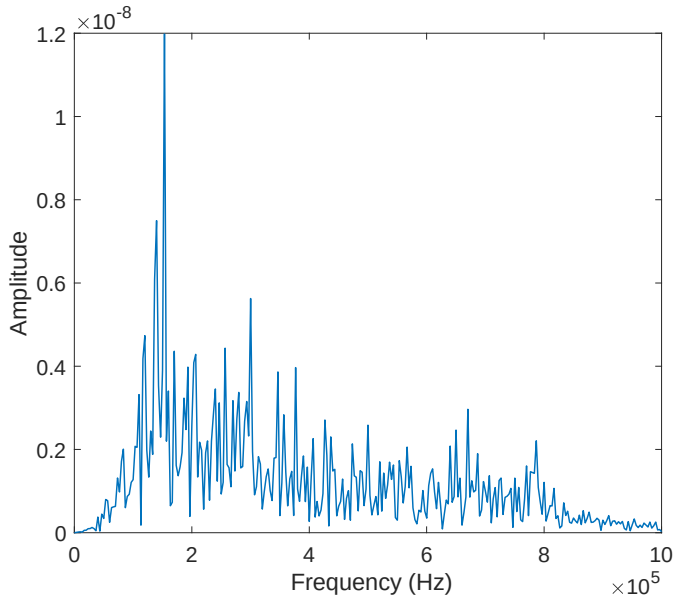

(a)

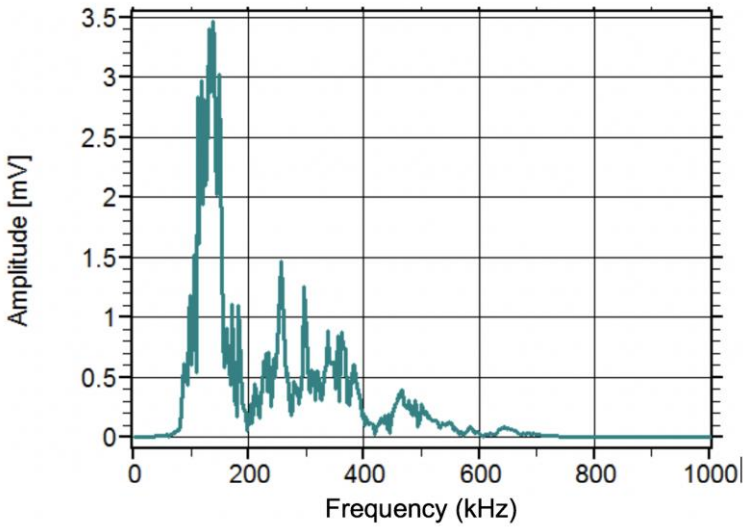

(b)

Figure 3-12 Frequency domain (a) applied with Butterworth filter (range from 100 - 900 kHz) on simulated signal (b) experimental signal recorded from VS900-RIC

It is clearly shown that that different frequency filters will result in different amplitudes of signals, which therefore will have an influence on the signal features. The quantitative analysis on the sensor effect on the acoustic emission signals from fracture is discussed in chapter 4.

It is shown that the signals obtained from the sensors agree well with the filtered signals from the modelling. For the case of frequency filter 1 and 2,

distinct S_0 and A_0 wave modes are shown in both modelling results and experimental results. For the signal from VS150-RIC and the filtered signal, see Figure 3-7, the signals show a lower amplitude of S_0 wave mode. However, for the signal from VS375-WIC, it show a higher amplitude of S_0 wave mode.

Through the above investigation, It is concluded that the sensor's sensitivity has an influence on the amplitudes of the simulated acoustic emission wave modes. Therefore, when applying modal acoustic emission analysis to distinguish different damage modes, the acoustic emission signals need to come from the same sensor and it is suggested to apply other techniques to examine the results.

In order to investigate on the relationship between the crack size and the resulted acoustic emission signals. The amplitude of the S_0 and A_0 wave modes from different crack sizes through the plate is plotted in Figure 3-13. The amplitudes of the S_0 and A_0 are based on the signal filtered by filter 1 (Gaussian window, central frequency 150 kHz, band pass 250 kHz). It shows that the amplitude of S_0 and A_0 increases with the bigger crack sizes.

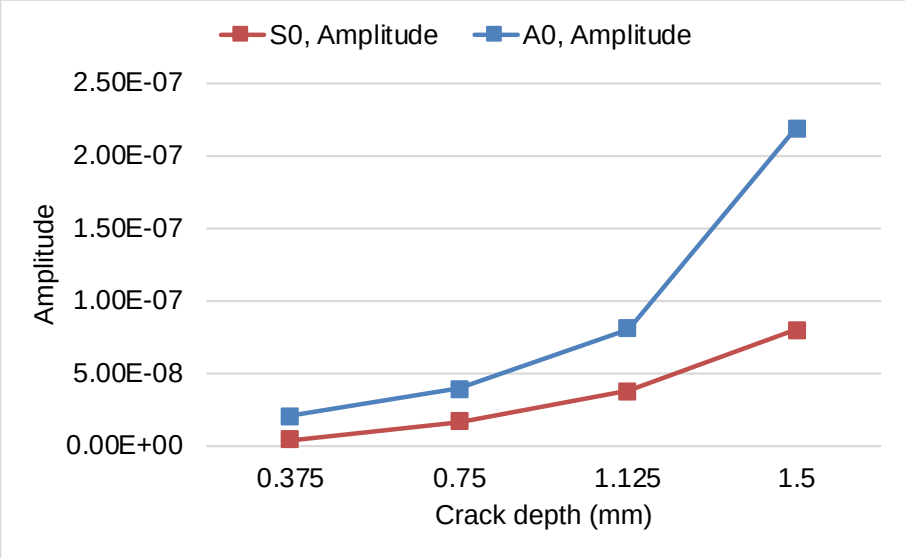

Figure 3-13 Simulation result - amplitude of S_0 and A_0 from different crack sizes

3.3 Mode II Fracture Simulation

3.3.1 Model setup

The geometry of the model chosen for this investigation is a 0.25 m × 0.25 m steel plate. For mode II fracture, the crack growth is simulated by artificially deleting elements by reducing the stiffness (Young's modulus) to around 0. The implementation is achieved by defining temperature-dependent material properties, see Table 3-4. Then crack growth is defined by assigning instantaneous temperature change over crack growth increment which is used as arbitrary variable to change stiffness over time. The model is developed assuming plane stress conditions (plane stress elements).

Table 3-4 Temperature dependent material properties

Young's modulus (Pa)	Poisson's ratio	Temperature (°C)
200e9	0.3	20
20	0.3	0

The basic procedure of modelling is shown in Figure 3-14. First the model is subjected to a static 100 kN traction load which is applied on the right surface, the left surface of the model is fixed. Then the crack growth is simulated by assigning instantaneous temperature to 0°C to change stiffness. This instantaneous change causes wave excitation. The larger crack size of crack growth 2 and 3 is simulated in the same way by applying the condition on the crack growth surface.

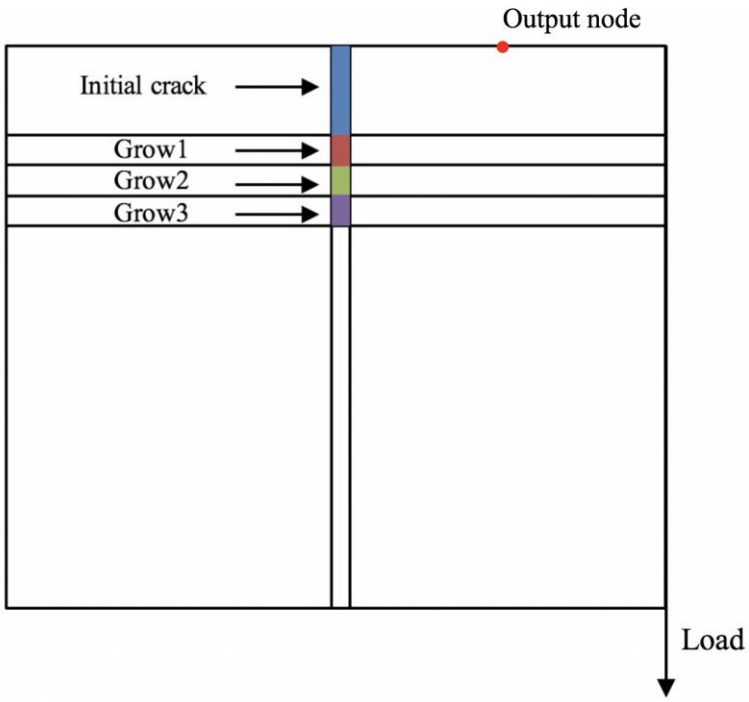

Figure 3-14 Mode II crack growth in a steel plate

The element size is calculated to be 0.1mm, and a time step of 10 ns is used. The calculations are based on the same methodology as explained in 3.2.1. Three different crack growths of 0.025 mm, 0.030 mm, and 0.035 mm are simulated.

3.3.2 Simulated Acoustic Emission

In the following, the results of the above model computation are presented. The history output from the output point is shown in Figure 3-15.

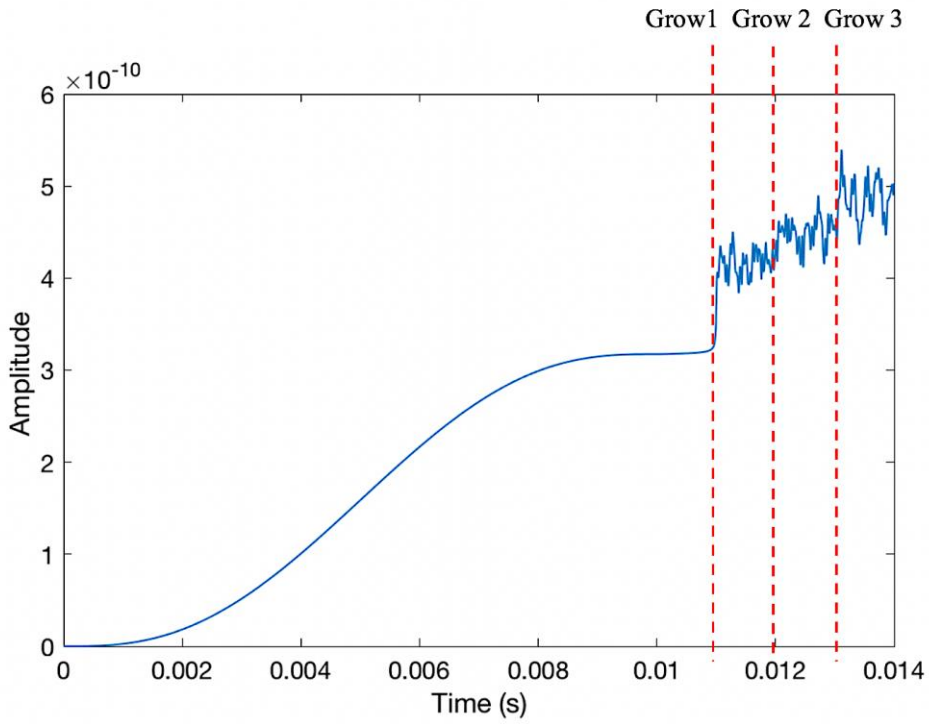

Figure 3-15 Simulated signal from output node

It is shown that there are elastic waves generated as cracks released. The amplitude of the signals increases as crack grows. The frequency responses of the cracks are investigated, see Figure 3-16. It is shown that the amplitude of the low frequency components increase as the crack grows.

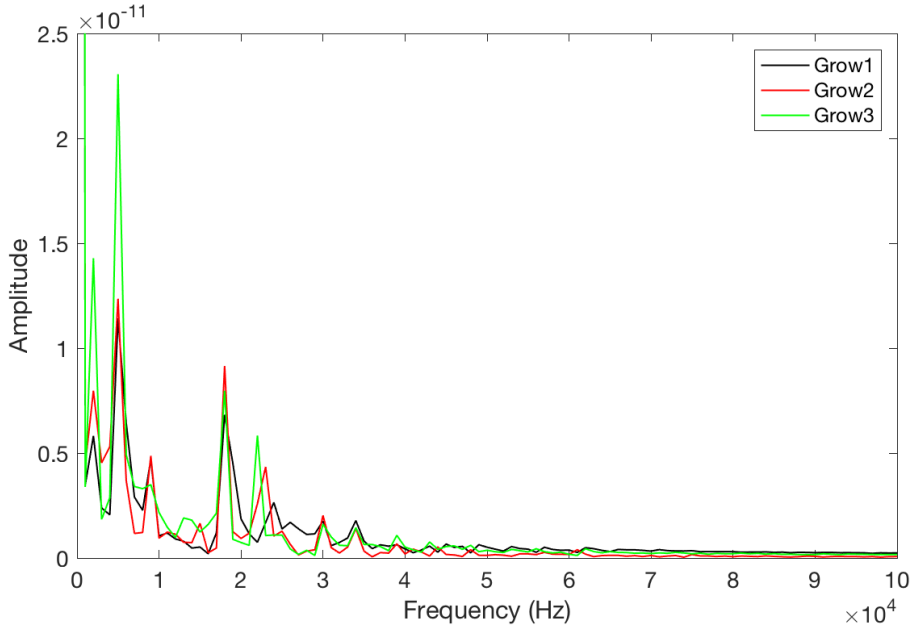

Figure 3-16 Simulated signal frequency response from the crack growth

3.4 Conclusions

The acoustic emission waves are reproduced using finite element modelling as the results of the interaction of elastic waves radiated by fracture mode I and mode II cracks. The source model incorporate different crack sizes for each fracture mode. The amplitude of the generated signals increases as the crack grows for both cases.

Acoustic emission signals generated by the mode I are validated against signals acquired during a tensile test on carbon steel specimen. Three acoustic emission sensors with different frequency ranges are used during the test. To compare, three different frequency filters which correspond to the frequency range of the sensors used during the experiment are applied on the signals generated from the modelling. The results show a good agreement between the modelling results and the experimental results for all three different scenarios.

Moreover, the effect of sensor frequency sensitivity on the acoustic emission signals is also investigated on the signals generated from the modelling. The results are compared with the signals obtained from three different sensors. It is shown that different frequency filters applied on the original acoustic emission signals result in different amplitudes of acoustic emission signals, this will thus have an impact on the values of the signal features.

Results also show that the amount of energy carried by S_0 and A_0 wave modes and therefore their amplitudes depends strongly on the sensor's frequency range. Therefore, when applying modal acoustic emission analysis to distinguish different damage modes, the acoustic emission signals need to come from the same sensor and it is suggested to apply other techniques to examine the results.

4 Influence of Sensor Sensitivity on Acoustic Emission Signals

4.1 Introduction

In chapter 2, it is explained that the source characterization methods are generally achieved by correlating the acoustic emission signal features with a particular damage mechanism. Sensor frequency characteristics have an effect on the acoustic emission signal features. This effect is investigated in chapter 3 on the simulated acoustic emission waves. In this chapter, this effect is investigated on acoustic emission signals from lab based experiments carried out on both metal and composite materials. During the test, different types of sensors are used.

First, variations in acoustic emission signal features of the signals obtained from different sensors are analysed during tensile tests carried out on carbon steel and CFRP specimens. The aim is to investigate the acoustic emission response from damage mechanisms in metals and composite materials.

The second objective of this chapter is to quantify the characteristics of the acoustic emission signals from plastic deformation. First, several acoustic emission signal features (including time domain features and frequency domain features) are being investigated by plotting with respect to load-displacement curve. The acoustic emission signals are synchronized with the load-displacement curve, therefore the signatures of acoustic emission signal features from plastic deformation can be identified.

Finally in this chapter, an effective pattern recognition approach is developed to identify the plastic deformation. Through this approach, a novel feature selection algorithm is proposed. The developed pattern recognition algorithm is applied on the signals obtained from different sensors.

4.2 Tensile Test on Carbon Steel

4.2.1 Materials and Specimens

Carbon steel is a steel with carbon content up to 2.1 %, it is widely used in construction, manufacturing and offshore industries. It is essential to thoroughly and effectively monitor the defects in carbon steel structures.

The acoustic emission sources in carbon steel are closely associated with the dislocation movement accompanying plastic deformation and the crack initiation and growth. To monitor acoustic emission events generated from plastic deformation, tensile tests on notched S355 carbon steel specimens are carried out. During which three different types of sensors are used. The detail of the testing specimens is described in 3.2.3.

4.2.2 Experimental Procedure

Two different loading settings are applied during the test. For the first test, the specimen is following a few loading – unloading steps. During the loading – unloading process, a constant displacement speed of 1mm/min is used. For the second specimen, a regular tensile test is carried out with constant displacement speed of 1mm/min throughout the test.

4.2.3 Results and Discussion

4.2.3.1 Felicity Ratio Analysis to Monitor Progressive Damage

In this section, Kaiser effect and Felicity effect are investigated on the signals obtained by different sensors. Knowledge of these two effects can be used to determine if major structural defects are present. Influenced by the materials and stress level, the Kaiser effect does not always apply. On the contrary, another phenomenon which describes the presence of significant acoustic emission events that begin to increase significantly at stress levels below those previously applied is introduced, it is called the Felicity effect. The analytical parameter that qualifies the Felicity effect is known as Felicity ratio which is given by:

$$\mathrm{FR} = \frac{\mathrm{P}_{\mathrm{AE_i}}}{\mathrm{P}_{\mathrm{max}_{(\mathrm{i}-1)}}} \tag{33}$$

where P_{AE_i} is the stress level when acoustic emission events begin to increase significantly in the ith loading-unloading cycle, and $P_{max_{(i-1)}}$ is the maximum stress level in the $(i-1)$th loading - unloading cycle, see Figure 4-1. The Felicity ratio is a description to irreversibility of the acoustic emission process of materials and can reflect the severity of original damages, and therefore has become an important evaluation index of defect severity. When $FR < 1$, it is often an indication of the significant accumulated damage in the structure [97].

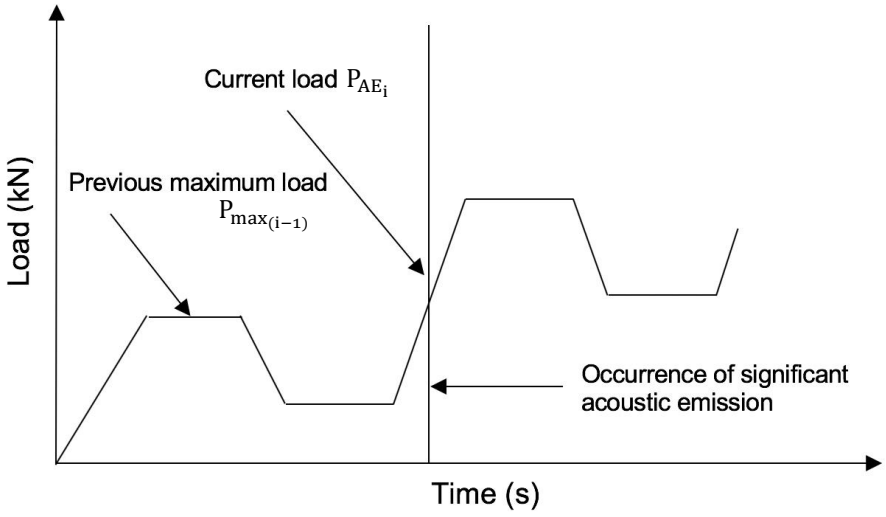

Figure 4-1 Example calculation of the Felicity ratio

Determining the stress level when acoustic emission events begin to increase significantly in the loading process is the key to obtain the Felicity ratio. However there is no agreed standard on using one specific acoustic emission signal feature to determine the “sharp” increase point. Several researchers used the acoustic emission signal feature, number of counts, correlating with the stress level to demonstrate Felicity effect and calculate Felicity ratio successfully [98], [99], [100]. I. Stavrakas determined the stress level using number of hits during the compression tests of Dionysos marble [101].

Another parameter which can lead to a false determination of the stress level is the existence of acoustic emission signals generated from noise. During the tensile test, the noise sources include environment noise and the friction noises from jaws holding the specimen. Therefore, background noise filtering is performed before Felicity ratio calculation in this work:

First, in order to eliminate these unwanted signals from the environment noise, the signals with fewer than 3 counts and of duration less than 3 μs are discarded [102].

Secondly, the left acoustic emission signals are examined using source location method. All the events that are located outside the gauge length are considered as acoustic emission events generated from grip noise. Therefore the signals generated from those events are discarded.

After the noise filtering method has applied, the rest of the acoustic emission signals were considered generated from defect growth related sources. A comparison is made between the signals before (left) and after the above filter (right), see Figure 4-2. As the acoustic emission signals from the noise is filtered out, therefore the figures on the right side have less events. It can be observed that a small number of acoustic emission events were generated during the elastic stage, when the load drops, almost no events happen, however, when it passes the previous maximum loading, a significant number of acoustic emission events happen, the same trend happens to the next three cycles of loading – unloading. This behaviour is following the Felicity effect.

The signals are represented with the number of counts. It can be seen that the acoustic emission signals from the noise generally have a lower value of number of counts.

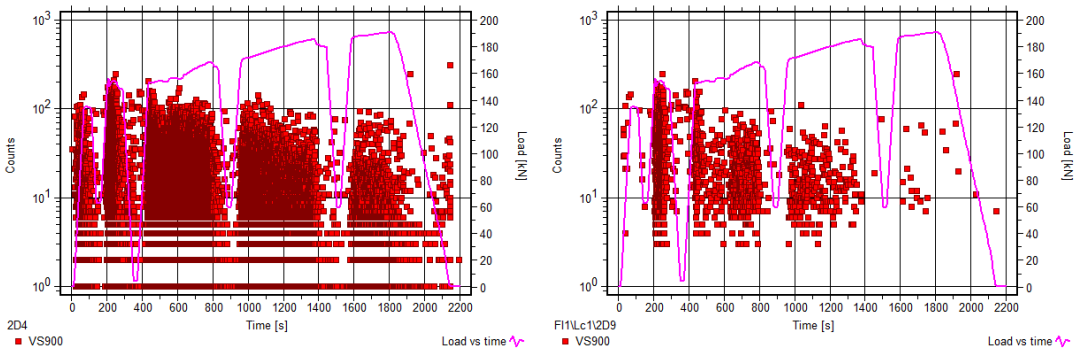

(a)

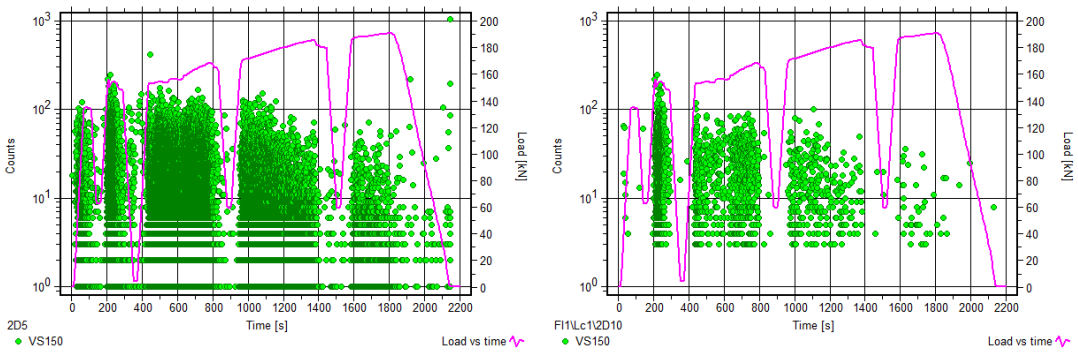

(b)

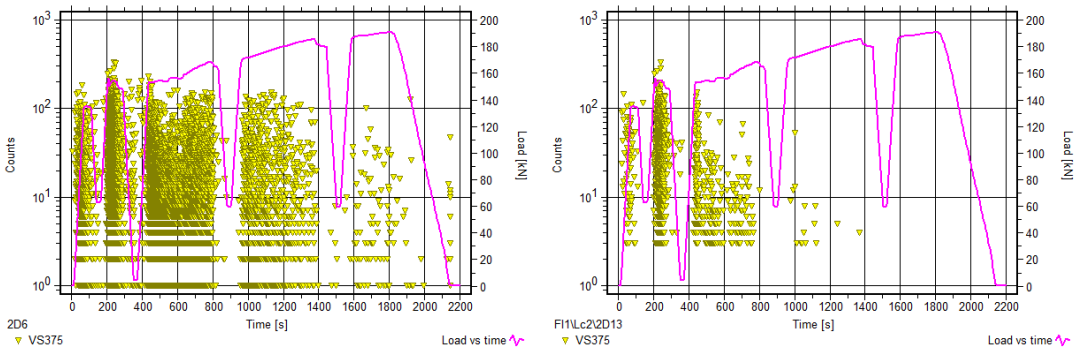

(c)

Figure 4-2 Number of counts distribution for raw data (left) and filtered data (right) of (a) VS900-RIC (b) VS150-RIC (c) VS375-WIC

In order to calculate the Felicity ratio, a 'significant' increase of acoustic emission event growth needs to be identified. ASTM provides sensor-placement and guideline for a composite tanks and vessels:

12.2.2.2 More than $N_c/25$ counts during a 10% increase in load.

Therefore the cumulative number of counts of the three sensors are plotted to determine the "sharp" increase point for the stress level identification.

Four loading-unloading cycles are applied during the test: the first cycle is in the elastic stage, the rest three cycles are in plastic deformation stage. The Felicity ratio for all four cycles is investigated for the signals acquired by three different sensors. The cumulative number of counts history is plotted on the same plot the loading history, see Figure 4-3. The results of the felicity ratio calculations are shown in Table 4-1.

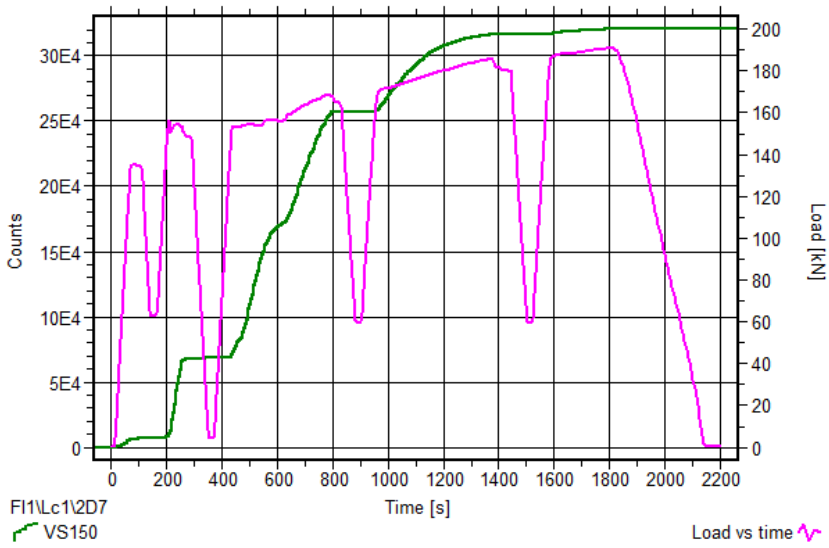
Counts
Load [kN]
Time [s]
FI1\Lc1\2D7
VS150
Load vs time

(a)

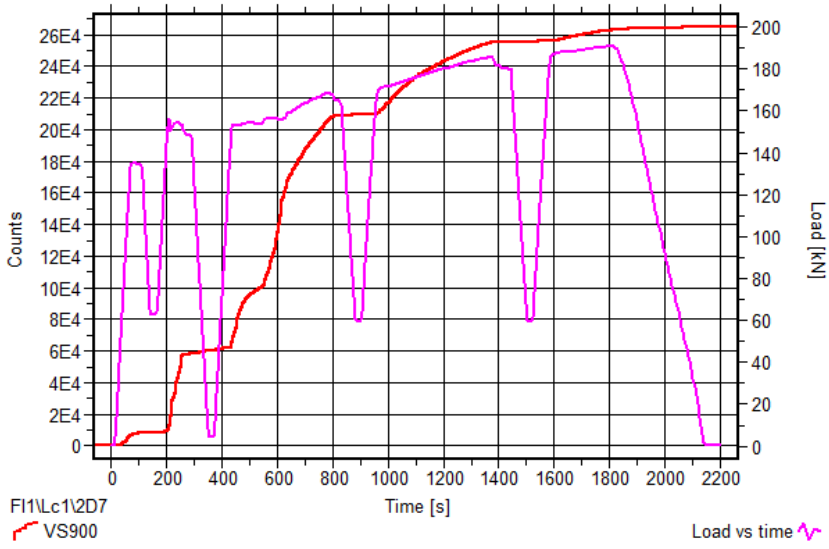
Counts
Load [kN]
Time [s]
FI1\Lc1\2D7
VS900
Load vs time

(b)

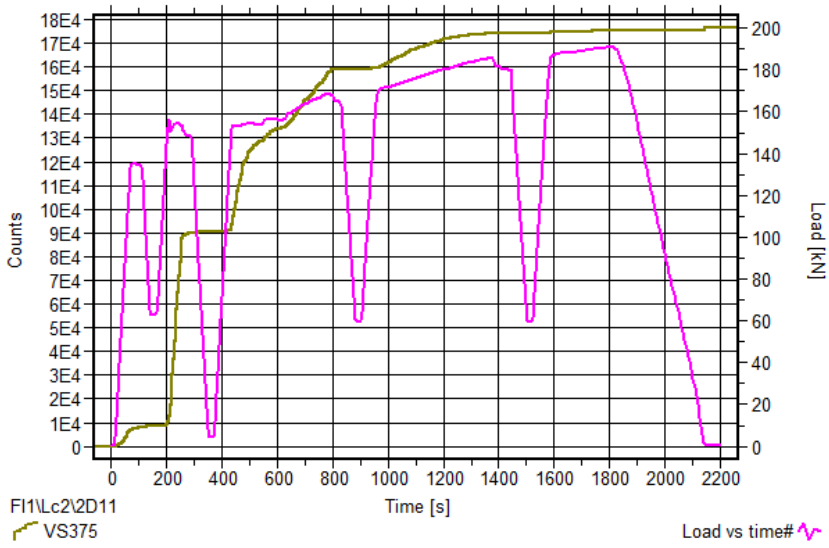
Counts
Load [kN]
Time [s]
FI1\Lc2\2D11
VS375
Load vs time#

(c)

Figure 4-3 Cumulative number of counts vs Loading path for (a) VS150-RIC (b) VS900-RIC (c) VS375-WIC

Table 4-1 Felicity ratio for four cycles during the test

Sensor	Cycle			
	1	2	3	4
VS150-RIC	1.05	0.91	0.89	0.96
VS900-RIC	1.06	0.34	0.96	1.01
VS375-WIC	1.05	0.82	1.01	N/A

Carbon steel materials have presented different phenomena in different stages. During the elastic stage, Kaiser effect is observed by all three different sensors, as the acoustic emission didn't start to accumulate when the load exceeds the previous maximum load, this is represented by $\mathrm{FR} > 1$. After the yielding happens, the Felicity effect is observed.

J. M. Waller et al. found that Felicity ratio decreases with the increasing stress in during the damage accumulation test in composite materials [103]. However, this phenomenon is not observed for this test. For all three sensors, the Felicity effects are clearly observed when plastic deformation starts, however the value of Felicity ratio in the later plastic deformation stage is even bigger than the earlier plastic deformation stage. For the VS375-WIC, there are no events captured in the fourth cycle, this could be due to the high resonant frequency of the sensors, it is not able to pick up the low frequency acoustic emission events. The above proved that using Felicity ratio value to indicate the severe damage in carbon steel is not a very reliable method. Therefore, further investigation on other methods using acoustic emission signals to indicate plastic deformation is carried out.

4.2.3.2 Plastic Deformation Detection Using Acoustic Emission Signal Features

In this section, the identification of plastic deformation is achieved by looking at the acoustic emission signal features. The data processing is focusing on the data obtained from the test on the second specimen, which is being applied a constant displacement-speed loading control until fracture happens.

For the second specimen, the load and displacement data, which is synchronized with the acoustic emission system, is recorded during the test, see Figure 4-4. Beyond the elastic limit, yielding occurs, there will be thus permanent deformation. After the upper and lower yield point, the specimen is in uniform plastic deformation stage. A further increase in the load will lead the specimen to fracture, which will cause an accident. Therefore it is very important to detect the yielding and plastic deformation when it happens.

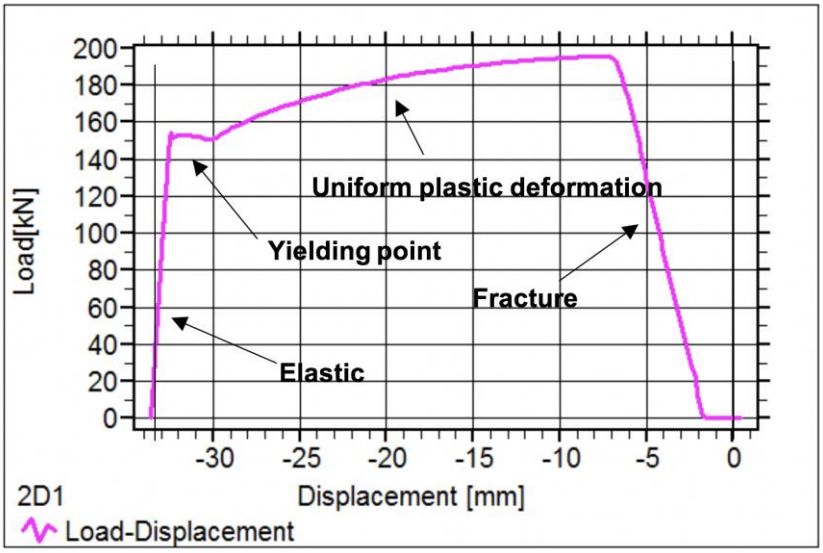

Figure 4-4 Load vs displacement curve

Identifying plastic deformation using cumulative trends of acoustic emission signal features

There exists a correspondence between the obtained acoustic emission signal features and the dislocation activities in different stages. A graph of cumulative number of hits and energy is plotted against the load-displacement curve. Both the cumulative number of hits and cumulative energy increased rapidly at the beginning of the plastic deformation, see Figure 4-5. This trend is same for the signals from all three different sensors. The reason is due to that the main acoustic emission events are generated from massive dislocation activities in grain boundaries during the deformation process, the first dislocation activities take place at the yielding stage, intensive increasing of dislocation activities is observed, which is when plastic deformation begins. Then the number of

events reduced at the later stage of uniform plastic deformation which is due to the reduction of dislocation activities [104].

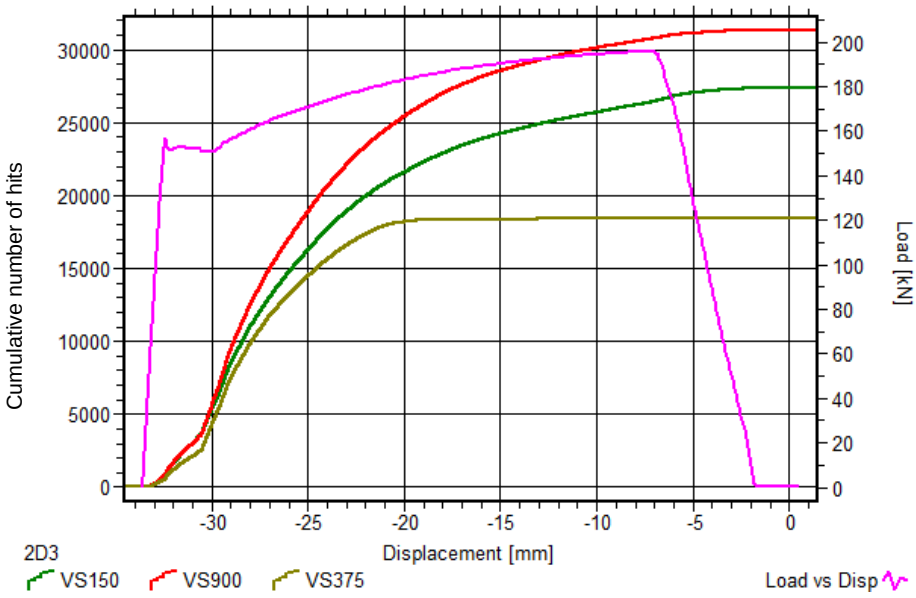

(a)

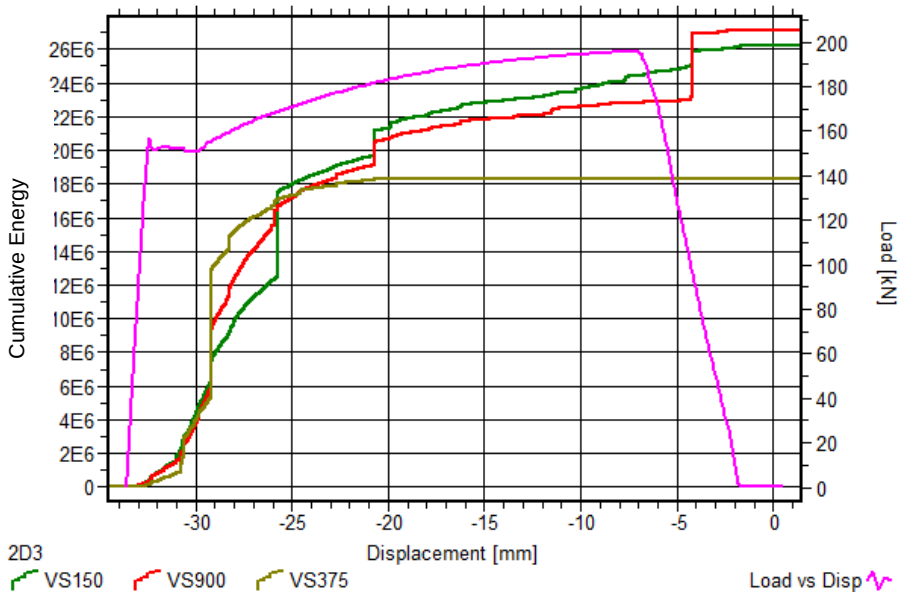

(b)

Figure 4-5 (a) Cumulative number of Hits (b) Cumulative energy

Identifying plastic deformation using acoustic emission signal frequency domain features

The total number of events acquired by three different sensors are 31,366 (VS900-RIC), 27,404 (VS150-RIC) and VS375-WIC (18,443) respectively. The resonant sensor VS375-WIC acquired much less acoustic emission

events in comparison with VS150-RIC and VS900-RIC. Especially after the unique plastic deformation begins, there are almost no events captured. This indicates that during the test, the frequency range of generated acoustic emission signals are concentrated in low (20 kHz – 100 kHz) and standard (100 kHz – 400 kHz) frequency range.

Referring to the results, the broad band sensor, VS900-RIC acquires more acoustic emission events than the resonant sensor VS150-RIC. This can be because the broad band sensor combine a good response from the standard to the high frequency range, therefore a lot of events which are not in the frequency range of the resonant sensors are captured by the broadband sensors. In order to prove this, the frequency ranges of the acquired signals are analysed. In order to access the frequency information of the obtained signals, FFT analysis is carried out. Peak frequency in the spectrum can be attributed to the predominant in the specimen, therefore it has been studied for all sensors. The peak frequency of the signals are classified into three frequency regimes including low (20 kHz – 100 kHz), standard (100 kHz – 400 kHz) and high (>400 kHz). The number of events captured by each sensor for these three regimes are presented in Table 4-2.

Table 4-2 Cumulative number of hits acquired by VS900-RIC, VS150-RIC, and VS375-WIC for three different frequency regimes

Frequency regime	Cumulative number of hits		
	VS900-RIC	VS150-RIC	VS375-WIC
20 kHz – 100 kHz	98	315	0
100 kHz – 400 kHz	28,484	27089	18,306
>400 kHz	2782	0	137

It can be observed that there are acoustic emission signals of peak frequency range above 400 kHz for the broad band sensor VS900-RIC, and not for the resonant sensor VS150-RIC. This explains the fact that the broadband senor VS900-RIC captures the most number of acoustic emission signals.

The peak frequency of acoustic emission signals from different stages is then compared with the load-displacement curve. M. Akbari et al. compared the acoustic emission signals during tensile deformation of notched and

unnotched specimens, the sensor used is with a resonant frequency at 125 kHz. It is found that high peak frequency signals are associated with plastic deformation in unnotched specimen, whereas peak frequencies are scattered during test for the notched specimen [105]. This doesn't agree with our results for the notched specimen, as the for VS150-RIC and VS900-RIC, high peak frequency signals (> 350 kHz for VS150-RIC, > 600 kHz for VS900-RIC) are only generated when yielding started, whereas the peak frequency of the signals acquired by VS375-WIC are scattered during the test, see Figure 4-6.

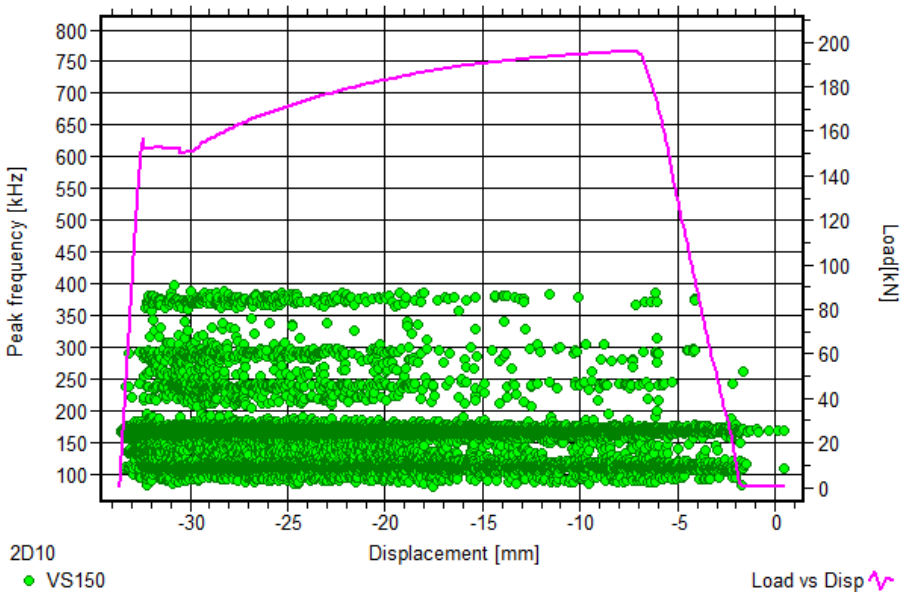

(a)

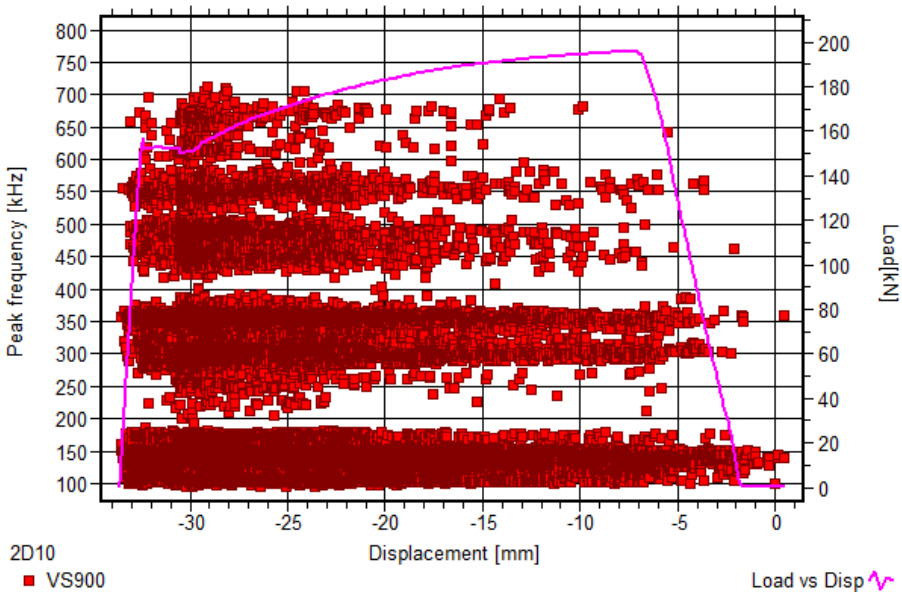

(b)

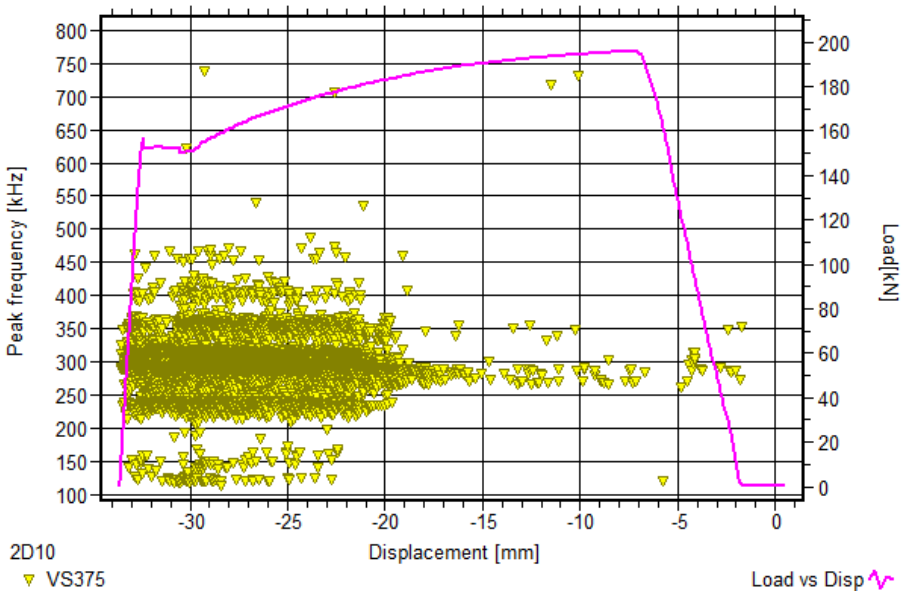

(c)

Figure 4-6 Peak frequency distribution of signals acquired by (a) VS150-RIC (b)VS900-RIC (c)VS375-WIC

FFT result shows that both broadband sensor VS900-RIC and low resonant frequency sensor VS150-RIC have characteristic frequencies when plastic deformation begins. However this phenomenon is not clearly revealed by the high resonant frequency sensor VS375-WIC. An example of the signals acquired by each sensor is shown in Figure 4-7.

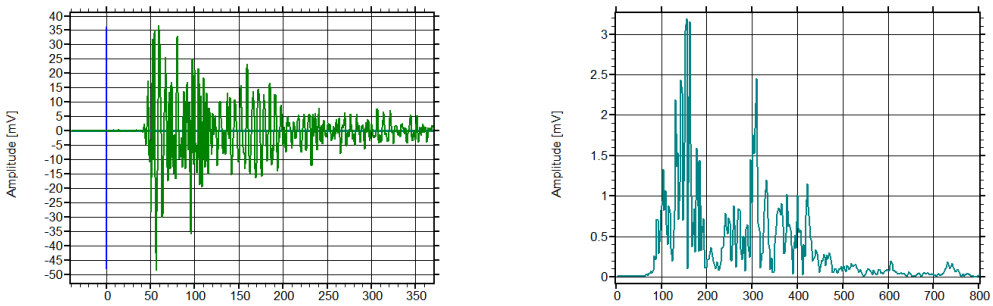

(a) Time domain (left) and frequency domain of signal acquired by VS150-RIC

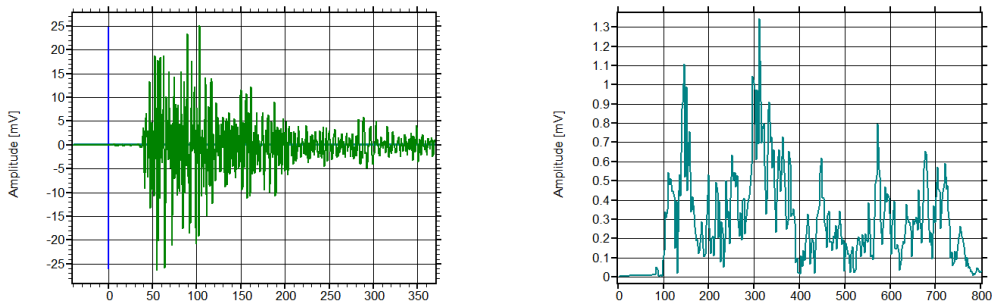

(b) Time domain (left) and frequency domain of signal acquired by VS900-RIC

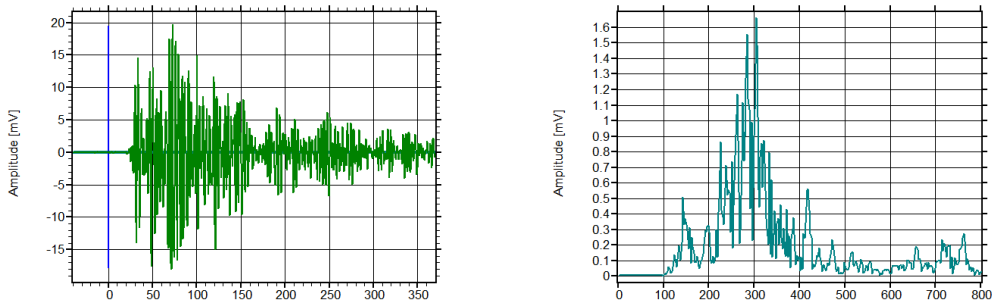

(c) Time domain (left) and frequency domain of signal acquired by VS375-RIC

Figure 4-7 Represented signals acquired by VS150, VS900 and VS375 respectively.

Identifying plastic deformation using acoustic emission signal time domain features

The identification of plastic deformation is also investigated using acoustic emission time domain features. The influence of sensor frequency characteristics on acoustic emission time domain features is also analysed. S. Schnabel et al. found that the peak amplitude of acoustic emission signals increased after passing the yielding stress [106]. The same phenomenon is observed in this test.

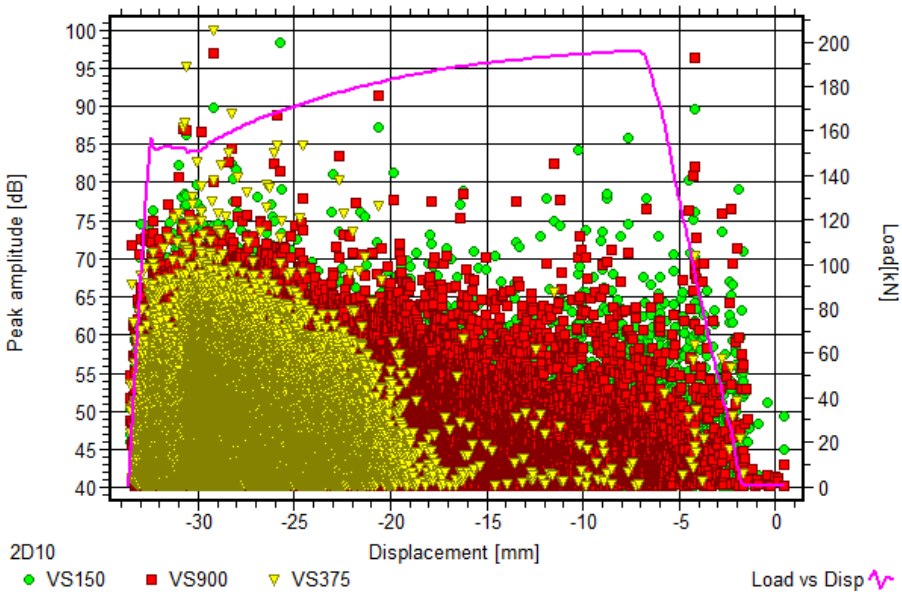

Figure 4-8 showed the high peak amplitude events (>75dB) only occurred after the yielding started. High peak amplitude acoustic emission signal is often a sign of high energy, therefore, the energy distribution for three sensors is investigated.

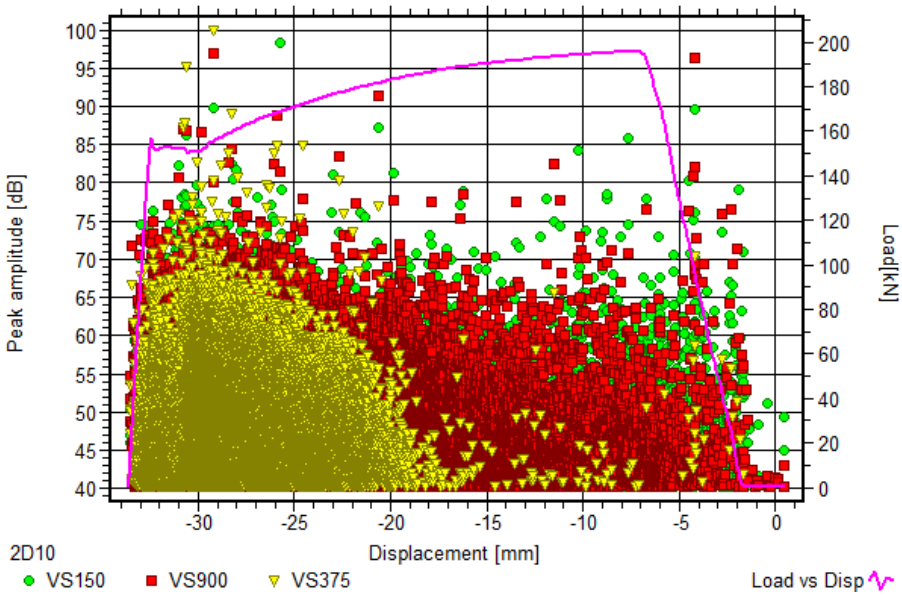

Figure 4-8 Peak amplitude distribution over the load-displacement curve for different sensors

Through the investigation in the material uniform plastic deformation region, it is found that the energy of the acoustic emission signals generated during the plastic deformation stage are significantly increased. This is the same for

signals acquired by all three sensors, see Figure 4-9. This is because that during the yielding stage, new dislocations are generated and slip bands are spread, which will generate acoustic emission events with high energy. These events result in high energy signals. R. Kocich et al. also found there is a significant activity of acoustic emission signals with high energy after the yielding point during the tensile tests on Mg alloys and low carbon steel [107]. In the last stage of the uniform deformation, the energy of acoustic emission events decrease due to the reduction of dislocation activities.

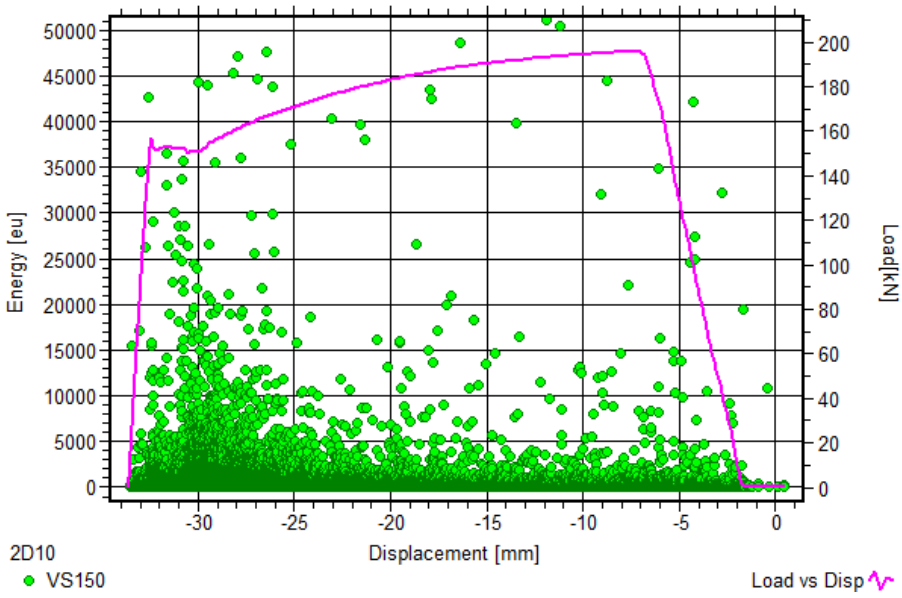

(a)

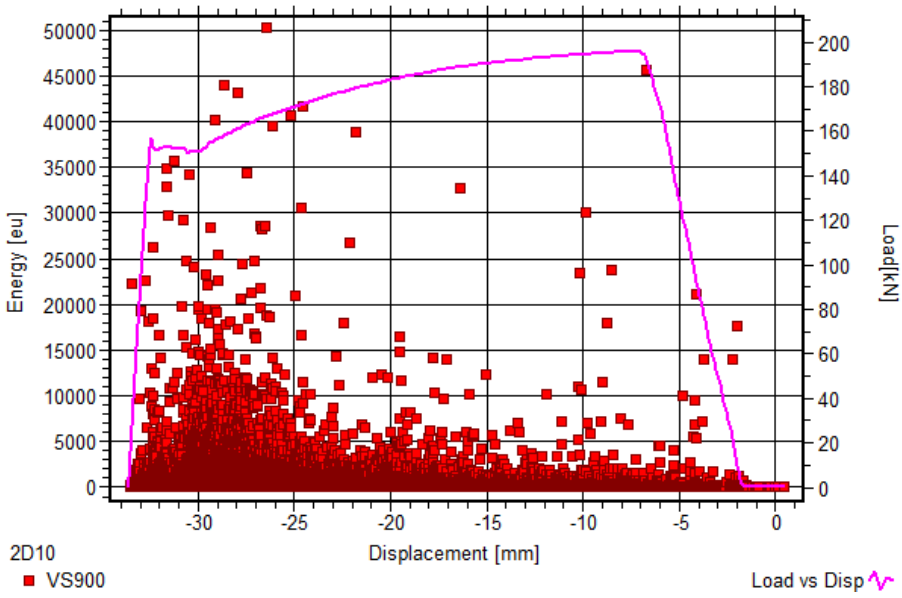

(b)

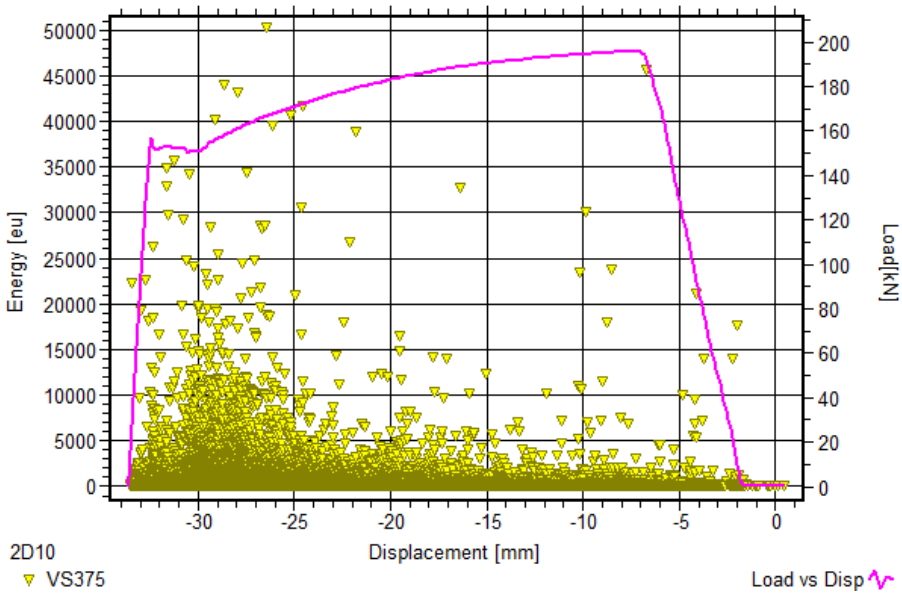

(c)

Figure 4-9 Energy distribution over the load-displacement curve for (a) VS150 (b) VS900-RIC (c) VS375-WIC

The above results show that during this experiment, signals with high peak amplitude and energy are generated during the plastic deformation. This conclusion applies to the signals from all three different sensors. Therefore it is concluded that the sensor frequency characteristics don't have a significant influence on the acoustic emission signal time domain features.

Plastic deformation detection using pattern recognition technique

The above conclusion is presented based on the fact that acoustic emission test is carried out in a lab environment, where there are much less unidentified noise in the data contributing to an inaccurate result. The loud service environment contributes extraneous noise to the acoustic emission signals. Currently none of the codes and standards discusses in depth filtering process and in most cases the quality of acoustic emission data and noise filtering strongly depend on operator experience [66]. Therefore there is a need to present a more advanced automated signal interpretation which utilizes the information available in each one the parameters collectively is needed to help operators in noise identification and achieve a higher performance and faster industrial industry production. This is the basis on which we proposed and pursued pattern recognition in acoustic emission analysis [108].

Since there is no set of training patterns indicating multiple mechanisms, for this study, the unsupervised pattern recognition technique is applied. Following the introduced steps for unsupervised pattern recognition in 2.3.3, below details the results obtained from each of the step.

After a successful collection of good quality data, the unwanted signals from noise need to be filtered out before applying the clustering analysis. The noise mainly include the frictions between the specimens and jaws of the tensile test machine, and environment noise. In order to eliminate these signals generated from unwanted noise, the signals with number of counts less than 3 and duration less than 3 μs are disregarded [102]. Figure 4-10 shows the peak amplitude versus MARSE distribution for the signals generated by noise and the signals generated from real damage acquired by VS150-RIC.

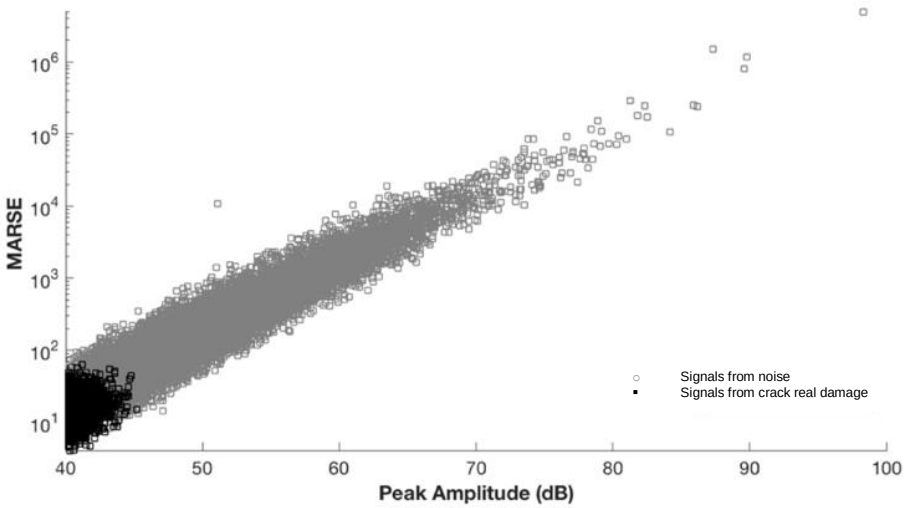

Figure 4-10 Peak amplitude vs. MARSE distribution of signals generated from noise and signals generated from real damage acquired by VS150-RIC, respectively

The next step for unsupervised pattern recognition is to classify signals into groups based on similarities, of which the key point is a successful feature selection methodology. Time domain features including peak amplitude, duration, MARSE, rise time, average frequency, as well as frequency domain features including peak frequency and frequency centroid are extracted as features for clustering. The features are then normalized over the range [0, 1] using the equation:

$$X = \frac{X - X_{min}}{X_{max} - X_{min}} \tag{34}$$

The feature selection method is inspired by D. D. Doan et al. [74], who introduced a sequential method based on clustering algorithm. The subset of features is selected by minimizing the Davies-Bouldin (DB) index, which is a metric for the evaluation of classification algorithms.

The principle of this feature selection processing is to gradually combine each feature from the available feature space with an initial feature subset. Considering an initial subset of features S (empty by default), the algorithm takes each of the available features to update S. Feature selection is achieved by minimizing the value of DB index partitioned by k-means algorithm (see Appendix C):

$$DB = \frac{1}{k}\sum_{i=1}^{k} max_{i \neq j}\left\{\frac{d_i + d_j}{D_{ij}}\right\} (i, j = 1 \dots k) \tag{35}$$

where d_i is the average Euclidean distance between each point in the ith cluster and the centroid of the ith cluster, and d_j is the average Euclidean distance between each point in the jth cluster and the centroid of the jth cluster. D_{ij} denotes the Euclidean distance between the centroids of the ith and jth clusters. The maximum value of D_{ij} represents the worst-case within/between the centroids of the ith and jth clusters. Therefore the lower the DB value, the better the compactness and the separability within the partition. The computation of the DB index makes use of the Euclidean distance obtained by the k-means algorithm to estimate the distance between acoustic emission hits and cluster centres and finally obtains an estimate of the average within-class distances used in equation (35) (d_i and d_j). An initial feature needs to be chosen for the first interaction, the initial feature and the selected feature that minimizes the value of the DB index is then selected. For the next interaction, the initial feature and the selected feature are used together to evaluate by the

DB index. An improvement rate $\mathrm{IR(k)}$ is defined to indicate whether the DB criterion is improved:

$$\mathrm{IR(k)} = \frac{\mathrm{DB(S_k)} - \mathrm{DB(S_{k-1})}}{\mathrm{DB(S_{k-1})}} \tag{36}$$

where $\mathrm{DB(S_k)}$ and $\mathrm{DB(S_{k-1})}$ represent the value of the minimum DB index for the kth and $(\mathrm{k}-1)$th interactions, respectively. A negative value of $\mathrm{IR(k)}$ indicates that the DB criterion is improved.

Considering the sensitivity impact on the data processing results, the unsupervised pattern recognition is carried out on signals acquired by different sensors separately. Since MARSE has been proven to be an effective parameter to represent different damage mechanisms and is therefore to initiate the feature selection process for all the sensors. The number of clusters for k-means clustering is selected as 3 as there are three phases during the tensile test (elastic, plastic deformation and fracture).

At the first interaction for signals acquired by VS150-RIC, the lowest DB index is given by the combination with duration, see Figure 4-11. No more improvement of the DB criterion occurs at the next interaction, see Figure 4-12. Therefore, MARSE and duration are selected for the clustering algorithm.

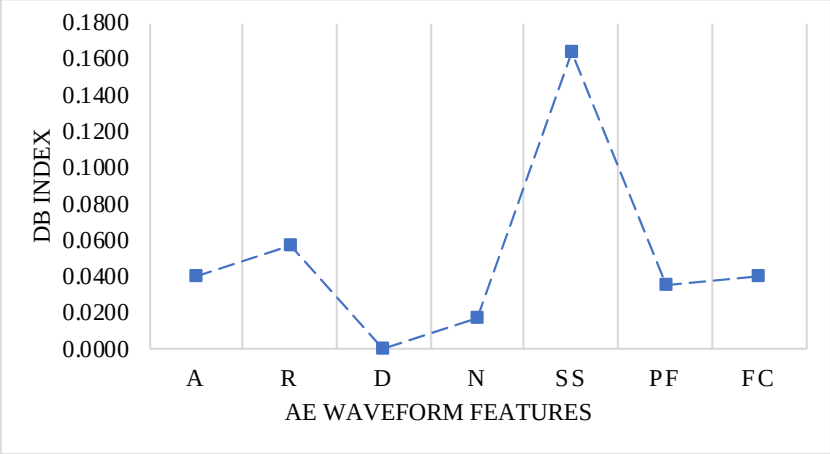

AE Signal Feature	DB Index
Peak Amplitude (A)	0.0402
Rise Time (R)	0.0569
Duration (D)	0.0001
Counts (N)	0.0168
Signal Strength (SS)	0.1643
Peak Frequency (PF)	0.0356
Frequency Centroid (FC)	0.0399

Figure 4-11 First interaction giving duration as the best feature of 3 clusters – VS150-RIC

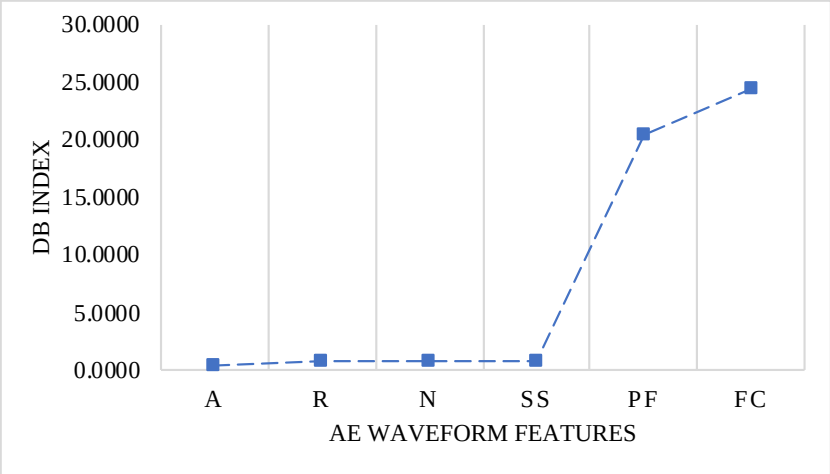

AE Signal Feature	DB Index
Peak Amplitude (A)	0.4969
Rise Time (R)	0.8976
Counts (N)	0.8250
Signal Strength (SS)	0.7595
Peak Frequency (PF)	20.3466
Frequency Centroid (FC)	24.3955

Figure 4-12 Second interaction giving duration as the best feature of 3 clusters – VS150-RIC

Figure 4-13 shows the partition of acoustic emission signals obtained by the above unsupervised patter recognition method. Time domain features MARSE and duration are used to visualize the position of the signal clusters. It can be observed that the acoustic emission signals are well separated into three clusters in the MARSE-duration space. Acoustic emission signals originating from cluster 1 are related to high duration and high MARSE. Figure 4-14 shows the duration distribution of the signals acquired by VS150-RIC versus the load-displacement history. This reveals that acoustic emission signals with high duration are generated during the plastic deformation stage and thus proves that the cluster 1 of signals with high duration and MARSE correspond to the plastic deformation stage.

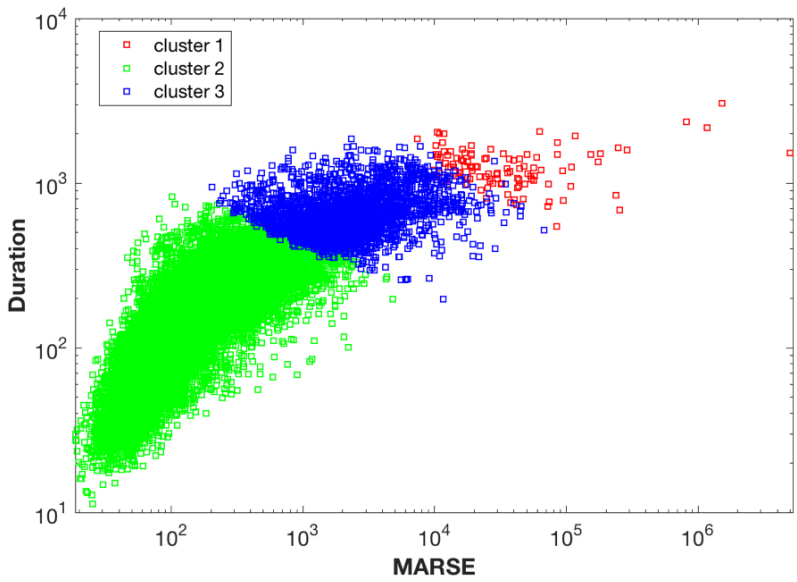

Figure 4-13 Clustering results on signals obtained from VS150-RIC

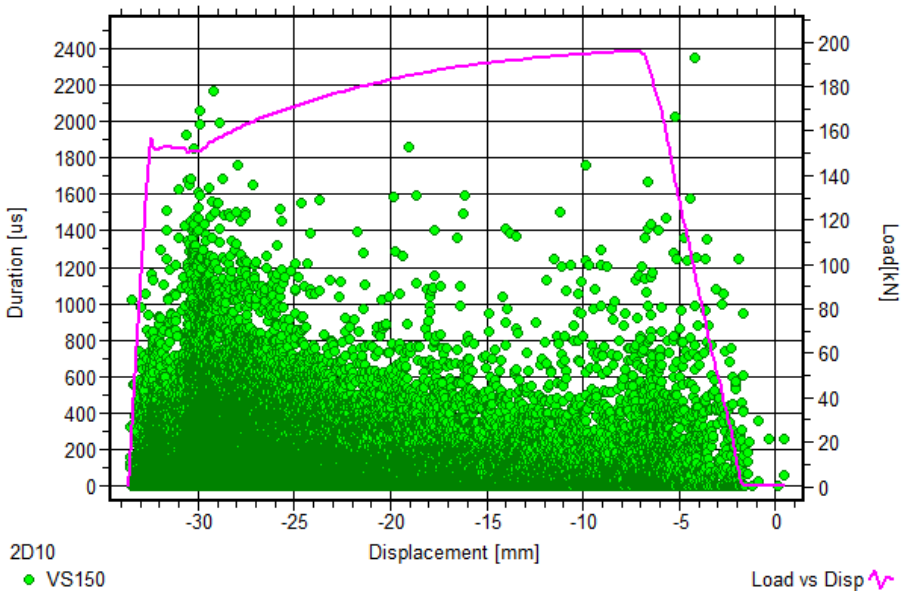

Figure 4-14 Duration distribution of the signals acquired by VS150-RIC

The same algorithm is applied on the signals acquired by VS900-RIC and VS375-WIC. For the signals acquired by VS900-RIC, the lowest DB index is given by the combination with peak frequency at the first interaction, see Figure 4-15; and for signals acquired by VS375-WIC, the lowest DB index is given by the combination with signal strength, see Figure 4-18. No more improvement of the DB criterion occurs at the next interaction. Therefore, peak frequency and MARSE are selected for the clustering algorithm on the signals acquired by VS900-RIC; signal strength and MARSE are selected for the clustering algorithm on the signals acquired by VS375-WIC.

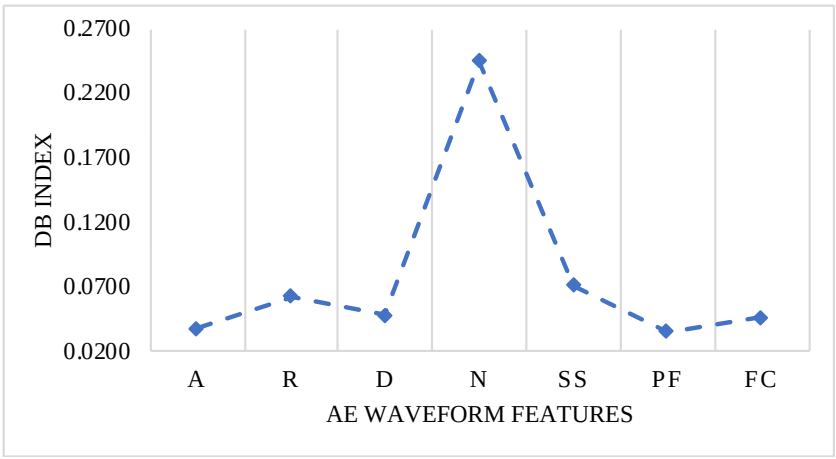

AE Signal Feature	DB Index
Peak Amplitude (A)	0.0375
Rise Time (R)	0.0623

Duration (D)	0.0481
Counts (N)	0.2453
Signal Strength (SS)	0.0712
Peak Frequency (PF)	0.0515
Frequency Centroid (FC)	0.0458

Figure 4-15 First interaction giving peak amplitude as the best feature of 3 clusters – VS900-RIC

Figure 4-16 shows the grouping of the acoustic emission events obtained by VS900-RIC on plot MARSE vs peak amplitude. Signals in cluster 1 are with lower peak amplitude and MARSE, signals in cluster 2 are with higher peak amplitude and MAESE, signals in cluster 3 are with the highest peak amplitude and MARSE, which is highly likely to be correlated with the events generated by the plastic deformation. In order to prove this, peak amplitude distribution of the signals obtained by VS900-RIC is plotted against the load-displacement curve, see Figure 4-17. It is shown that a clear increase of the peak amplitude values when the plastic deformation happens. This proves that the signals in cluster 3 correspond to the plastic deformation.

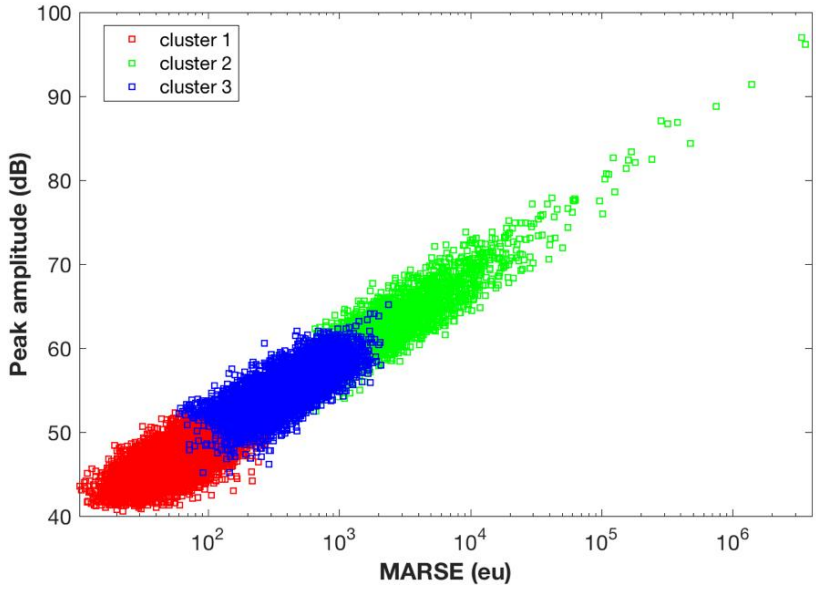

Figure 4-16 Clustering results on signals obtained from VS900-RIC

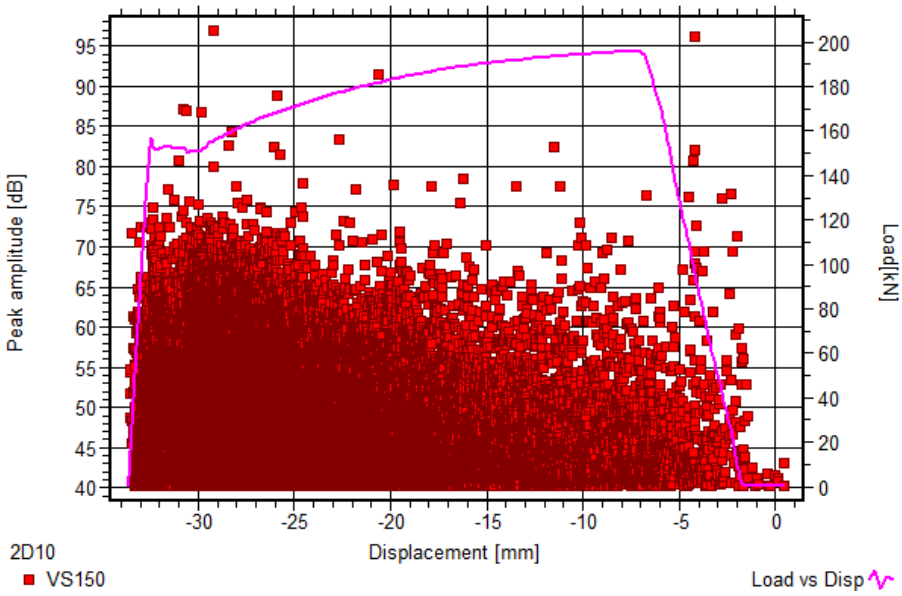

Figure 4-17 VS900-RIC – Peak amplitude vs time & Load vs time

For the signals acquired by sensor VS375-WIC, the signal strength is selected as the feature to be used for clustering analysis.

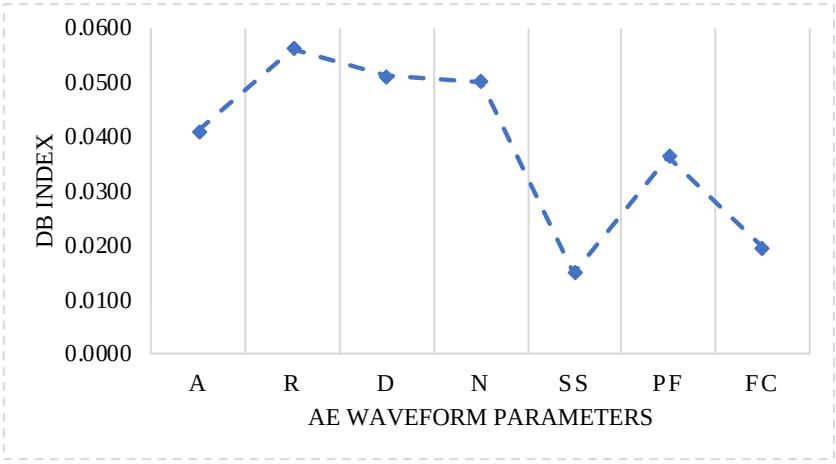

AE Signal Feature	DB Index
Peak Amplitude (A)	0.0410
Rise Time (R)	0.0562
Duration (D)	0.0511
Counts (N)	0.0502
Signal Strength (SS)	0.0149
Peak Frequency (PF)	0.0364
Frequency Centroid (FC)	0.0196

Figure 4-18 First interaction giving signal strength as the best feature of 3 clusters – VS375-WIC

The same algorithm is applied to clustering analysis of acoustic emission signals obtained by VS375-WIC. The data is divided mainly into two categories, as shown in Figure 4-19. The distribution diagram MARSE – signal strength is used for presenting the clustering results. It can be seen that cluster 3 correspond to low signal strength and MARSE, while for cluster 1 & 2, signals have similar trend with higher MARSE and signal strength. Correlations between the clustering results and the deformation in different stages is then analysed. Figure 4-20 shows the signal strength distribution for VS375-WIC. It is quite clear that the when the plastic deformation happens, there is an increase in high signal strength acoustic emission signals. Therefore it can be concluded that signals in cluster 2 represent the signals that generated from the plastic deformation.

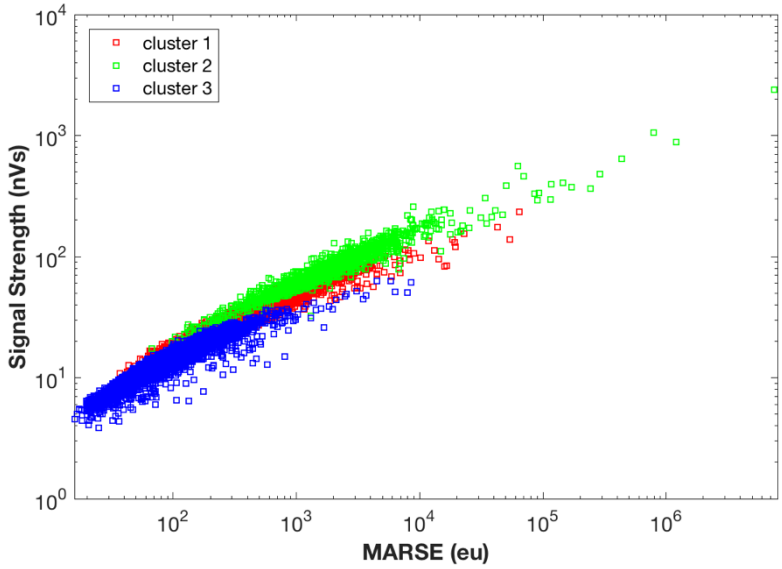

Figure 4-19 Clustering results on signals obtained from VS375-WIC

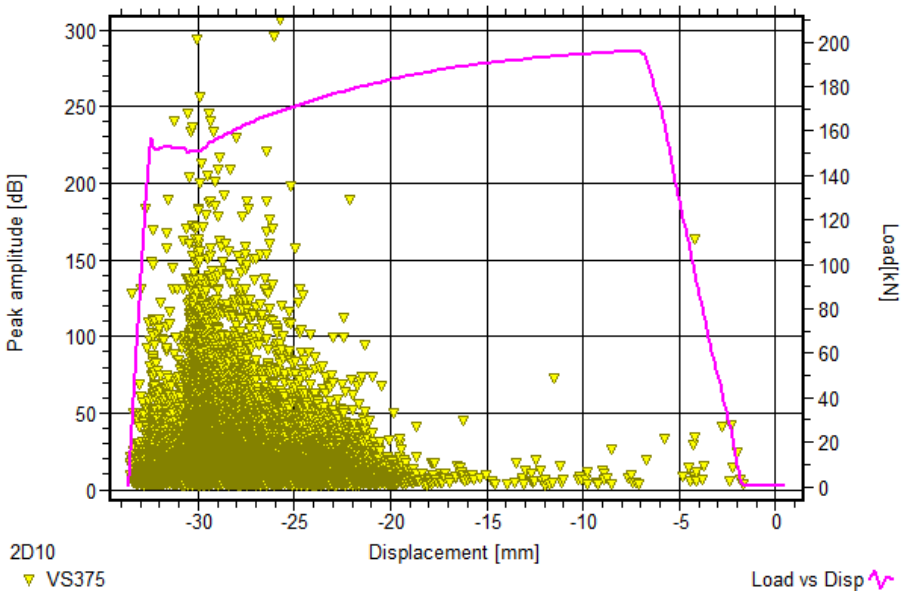

Figure 4-20 VS375-WIC - Signal strength vs time & Load vs time

In summary, the objective of this section is to identify plastic deformation using acoustic emission technique. During this process, the influence of sensor frequency characteristics on the acoustic emission signal features is also investigated. First, acoustic emission signal features distributions are used to identify the plastic deformation, both time domain and frequency domain features are examined. For the time domain features, high MARSE and peak amplitude are proved to be an indication of plastic deformation for all three different frequency range sensors. As for the frequency domain signal features, the results for three sensors are different. Both broadband sensor VS900-RIC and low resonant frequency sensor VS150-RIC have characteristic frequencies when plastic deformation begins. However this phenomenon is not clearly revealed on the signals acquired by high resonant frequency sensor VS375-WIC. The sensor sensitivity has a significant influence on the frequency domain of the obtained signals. The influence on the time domain is not quite obvious.

Finally an unsupervised pattern recognition method is applied. The algorithm identified the unique optimal parameter together with MARSE to represent plastic deformation for signals obtained by each sensor.

For broadband sensor VS900-RIC, plastic deformation is identified by signals with high MARSE and duration; for low resonant frequency sensor VS150-RIC, plastic deformation is identified by signals with high MARSE and high peak amplitude; for high resonant frequency sensor VS375-WIC, plastic deformation is identified by signals with high MARSE and high signal strength.

4.3 Tensile Test on CFRP Specimen

Apart from the investigation on damage mechanism in carbon steels, the damage mechanisms in composite materials are also investigated using acoustic emission technique. CFRP composites display several advantageous properties for structural application in the wind turbine blade and aeronautics industry. Therefore a tensile test is carried out on CFRP specimen, the three sensors used for the tensile tests on carbon steel specimens are also used in this test. The influence of the sensor frequency characteristics on the acoustic emission signals from different damage mechanisms is investigated.

4.3.1 Materials and Specimens

A CFRP laminate of [0°/90°]s is used in this study. The dimensions of the specimen is 250mm×25mm×2mm, this is based on ASTM D3039 standard. The aluminium tabs are bonded at both ends of the specimen using Araldite® 2000 PLUS adhesives. This is to reduce the signal from the grip during loading, also to prevent the specimen to be broken at the grip, see Figure 4-21.

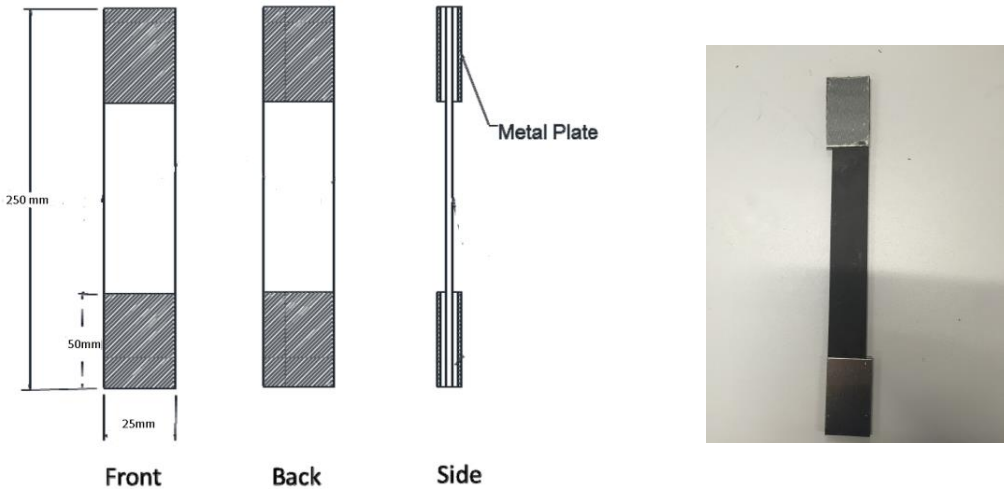

Figure 4-21 CFRP specimen with aluminium tabs

4.3.2 Experimental Procedure

An uniaxial tensile test is performed on the CFRP specimen. A 2mm depth notch is implanted in the middle of the specimen. During the test, three different sensors, VS150-RIC, VS900-RIC and VS375-RIC are placed at symmetrical distance from the notch, details of these sensors can be referred to 4.2.2. The threshold used of this test is 55dB to filter out the signals generated by the environmental noise. The detection parameter is shown in Table 4-3. A frequency filter range from 25 kHz – 850 kHz is applied. The stepped loading is applied for this test to observe the Kaiser effect. Displacement control is used during the test, the speed is 1mm/min.

Table 4-3 Detection parameter for data acquisition

Detection parameter	Value
Threshold	55 dB
Sampling Rate	5 MHz
HDT	50 μs

Figure 4-22 CFRP specimen on the tensile test machine

4.3.3 Results and Discussion

4.3.3.1 Felicity Ratio Analysis to Monitor Progressive Damage

In this section, the failure process of the CFRP specimen during the test is studied. There are mainly three kinds of damages of CFRP specimen with a

[0°/90°] architecture: matrix, delamination and fibre breakage. Once the matrix is lost, the strength along the fibre direction is decreased rapidly, when the matrix and fibre are separated, the delamination damage occurs.

While the existence of the Kaiser effect is undisputed for a variety of metallic materials, the Felicity effect has been observed by many researchers in composite materials, especially within the range of high stress levels [109], [110]. In this section, Felicity ratios are measured. Figure 4-23 shows a plot of the cumulative number of hits through the test, the loading history is presented on the same figure. The onset of significant acoustic emission events is based on the cumulative number of hits. Five cycles of loading – unloading are carried out during the test. The results of the Felicity ratio calculations are presented in Table 4-4.

Table 4-4 Felicity ratio results

Sensor	Cycle	Felicity Ratio
VS900-RIC & VS375-WIC	1	1.36
	2	1.06
	3	1.03
	4	1.01
	5	1.01
VS150-RIC	1	1.36
	2	1.06
	3	1.06
	4	1.01
	5	0.97

During this test, a distinct Kaiser effect is observed even during the high stress level. This doesn't agree with the literature. One of the possible reasons could be because of the high threshold level. In order to eliminate the environmental noise, a high threshold of 55 dB is applied. Therefore, there could be some acoustic emission events happening before reaching the previous load, however they cannot trigger the threshold for acquisition. The Kaiser effect is calculated based on the cumulative number of hits plot, see Figure 4-23. During the last stage of the test, shortly before the specimen breaks in half, the Felicity effect is observed on the signals from VS150-RIC, despite the high threshold level. This implies that the lower resonant sensor - VS150-RIC is very sensitive to the damage modes in composite materials.

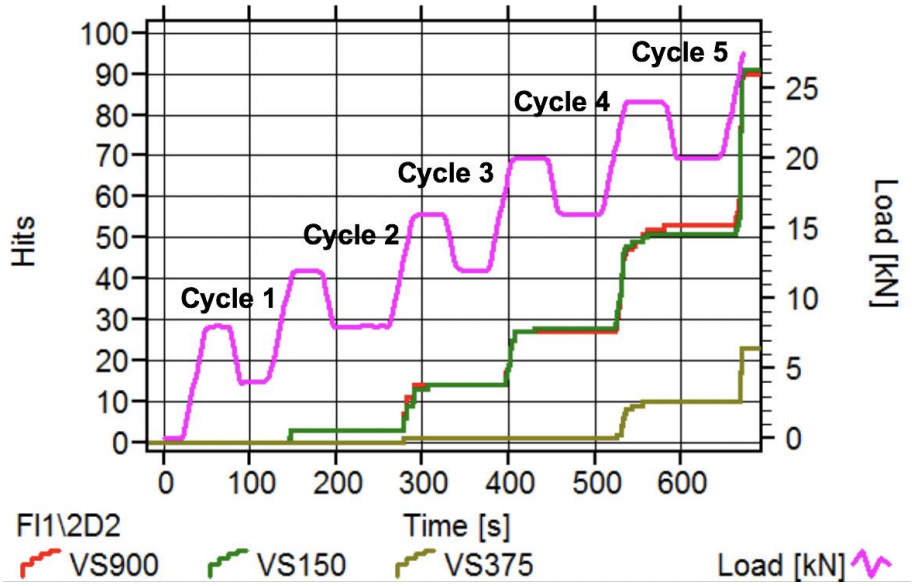

Figure 4-23 Load vs Cumulative number of hits

4.3.3.2 Damage Assessment Using Acoustic Emission Signal Features

This section describes the basics of an acoustic emission monitoring study, emphasizing on the signal features that are sensitive to the damage mechanisms in composite materials. The more important objective in this section is to investigate the influence of sensor frequency characteristics on the signals from different damage mechanisms in composite materials.

Using acoustic emission time domain signal features

The total number of hits acquired by each sensor is presented in Table 4-5. During the test, VS150-RIC and VS900-RIC capture more acoustic emission signals than VS375-WIC. This implies that the high resonant frequency sensor VS375-WIC is not suitable for damage detection in composite materials.

Table 4-5 Number of cumulative number of events captured with different sensors

Sensor	Total Nummer of Hits
VS150-RIC	94
VS900-RIC	92
VS375-WIC	23

As reviewed in 2.3.3, a lot research focused on using acoustic emission signal features for damage characterization. It is reported that signals with high peak

amplitude and high MARSE are associated with fibre failure and signals with low peak amplitude and low energy are associated with matrix cracking and delamination. In this regard, the peak amplitude and MARSE distributions are investigated, see Figure 4-24 and Figure 4-25.

It is shown that signals with high peak amplitude appear in the last stage of the test, when significant damage such as delamination and fibre breakage happen. The signals acquired by three different sensors respond the same. Therefore it is concluded that the sensor frequency characteristics don't have a significant influence on the acoustic emission signal time domain features.

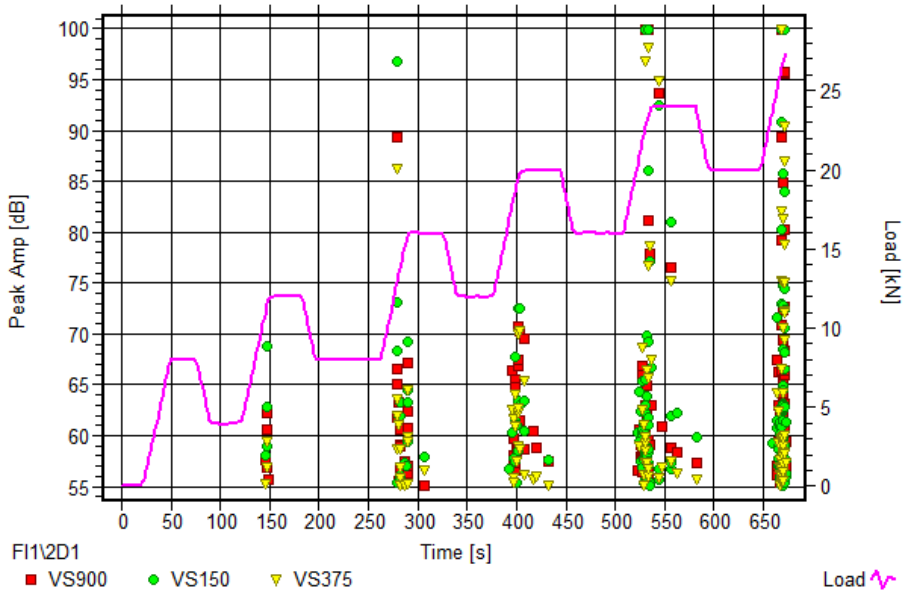

Figure 4-24 Peak amplitude distribution vs loading history for VS150-RIC, VS900-RIC and VS375-WIC

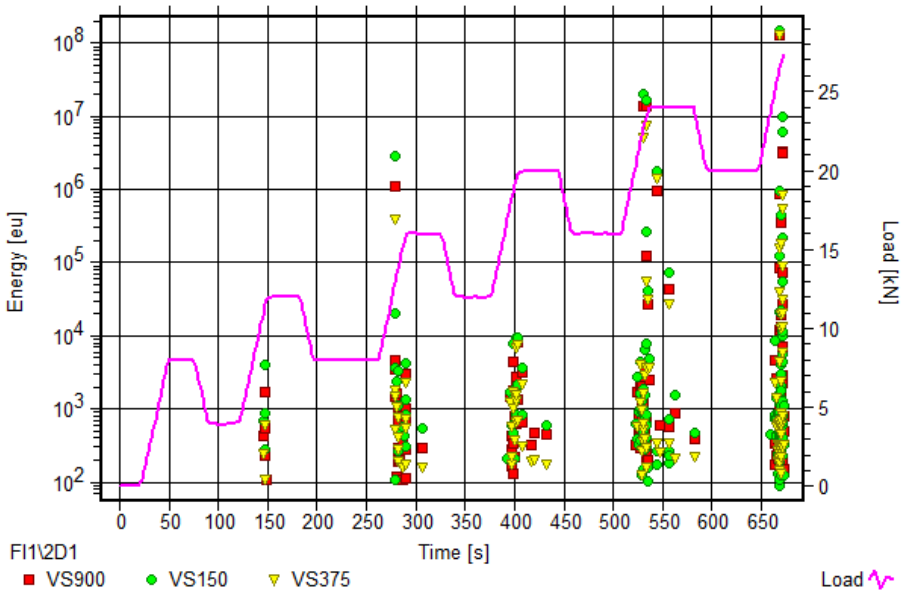

Figure 4-25 MARSE distribution vs loading history for VS150-RIC, VS900-RIC and VS375-WIC

Using acoustic emission frequency domain signal features

Acoustic emission signals can also be well characterized by using frequency domain analysis. In this regard, the identification of different damage mechanisms through frequency-based methodologies in acoustic emission data analysis is reviewed. It is concluded that the fibre breakage and fibre pull out show a relatively high frequency range (above 300kHz), while the frequency content of matrix cracking correspond to the low frequency range (30-150 kHz), delamination usually occur in the frequency range in between (200-300 kHz) [64], [111], [63]. Ni and Iwamoto conclude that peak frequency is a more reliable signal frequency domain characteristic [62]. Therefore classifications of failure modes based on peak frequency of acoustic emission signals acquired by all three sensors are investigated, see Figure 4-26.

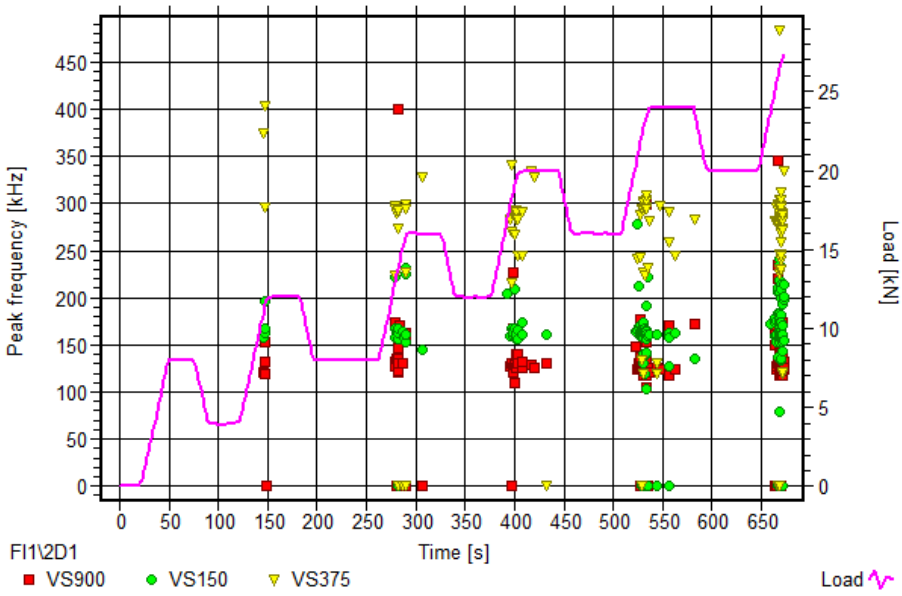

Figure 4-26 Peak frequency distribution & Load history for VS150-RIC, VS900-RIC and VS375-WIC

The peak frequency distribution shows that the different sensors have different peak frequency bands. For VS150-RIC, the peak frequency is clustered around its resonant frequency, 150 kHz, in the last stage of the test, some signals with higher peak frequency (above 200 kHz) are generated. As for the broadband sensor VS900-RIC, the peak frequency ranges from 100 kHz to 200 kHz throughout the test. For the higher resonant frequency sensor VS375-WIC, the peak frequency of the signals concentrates around 300 kHz throughout the test. Therefore, when using peak frequency content as a discriminating factor for damage mechanisms, the resonant sensor - VS150-RIC is proved to be more sensitive in responding to the different damage mechanisms.

As reviewed in 2.3.3, for plate-like structures, there are two modes of propagation – S_0 mode and A_0 mode. The out-of-plane displacement causes high amplitude A_0 mode and lower amplitude S_0 mode; the in-plane displacement causes high amplitude S_0 mode and lower amplitude A_0 mode. According to the dispersion curve, the S_0 mode travels faster than A_0 mode, therefore the S_0 mode always hits the sensor first. This concept allows to develop an approach to the acoustic emission analysis by presenting the signals in time and frequency domain.

In order to identify the wave modes in the received signals, wavelet transform analysis is carried out on the signals obtained from three different sensors resulted from one acoustic emission event. The objective of investigation in this section is to study the influence of sensor characterises on the acquired signals.

Based on the wavelet transform analysis of the signal acquired by VS150-RIC, a clear out-of-plane displacement acoustic emission source is identified, see Figure 4-27. The wave mode separation is performed on continuous WT analysis. The signal is calculated as a function of frequency versus time based on the WT, which is performed via AGU-Vallen Wavelet [112]. Red colour represents the highest magnitude of the WT and pink represents the smallest or zero-magnitude region. It is clearly shown that the maximum energy is located in between 20 μs to 50 μs, which corresponds to the lower speed wave mode, A_0 mode. This represents an out-of-plane displacement crack. In the case of composite materials, an out-of-plane displacement represents a delamination crack.

The wavelet transform analysis also extracts the information of the dominant wave mode's frequency bandwidth. The frequency bandwidths are selected from the dominant WT magnitude regions of the fundamental modes. Therefore the A_0 mode is characterized by a lower frequency range from 150 kHz to 250 kHz, while the S_0 is characterized by a higher frequency range from 250 kHz to 350 kHz.

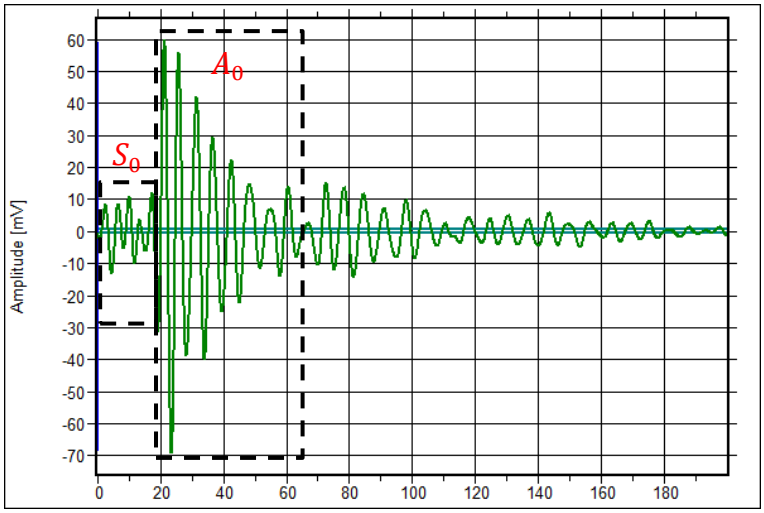

(a)

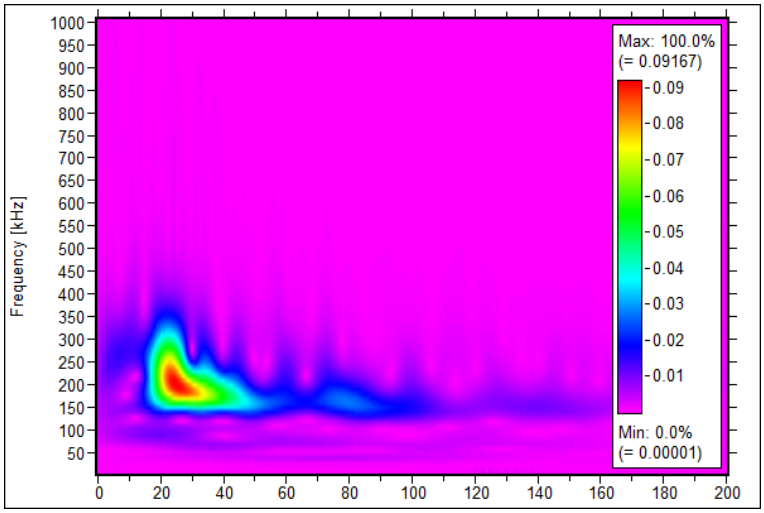

(b)

Figure 4-27 (a) Signal acquired by VS150-RIC (b) its wavelet transform analysis

It is worth noticing that the signals acquired by all three sensors respond differently to the above acoustic emission event. Figure 4-28 and Figure 4-29 represent the signals and the wavelet analysis acquired by VS900-RIC and VS375-WIC from this event. The results show that for VS900-RIC the A_0 mode is characterized by a lower frequency range from 100 kHz to 200 kHz, while the S_0 by a higher frequency range from 200kHz to 450 kHz. While for VS375-WIC, both the S_0 and A_0 are characterized by the frequency range from 150 kHz to 450 kHz.

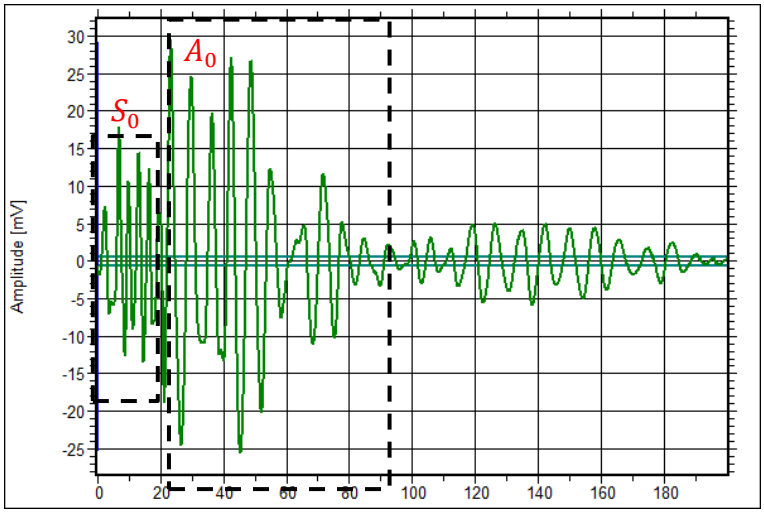

(a)

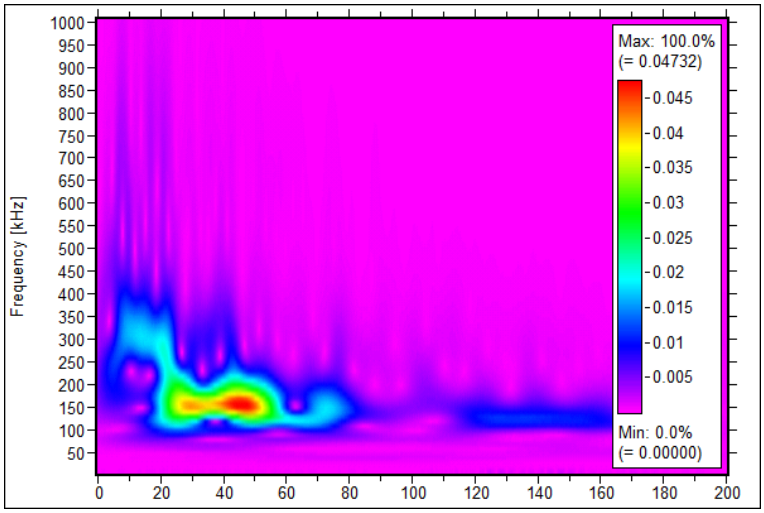

(b)

Figure 4-28 (a) Signal acquired by VS900-RIC from the same acoustic emission event (b) its wavelet transform analysis

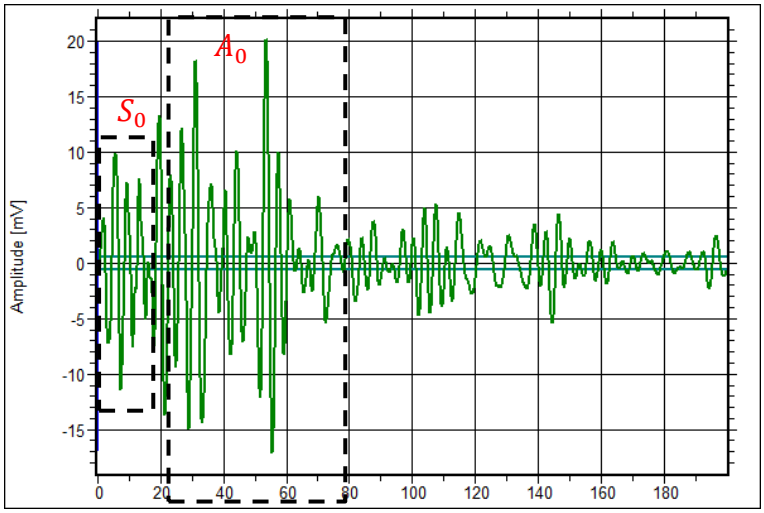

(a)

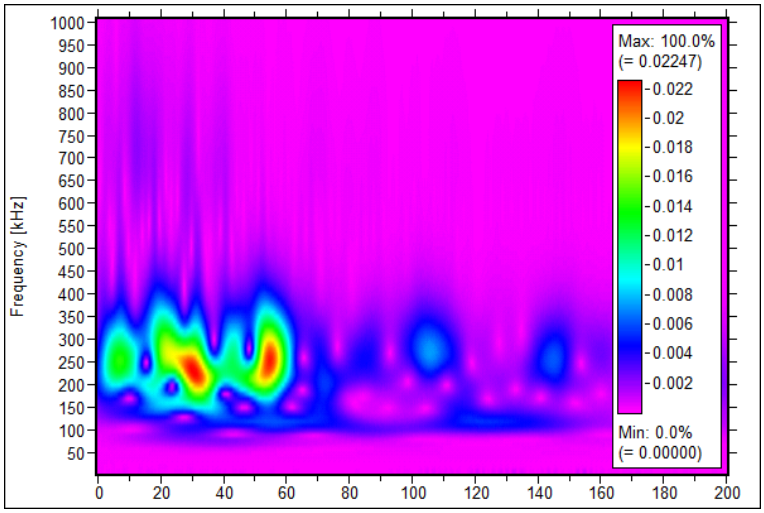

(b)

Figure 4-29 (a) Signal acquired by VS375-WIC from the same acoustic emission event (b) its wavelet transform analysis

The above investigations have shown clearly the influence of sensor frequency characteristics on the obtained signals. This influence reveals on the frequency domain features as well as time domain features.

For above acoustic emission event as an example, A_0 is the dominant wave mode, therefore the peak amplitude of the signals is recognized upon A_0 mode. It is shown that the peak amplitude of the signal acquired by VS150-RIC is the highest while the peak amplitude of the signal acquired by VS375-WIC is the lowest. This is because A_0 mode is identified to have a frequency range around 150 kHz based on the wavelet transform results on three different sensors.

For sensor VS150-RIC, which is with resonant frequency around 150 kHz, this provides the ability to obtain this wave mode to the relatively larger extend, for VS375-WIC on the other hand, the sensor is relatively more sensitive to the larger frequency wave modes, however the S_0 wave mode is not dominant in this case. Therefore that the peak amplitude of the signal obtained by VS150-RIC is the highest, whereas for VS375-WIC is the lowest.

Therefore, in order to understand the relationship between the dominant wave frequency and failure mode using wavelet transform analysis, it is recommended using the broadband sensors with a flat response curve.

However, broad band acoustic emission sensors are generally considered less sensitive than the resonant sensors. Resonant acoustic emission sensors are often used when the frequency content itself is not of interest but only acoustic emission signal features.

The pattern recognition technique requires a collection of good quality database which consists of acoustic emission signal features. Therefore in the applications of damage characterization using acoustic emission techniques a resonant sensor is preferred.

4.4 Conclusions

Tensile tests are carried out on carbon steel and CFRP specimens, during the tests, three different types of sensors are used.

For the tensile tests carried out on carbon steel, the main objective is to identify the plastic deformation process in carbon steel using acoustic emission technique. To achieve this, two general data processing techniques such as Felicity ratio measurement and acoustic emission signal feature distributions are applied. The effect of sensor's frequency effect on the signals is also investigated. Results show that the Felicity effects are clearly observed when plastic deformation starts, however, in the later stage, the felicity ratio measurements cannot indicate severe damage, especially when using the high resonant frequency sensors – VS375-WIC, therefore this method is not recommended.

As for using acoustic emission signal feature distributions to indicate plastic deformation, both time domain and frequency domain signal features are examined. For all three different sensors, time domain feature MARSE and peak amplitude are proved to be effective parameters to indicate plastic

deformation. On the other hand, frequency domain features from three different sensors respond differently. For the broadband sensor VS900-RIC and lower resonant frequency senor VS150-RIC, high peak frequency can be used to indicate plastic deformation whereas for high resonant frequency sensor, peak frequency cannot.

A more advanced unsupervised pattern recognition method is then applied to identify the plastic deformation. A novel feature selection algorithm is applied. Results show that for broadband sensor, plastic deformation is identified by signals with high MARSE and duration; for low resonant frequency sensor, plastic deformation is identified by signals with high MARSE and high peak amplitude; for high resonant frequency sensor, plastic deformation is identified by signals with high MARSE and high signal strength.

For the tensile test on CFRP specimen, through the Felicity ratio measurements, the low resonant frequency sensor VS150-RIC is proved to be the most sensitive sensor for damage assessment.

As for using acoustic emission signal feature distributions to assess damage mechanisms in composite materials. Both time domain features and frequency domain features are investigated, it is shown that signals with high peak amplitude appear in the last stage of the test, when significant damage such as delamination and fibre breakage happen. The peak frequency distribution shows that the different sensors have different peak frequency bands. For VS150-RIC, the peak frequency is clustered around its resonant frequency, 150 kHz, in the last stage of the test, some signals with higher peak frequency (above 200 kHz) are generated. As for the broadband sensor VS900-RIC, the peak frequency ranges from 100 kHz to 200 kHz throughout the test. For the higher resonant frequency sensor VS375-WIC, the peak frequency of the signals concentrates around 300 kHz throughout the test. Therefore, when using peak frequency content as a discriminating factor for damage mechanisms, the resonant sensor - VS150-RIC is proved to be more sensitive in responding to the different damage mechanisms.

Wavelet transform analysis is carried out on the signals obtained from three different sensors resulted from one acoustic emission event to further study the influence of sensor characterises on the acquired signals. It is concluded that broadband sensors with a flat response curve should be used when using wavelet transform to understand the relationship between the dominant wave frequency and failure mode. Resonant sensors are often used when only acoustic emission signal features are of interest. Pattern recognition technique requires a collection of good quality database which consists of acoustic emission signal features. Therefore in the applications of damage characterization using acoustic emission techniques a resonant sensor is preferred.

5 Influence of Detection Distance on Acoustic Emission Signals

5.1 Introduction

In chapter 4, the impact of sensor frequency characteristics on detected acoustic emission signal features is investigated.

Another important parameter that influences the acoustic emission signal features is the distance of wave propagation from acoustic emission source to the sensor. Acoustic emission signals lose energy as they propagate within the medium. This effect is called attenuation. The understanding of this effect is required to analyse acoustic emission signals accurately. In this chapter, an investigation of acoustic emission signals attenuation for monitoring of failures in GFRP laminates used in wind turbine blade is carried out.

First, the attenuation effect is investigated on the acoustic emission signals created using pencil lead breaks. The test is carried out on a GFRP panel, three sensors are placed on the panel with varied distances from the source. Wavelet transform analysis is applied to identify the wave modes in the acoustic emission signals generated by pencil lead breaks, the attenuation rates of the wave modes are analysed separately.

Secondly, the attenuation effect is investigated on the acoustic emission signals from damage mechanisms occurring during a three point bending test on the GFRP panel. A pattern recognition method is applied for the damage characterization.

5.2 Pencil Lead Break Test

5.2.1 Materials and Specimens

The GFRP specimen has a dimension of 1000mm $\times$ 40mm $\times$ 4.5mm. It is made of six layers, each containing glass fibres orientated at $\pm$ 45° and arranged in a twill weave pattern. The material properties of the GFRP specimen is listed in Table 5-1.

Table 5-1 Material properties for GFRP plate

ρ (kg/m^3)	E_1 (GPa)	E_2 (GPa)	E_3 (GPa)	ν_{12}	ν_{13}	ν_{23}	G_{12} (GPa)	G_{13} (GPa)	G_{23} (GPa)
1800	12.46	12.46	11.47	0.5	0.29	0.29	9.5	4.237	4.237

5.2.2 Experimental Procedure

The experiment used a Vallen AMSY-6 data acquisition system (DAQ) and three VS150-RIC sensors, which have a peak frequency of 150 kHz and a bandwidth from 100 kHz to 450 kHz. The sensors have built in preamplifiers which supply 34dB gain to the signal between the sensors and the DAQ. A band pass filter of 25kHz to 850kHz is further applied in the DAQ to compensate for the effects of background noise. The detection parameter is shown in Table 5-2.

Table 5-2 Detection parameter for data acquisition

Detection parameter	Value
Threshold	40 dB
Sampling Rate	3.3 MHz
HDT	50 μs

During the test, all sensors are placed along the centre of the plate to avoid edge effects. The sensors are spaced 100 mm with each other, see Figure 5-1. The pencil lead break (introduced in 2.3.3) is used to create an acoustic emission source. By changing the orientation and angle in which the lead broke determines which wave mode is dominant in the created signal. In this test, both in-plane and out-of-plane displacements are carried out in the (0, 0) position. The increasing spacing between the source and the sensors tracks the attenuation effects on both wave modes. PLB test is repeated 10 times for both in-plane displacements and out-of-plane displacements sources.

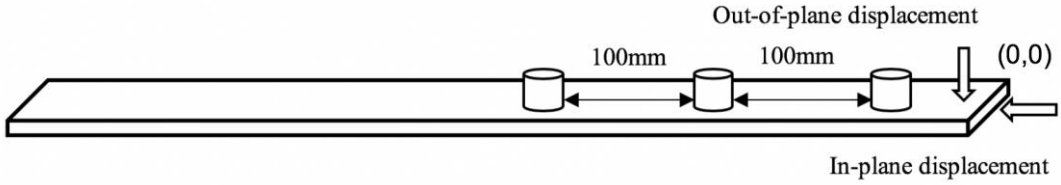

Figure 5-1Test set up for the attenuation test on GFRP plate

5.2.3 Results and Discussion

As discussed in 2.3.3, the out-of-plane displacement causes high amplitude A_0 mode and lower amplitude S_0 mode; the in-plane displacement causes high amplitude S_0 mode and lower amplitude A_0 mode. In this work, the wavelet transform analysis is carried out to differentiate wave modes in a signal. Figure 5-2 and Figure 5-3 give an example of the signal from three sensors and their wavelet transform analysis resulting from an out-of-plane displacement and in-plane displacement respectively.

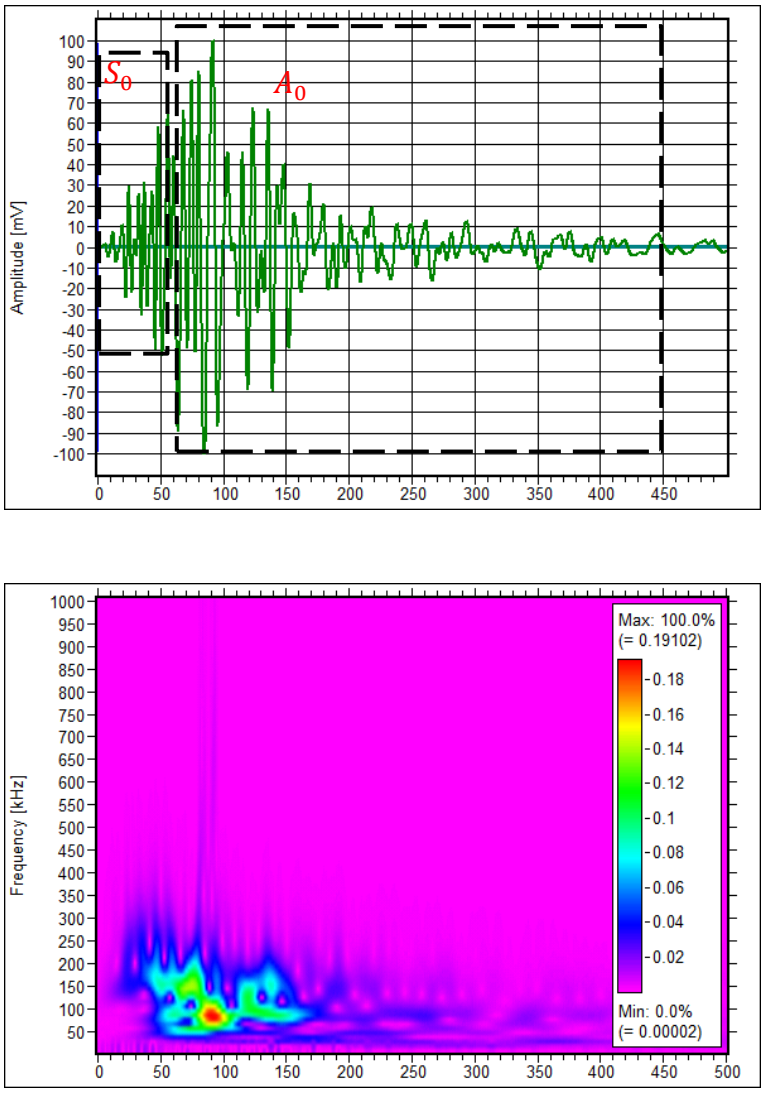

(a)

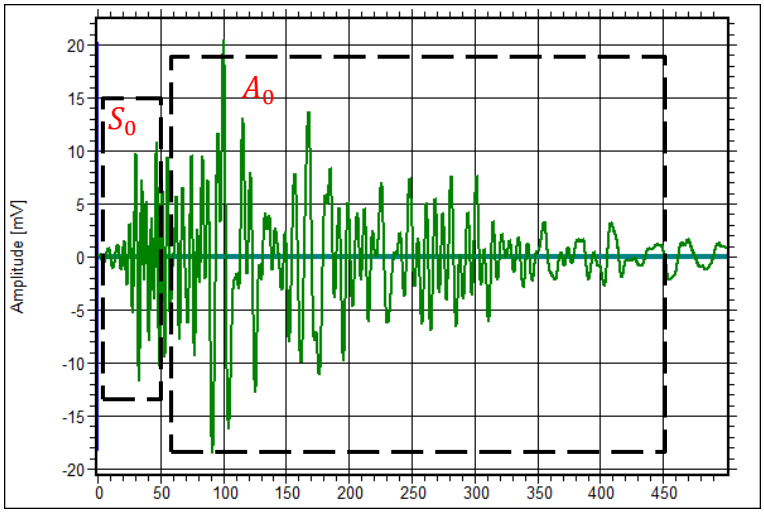
S_0
A_0
Amplitude [mV]
20
15
10
5
0
-5
-10
-15
-20
0
50
100
150
200
250
300
350
400
450

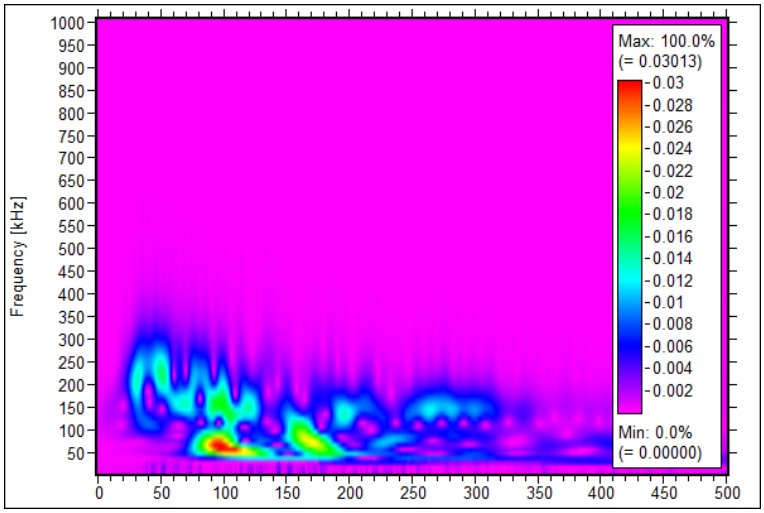
Frequency [kHz]
1000
950
900
850
800
750
700
650
600
550
500
450
400
350
300
250
200
150
100
50
0
50
100
150
200
250
300
350
400
450
500
Max: 100.0%
(= 0.03013)
0.03
0.028
0.026
0.024
0.022
0.02
0.018
0.016
0.014
0.012
0.01
0.008
0.006
0.004
0.002
Min: 0.0%
(= 0.00000)

(b)

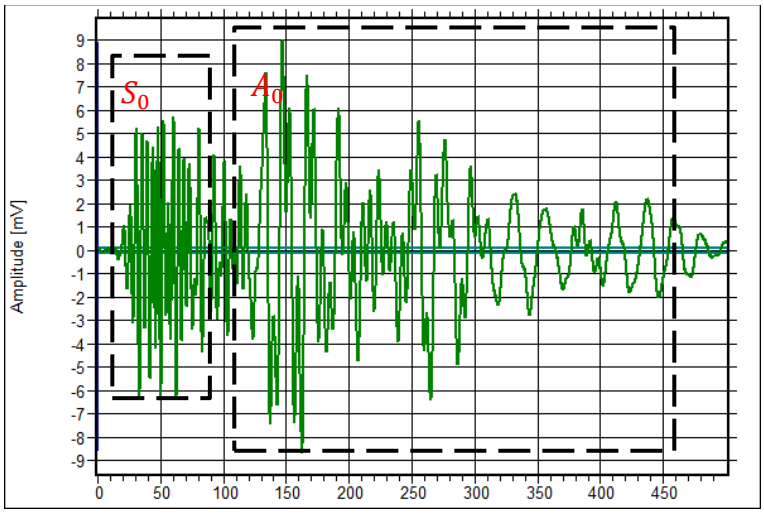
S_0
A_0
Amplitude [mV]
9
8
7
6
5
4
3
2
1
0
-1
-2
-3
-4
-5
-6
-7
-8
-9
0
50
100
150
200
250
300
350
400
450

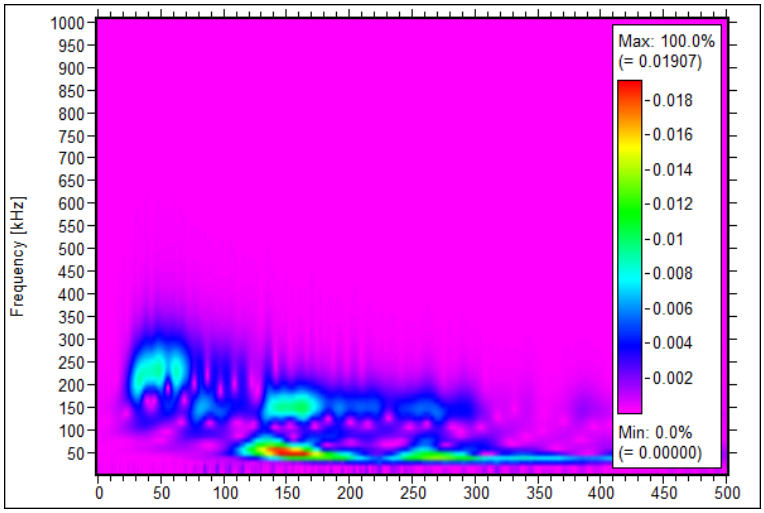

(c)

Figure 5-2 Signal and its wavelet transform analysis resulting from an out-of-plane displacement measured with (a) sensor 1 (b) sensor 2 (c) sensor 3

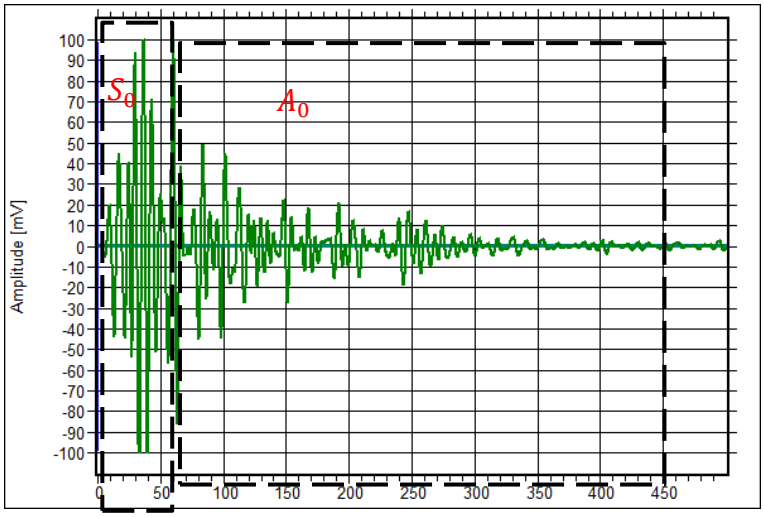

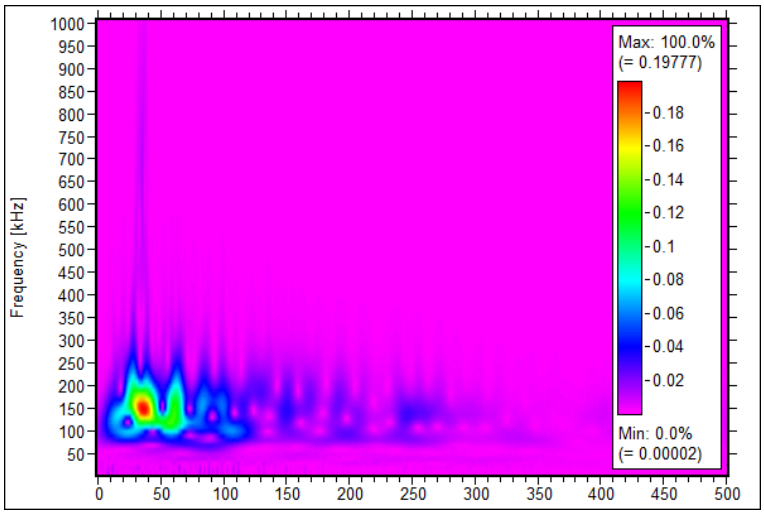

(a)

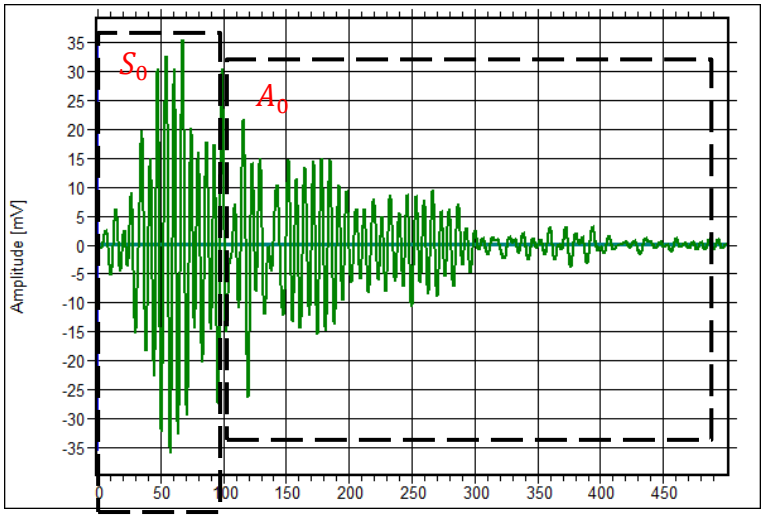
S_0
A_0
Amplitude [mV]

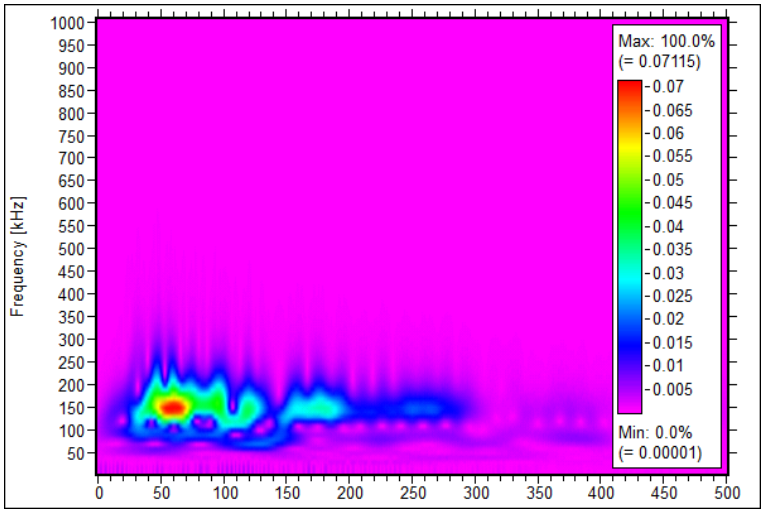
Frequency [kHz]
Max: 100.0%
(= 0.07115)
Min: 0.0%
(= 0.00001)

(b)

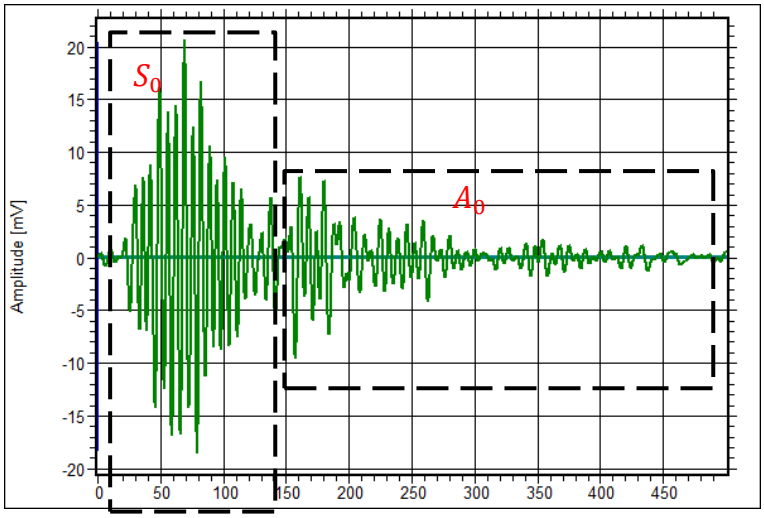
S_0
A_0
Amplitude [mV]

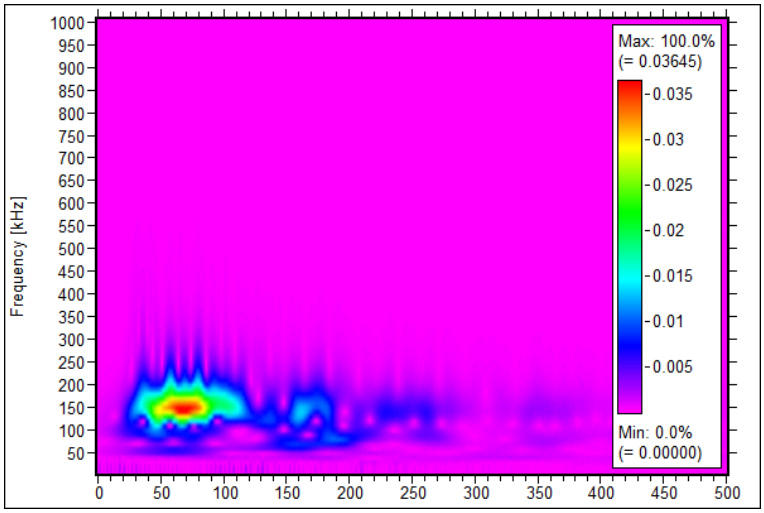

(c)

Figure 5-3 Signal and its wavelet transform analysis resulting from an in-plane displacement measured with (a) sensor 1 (b) sensor 2 (c) sensor 3

According to the dispersion curve, the S_0 mode travels faster than A_0 mode, therefore the S_0 mode always hits the sensor first. By applying wavelet transform analysis, the wave modes in the signals are successfully identified.

From the wavelet transform analysis, it is noted that S_0 mode has a high frequency feature. For the signals generated from out-of-plane displacements, as the distance from the source to the sensor increases, the energy of the signals moved towards the low frequency range, the energy of the high frequency components (above 200 kHz) can be seen fading. This is consistent with the theory that higher frequency components may experience greater attenuation rates than the lower frequency components [113].

Meanwhile, for the in-plane displacement generated acoustic emission signals, when the wave propagates to sensor 3, the energy of the signals is concentrating on the low frequency components. This reveals that, in this GFRP materials, high frequency components in acoustic emission signals from in-plane displacement sources are difficult to be detected outside a 300 mm radius.

It is noted that for acoustic emission signals generated by the out-of-plane displacement, the peak amplitude of the acoustic emission signal corresponds

to the peak amplitude of A_0 mode, which is the dominant wave mode. Meanwhile, for acoustic emission signals generated by in-plane displacement, the peak amplitude of the acoustic emission signal corresponds to the peak amplitude of S_0 mode.

In order to quantify the degree of the signal loss between the sensors, the loss in peak amplitude of the two wave modes is considered. The peak amplitude of both wave modes is measured in mV, and transferred to decibels (dB) using the equation below:

$$\mathrm{dB} = 20 \log_{10} \frac{\mathrm{V}}{\mathrm{V_{ref}}} \tag{37}$$

$\mathrm{V_{ref}}$ for acoustic emission waveform is $1\mu\mathrm{V}$. Results are shown in Table 5-3.

Table 5-3 Peak amplitude of both wave modes from sensors at varied distances from the source

Source type	Propagation distance (mm)	Peak amplitude (dB)	
		S_0 mode	A_0 mode
Out-of-plane	100	89.5	99.2
	200	80.2	86.3
	300	74.8	78.1
In-plane	100	100.0	100.0
	200	90.2	89.5
	300	86	77.5

The degree of the peak amplitude loss cannot reveal the attenuation effects concluded from the above WT analysis. Since recorded events saturated the amplitude scale, the degree of signal loss between the sensors is therefore quantified by the loss in energy.

Figure 5-4 shows the MARSE response from 3 sensors. The first 10 responses are from the out-of-plane displacement, and the later 10 responses are from the in-plane displacement. It is shown that the attenuation is less effective for the in-plane displacement generated acoustic emission signals.

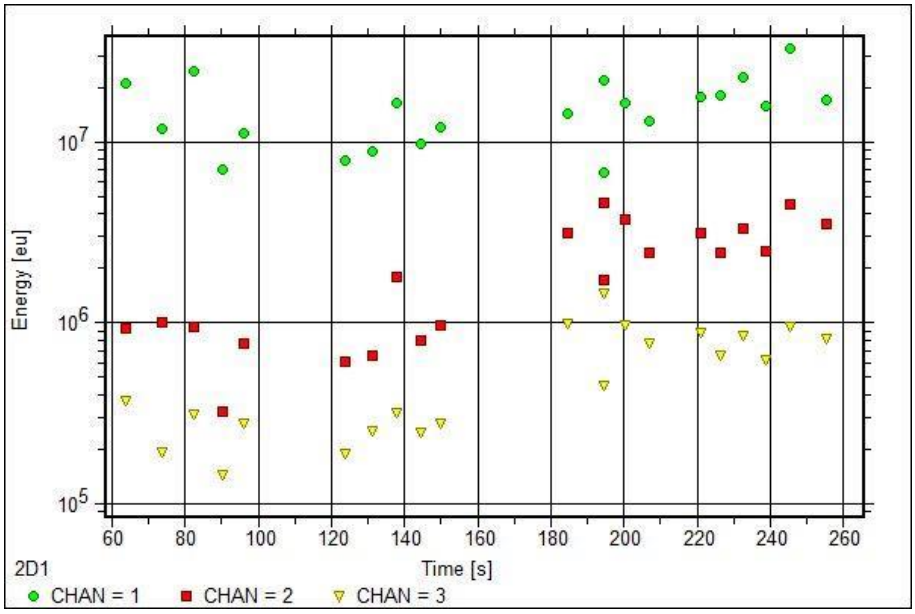

Figure 5-4 MARSE of 3 sensors from out-of-plane and in-plane displacement PLB tests

The ratio of MARSE is compared by dividing the MARSE from the further sensor by the MARSE of the nearer sensor from the acoustic emission source. The results are compared between out-of-plane source and in-plane source generated acoustic emission events, shown in Table 5-4. The MARSE ratio is the average value based on the 10 pencil lead breaks for both in-plane and out-of-plane sources.

Table 5-4 MARSE ratio between sensors for out-of-plane and in-plane sources

Source type	Sensor 1 to Sensor 2 (100mm)	Sensor 1 to Sensor 3 (200mm)
Out-of-plane Source	0.056	0.015
In-plane Source	0.194	0.059

A more significant drop of the MARSE ratio in the propagated waves is observed for the signals generated from the out-of-plane source. For an out-of-plane source, the dominant wave mode is A_0 mode, it is therefore concluded that the A_0 mode has a much higher attenuation rate than the S_0 mode in this material.

In summary, it's conclude that A_0 mode has a much higher attenuation rate than the S_0 mode in this material. In terms of effective signal detection distance,

it is recommended to place the sensor within a 300 mm radius distance from the source.

5.3 Three-Point Bending Test

In last section, the attenuation effect on the acoustic emission signals generated from pencil lead breaks is investigated. Based on the results, an effective signal detection distance is recommended. In this section, the attenuation effect on the acoustic emission signals from different damage mechanisms in GFRP panel during a three point bending test is investigated.

5.3.1 Materials and Specimens

The specimen used for three-point bending test is the same as the one used in pencil lead break test as illustrated in 5.2.1.

5.3.2 Experimental Procedure

Static three-point bending test is carried out. A constant supporting bar spacing is set at 76 mm. The test is performed using displacement control and a deformation rate of 1mm/min is used. The bending moment for the specimen is set as 8mm. A schematic diagram of the loading system and specimen is presented in Figure 5-5.

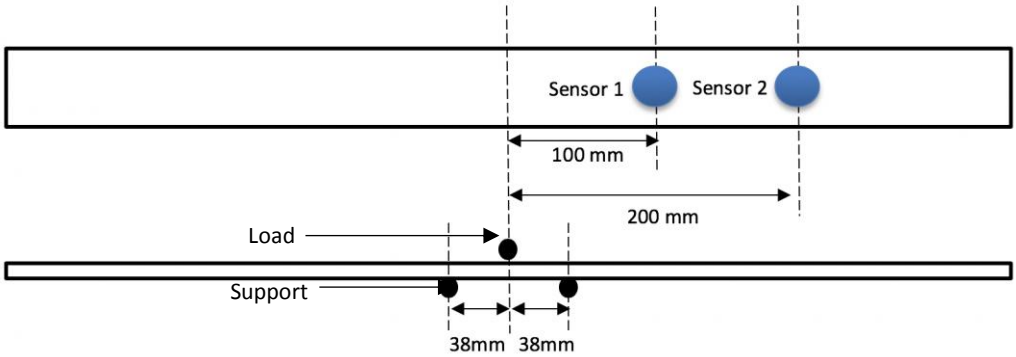

Figure 5-5 Loading configuration and sensor locations

For acoustic emission measurements, 2 VS150-RIC sensors with resonant frequency of 150 kHz are attached, as illustrated in Figure 5-6. Sensor 1 and sensor 2 are placed in a linear configuration which is 100 mm and 200 mm

away from the loading point respectively, see Figure 5-5. The acoustic emission sensors are fastened to the specimens by G-clamps. Grease is applied on the contact surface between sensors and specimens to improve the wave conduction. The experiment set up is shown in Figure 5-6. The signals are pre-amplified 34 dB and recorded by a Vallen 16-channel data acquisition system. The detection parameter is shown in Table 5-5. A computer is used to control the data acquisition system.

Table 5-5 Detection parameter for data acquisition

Detection parameter	Value
Threshold	40 dB
Sampling Rate	3.3 MHz
HDT	50 μs

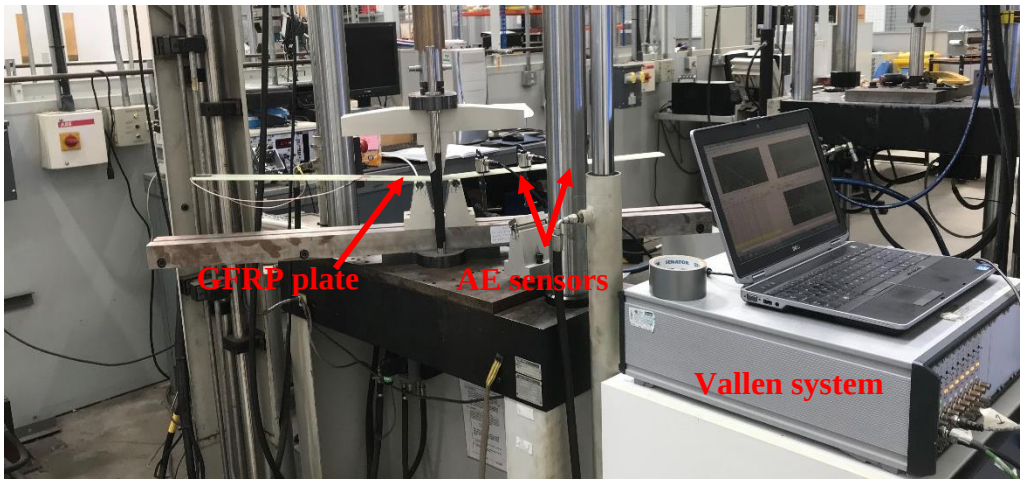

Figure 5-6 Three point bending test on GFRP specimen

5.3.3 Results and Discussion

5.3.3.1 Attenuation of Acoustic Emission Signals

First, the total number of acoustic emission hits captured by both sensors is investigated, the result is shown in Table 5-6.

Table 5-6 Cumulative number of hits for two sensors

Sensor	Cumulative number of hits
1	26360
2	8052

It is shown that sensor 1 acquires much more acoustic emission hits than sensor 2. This is because that sensor 1 is placed close to the damage area,

the acoustic emission signals with low energy attenuate and cannot trigger sensor 2 for acquisition. This is also evident in Figure 5-7 and Figure 5-8, the signals acquired by sensor 1 have a peak amplitude and MARSE values than the sensors acquired by sensor 2.

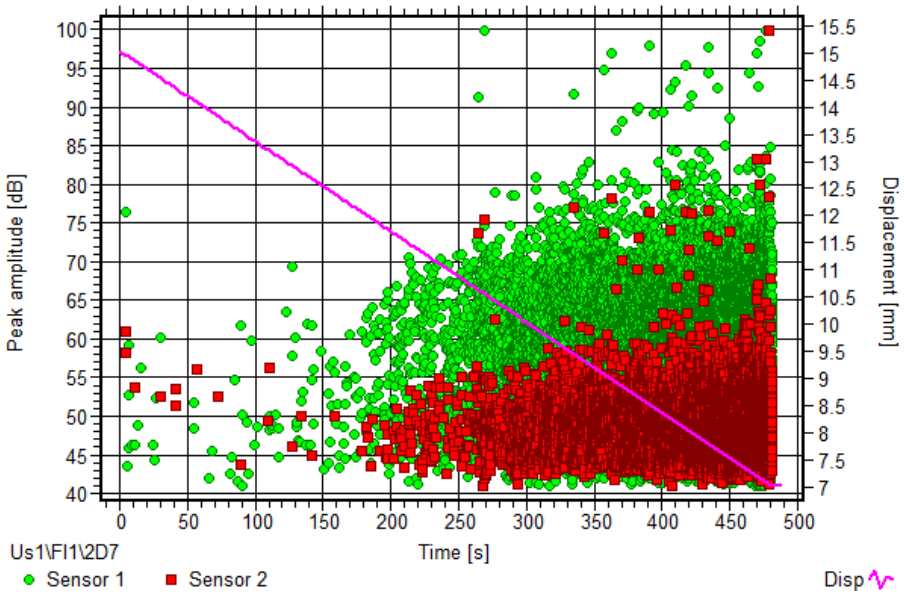

Figure 5-7 Peak amplitude distribution of sensor 1 and sensor 2

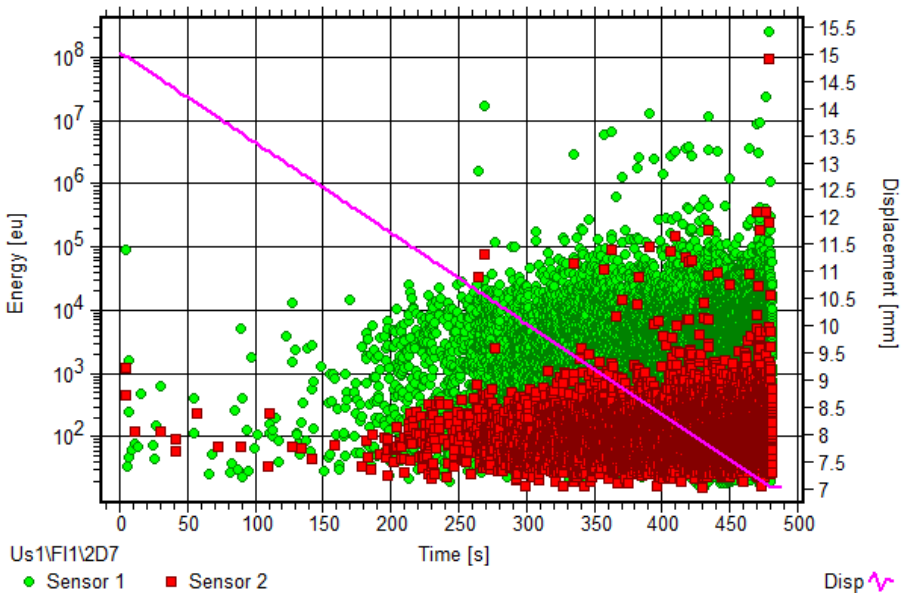

Figure 5-8 MARSE distribution of sensor 1 and sensor 2

The frequency content of recorded acoustic emission signals is also investigated. FFT analysis is applied on these signals. Peak frequency has

been the most widely adopted frequency parameter for describing damage in composite materials [114], [115]. The peak frequency distribution is shown in Figure 5-9. It can be seen that the peak frequency of acoustic emission signals acquired by both sensors concentrated around 150 kHz, which is the resonant frequency of the sensors. There is a group of signals with lower frequency peaks (<130 kHz) before 300s of the test have only been acquired by sensor 1. These signals could attribute to matrix cracking which generate acoustic emission signals with low frequency content as well as low MARSE. Some signals with high frequency components (above 200 kHz) occur in the final stage of the test, which can be due to the fibre breakage damage.

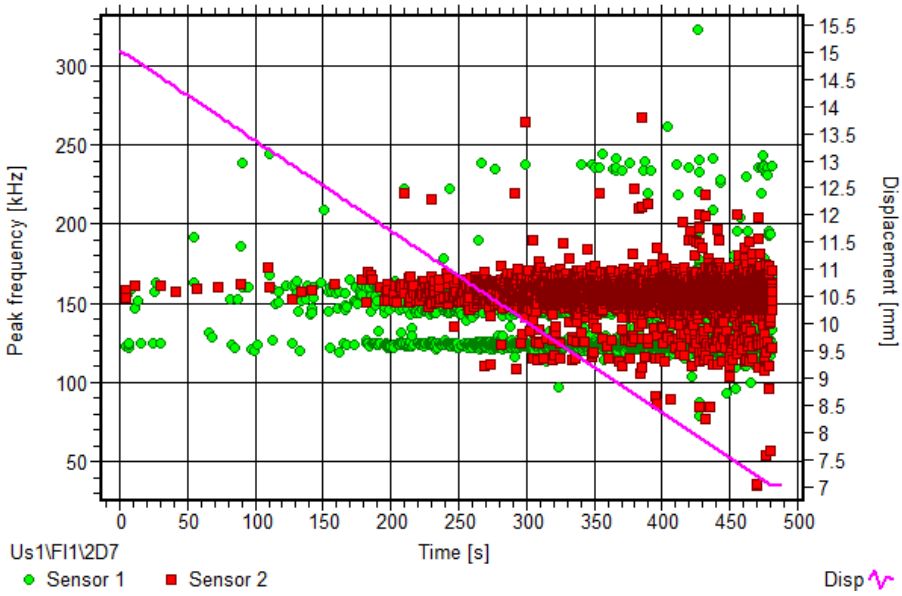

Figure 5-9 Peak frequency distribution of sensor 1 and sensor 2

From the above investigations, it is concluded that the attenuation effect on acoustic emission time domain features is quite significant. On the other hand, the effect on the acoustic emission frequency domain features is not as obvious.

5.3.3.2 Source Characterization

In this section, the objective is to find the relationship between acoustic emission signal features and damage mechanisms in GFRP materials. The

pattern recognition method proposed in 4.2.3.2 is applied on the signals acquired from sensor 1 and sensor 2 respectively.

In the last section, it shows that the acoustic emission frequency domain features are less affected by the attenuation effect. Besides, the identification of the different damage mechanisms through frequency-based methodologies in acoustic emission data analysis from loaded composite materials has also been studied in [116], [63]. In these experiments, both carbon and glass fibre breakage and fibre pull out showed a relatively high frequency range (above 300 kHz), while the frequency content of matrix cracking corresponded to the low frequency range (30–150 kHz), and delamination and debonding usually occurred in the frequency range in between (200–300 kHz).

Therefore, peak frequency is selected to initiate the clustering process. Due to the number of damage mechanisms in the specimen is unknown, the feature selection algorithm is applied with 2, 3 and 4 clusters. The data processing process is separated for the data obtained by sensor 1 and sensor 2. For the data obtained by sensor 1, at the first interaction, the lowest DB index is given by the combination with MARSE for all three cases which are 2, 3 and 4 clusters, see Figure 5-10.

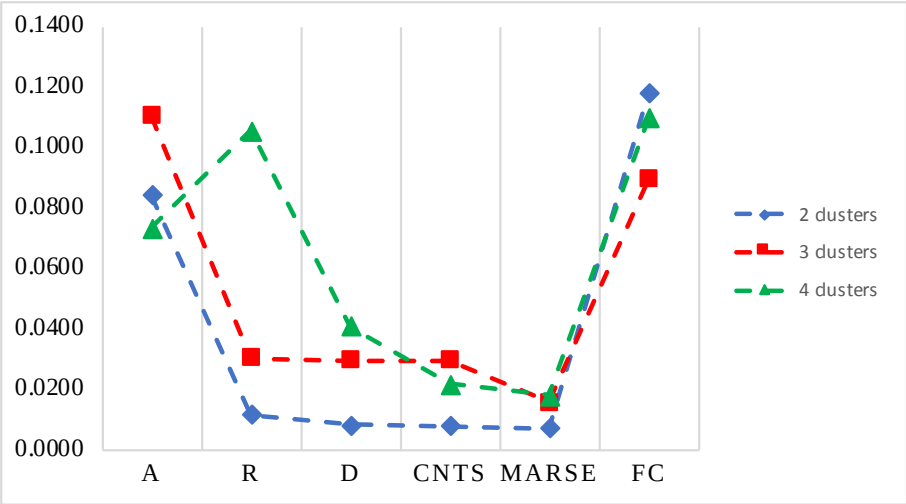

Features	DB index		
	2 clusters	3 clusters	4 clusters
Peak amplitude (A)	0.0843	0.1104	0.0734

Rise Time (R)	0.0120	0.0305	0.1055
Duration (D)	0.0085	0.0299	0.0409
Number of counts (CNTS)	0.0082	0.0298	0.0222
Energy (MARSE)	0.0076	0.0160	0.0181
Frequency centroid (FC)	0.1180	0.0896	0.1096

Figure 5-10 Channel 1 – two clusters using peak frequency as a reference

Therefore, peak frequency and MARSE are selected as the input parameters for K-means clustering. An investigation of choosing the optical number for the number of clusters is carried out.

A widely used method to choose an optimal value for the number of clusters is Silhouette analysis. A Silhouette coefficient is defined to study the separation distance between the resulting clusters with a higher value, indicating better cluster quality. R. Gutkin et al. investigated failure in CFRP using three different pattern recognition techniques including k-means, self-organizing maps combined with k-means, and competitive neural networks on acoustic emission signals [64]. The number of clusters, k, is chosen between 0 and 2 so that the Silhouette coefficient is maximized. The results from the clustering analysis follow the pattern found in peak frequencies distributions. Li Li et al. identified a framework for the analysis of a link between the damage mode and acoustic emission signals originating from the damage initiation and development of 2D and 3D glass/epoxy woven composites loaded in tension. The number of clusters for k-means ++ analysis is evaluated using both Silhouette coefficient and the Davies-Bouldin index. Acoustic emission signals are divided into four groups which corresponds to matrix cracking, fibre/matrix debonding, delamination, and fibre breakage, respectively [117]. Crivelli, D. et al. developed a technique based on Self-organizing Mapping in conjunction with the k-means clustering algorithm to separate the acoustic emission signals from tensile tests of pultruded GFRP specimens [118]. The optimal number of clusters is evaluated using three performance indexes including Davies-Bouldin, Silhouette and Calinski-Harabasz. The result is selected depending on the most voted number of clusters. In this work, the optimal number of clusters is chosen by taking into account both Calinski-Harabasz

and Silhouette quality indexes [119]. The calculation is based on the selected feature, peak frequency and MARSE.

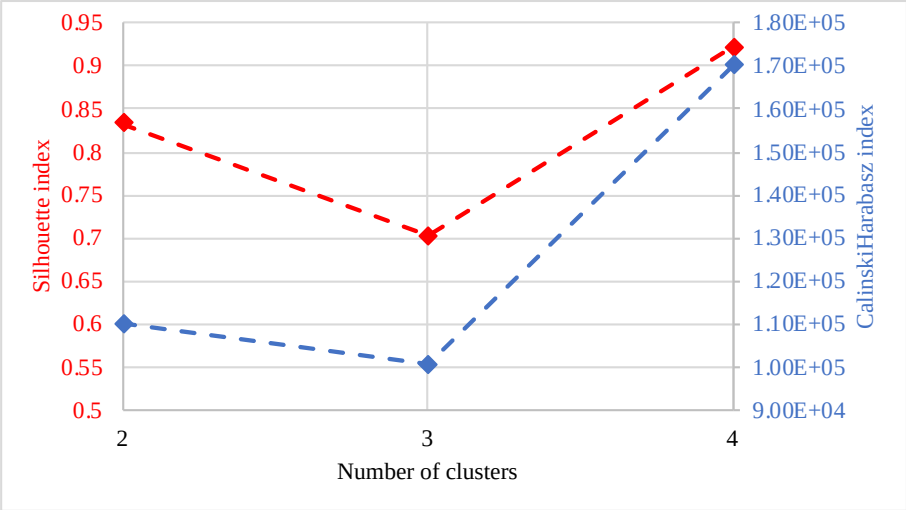

Quality index	Value		
	2 clusters	3 clusters	4 clusters
Silhouette	0.8328	0.7028	0.9212
Calinski-Harabasz	1.10E+05	1.01E+05	1.70E+05

Figure 5-11 Number of clusters evaluated by the Silhouette index and the Calinski-Harabasz index.

Both Silhouette and Calinski-Harabasz indexes identify 4 as the best performing clustering number. Based on the above calculations, 4 is therefore selected as the optimal number of clusters. Figure 5-12 shows the partition of acoustic emission signals obtained by the clustering analysis. Peak frequency and MARSE are used to visualize the position of the signal clusters. It is shown that the acoustic emission signals are well-separated into 4 clusters in the peak frequency – MARSE space. Acoustic emission signals originating from cluster 1 are related to the peak frequency ranging from 130 kHz to 175 kHz. The signals with peak frequency ranging from 125 kHz to 150 kHz and 125 kHz to 175 kHz are grouped as cluster 3 and 4 respectively. Cluster 2 are identified with a group of signals of peak frequency ranging from 200 kHz to 250 kHz.

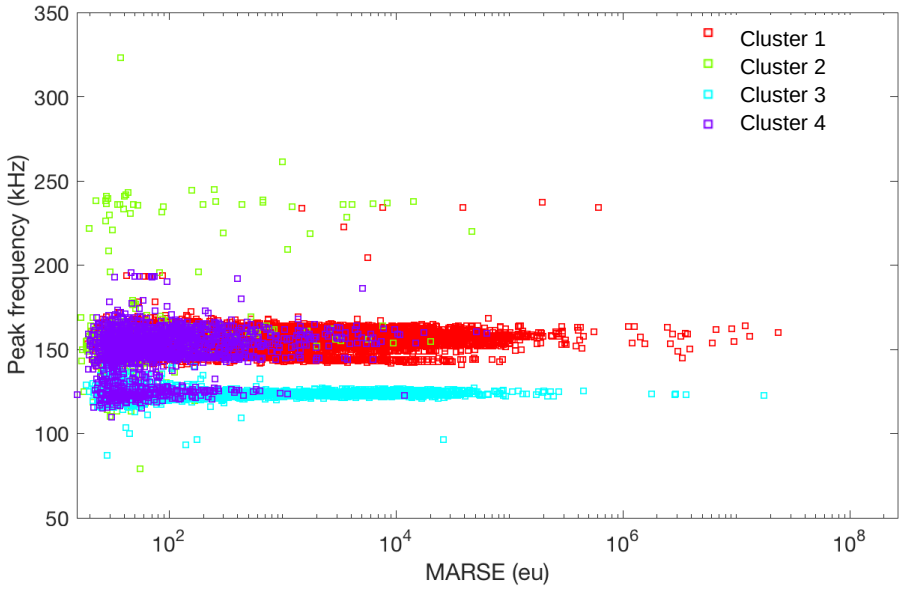

Figure 5-12 Clustering results: the partition of AE signals on MARSE - peak frequency

The characteristic frequency range of each failure mode signals are well identified in literature review, see Table 5-7.

Table 5-7 Frequency analysis results

Failure Modes	Frequency Range (kHz)			
	Glass/ Polyester [120]	Glass/ Polypropylene [63]	Carbon/ Epoxy [121]	Carbon/ Epoxy [64]
Matrix cracking	30–150	×	<100	0–50
Delamination	×	×	×	50–150
Debonding	180–290	100	200–300	200–300
Fibre breakage	300–400	450–550	400–450	400–500
Fibre pull out	180–290	200–300	×	500–600

The four groups of acoustic emission signals are finally correlated with the damage mechanisms by comparing their peak frequency characteristics with literature review results.

The literature review stated that signals generated from debonding have a frequency range above 200 kHz, therefore signals from cluster 2 are associated with debonding. As for signals in cluster 1, 3, and 4, which correspond to a lower peak frequency range, signals in these three clusters can be linked with matrix cracking and delamination. In order to further

discriminate the damage mechanisms of the signals from cluster 1, 3, 4. Other acoustic emission signal features are investigated.

D.J. Collins investigated the abilities of acoustic emission testing to detect and characterize damage in composite materials, and concluded that peak amplitude, peak frequency and average frequency are all accurate methods of detecting and characterizing damage in composite materials [122]. De Groot et al. found that the classification in CFRP using average frequency can separate the signals into four types: the matrix cracking (90 kHz – 180 kHz), the debonding (240 kHz – 310 kHz), the fibre pull-out (180 kHz – 240 kHz) and fibre breakage (>300 kHz) [115]. Therefore, the positions of these clusters in time domain features such as average frequency, peak amplitude, duration, number of counts are presented in Figure 5-13.

It is shown that signals from cluster 2 which are recognized generating from debonding have a relatively higher average frequency response (above 150 kHz). The average frequency values are not completely consistent with De Groot et al. ‘s findings, however the results show the same trend which is that in comparison with the signals from matrix cracking and delamination, the signals debonding have a relatively high average frequency response.

N. Fallahi et al. use Self-Organizing Map (SOM) method to cluster the acoustic emission signals according to the fracture modes in carbon-epoxy composite laminates during Double Cantilever Beam. They concluded that the signals from fibre breakage and delamination have a higher peak amplitude response than the ones from matrix cracking. Signals from cluster 1 and 4 have similar peak frequency distributions, however the signals of cluster 4 have relatively lower MARSE values. Figure 5-13 (a) show that signals of cluster 4 also have a relatively lower peak amplitude response, therefore this group of signals correspond to matrix cracking. For signals from cluster 1 and 3, signals of cluster 1 have a higher peak frequency response than signals of cluster 3, however no significant differences can be found on acoustic emission time domain features (peak amplitude, duration, rise time and number of counts). Therefore, it is believe that signals from cluster 1 and cluster 3 correspond to

the same fracture mechanism. Signals in these two clusters have a higher peak amplitude response in comparison with the events in cluster 4. Therefore, in the author's opinion, events in cluster 1 and 3 correspond to delamination.

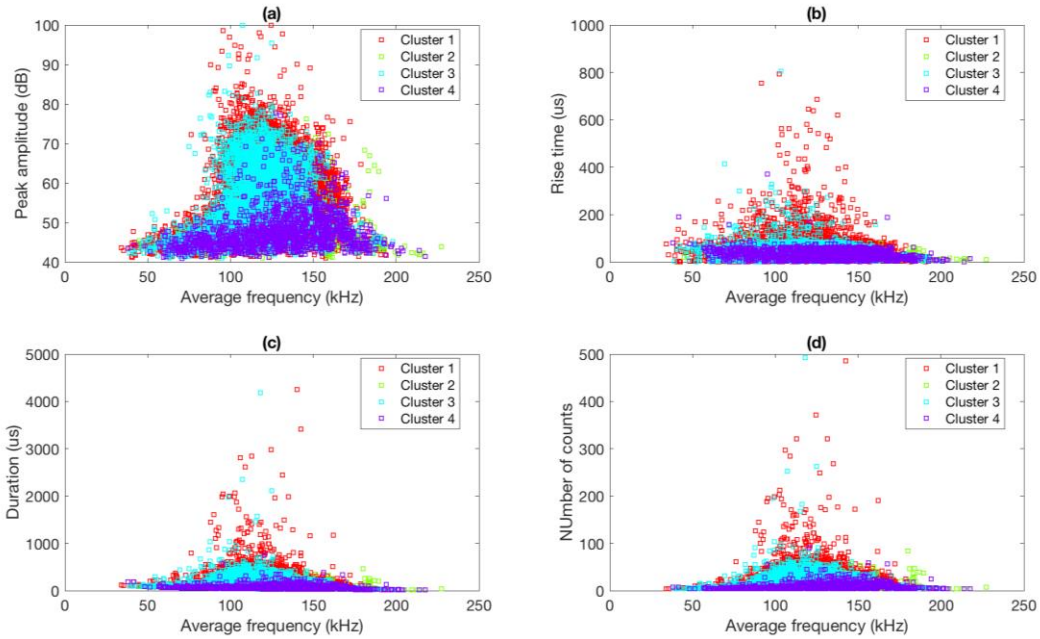

Figure 5-13 Clustering results: the partitions of AE signals on time domain features (a) average frequency vs peak amplitude (b) average frequency vs rise time (c) average frequency vs duration (d) average frequency vs number of counts

The above pattern recognition method demonstrates an effect way of discriminating the signals from different damage mechanisms. Since the main objective of this chapter is to investigate on the influence of attenuation on acoustic emission signals in composite materials. The same algorithm is applied on the signals obtained by sensor 2, which is further away from the source.

In 5.3.3.1, the attenuation of acoustic emission signals are evaluated. The loss of peak amplitude and MARSE are evident between the sensors. On the other hand, the peak frequency distributions of the signals obtained from these two sensors don't show a big difference from each other. Therefore, for signals obtained by sensor 2, peak frequency is also selected to initiate the feature selection process.

The selection algorithm is applied with 2, 3 and 4 clusters. For the signals acquired by sensor 2, instead of MARSE, the lowest DB index is given by the combination with number of counts for all three cases which are 2, 3 and 4 clusters, see Figure 5-14.

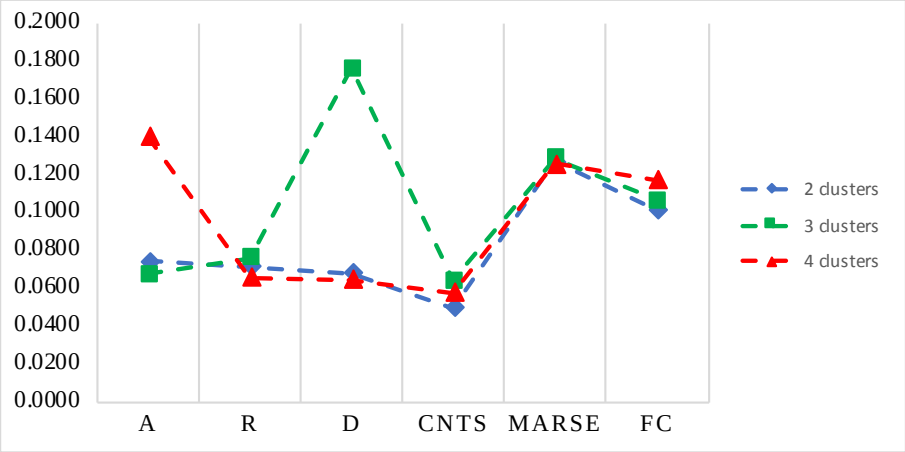

Features	DB index		
	2 clusters	3 clusters	4 clusters
Peak amplitude (A)	0.0739	0.0671	0.1400
Rise Time (R)	0.0714	0.0760	0.0655
Duration (D)	0.0676	0.1757	0.0647
Number of counts (CNTS)	0.0496	0.0641	0.0574
Energy (MARSE)	0.1267	0.1282	0.1256
Frequency centroid (FC)	0.1008	0.1060	0.1167

Figure 5-14 Channel 2 – DB index using peak frequency as a reference for 2, 3, 4 clusters

Concerning pattern recognition using k-means clustering, both Calinski-Harabasz and Silhouette quality indexes are used to calculate the optimal number of clusters, see Figure 5-15.

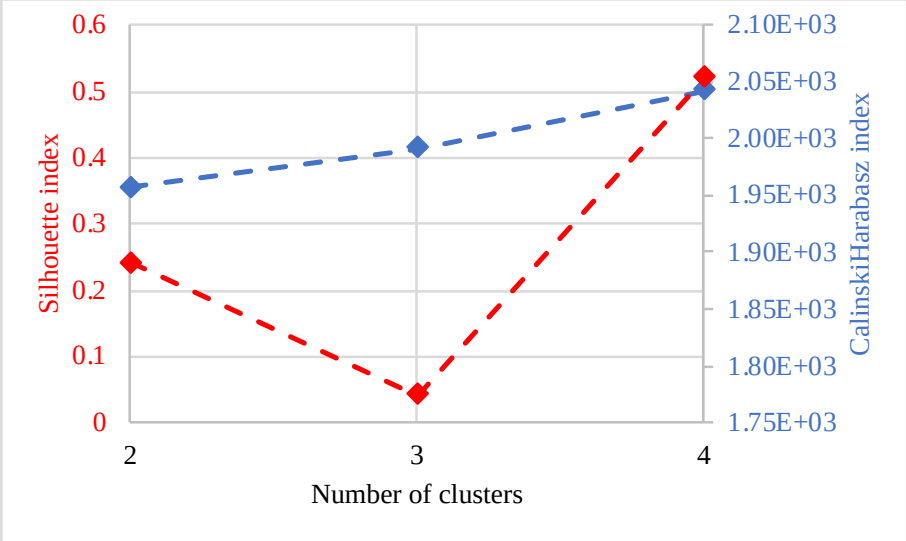

Quality index	Value		
	2 clusters	3 clusters	4 clusters
Silhouette	0.3548	0.4142	0.501
Calinski-Harabasz	1.89E+03	1.77E+03	2.05E+03

Figure 5-15 Number of clusters evaluated by the Calinski-Harabasz and Silhouette quality indexes

The same as the results from channel 1, both Calinski-Harabasz and Silhouette quality indexes identify 4 as the optical number of clusters. Therefore, 4 clusters is selected for k-means clustering.

Figure 5-16 shows the partition of acoustic emission signals obtained by the above pattern recognition method. Number of counts and peak frequency are used to visualize the position of the signal clusters. It can be seen that three clusters with peak frequency range from 50 kHz – 140 kHz, 140 kHz – 170 kHz and 170 – 250 kHz respectively. Another cluster also features the peak frequency range from 140 kHz – 170 kHz, but with a higher number of counts.

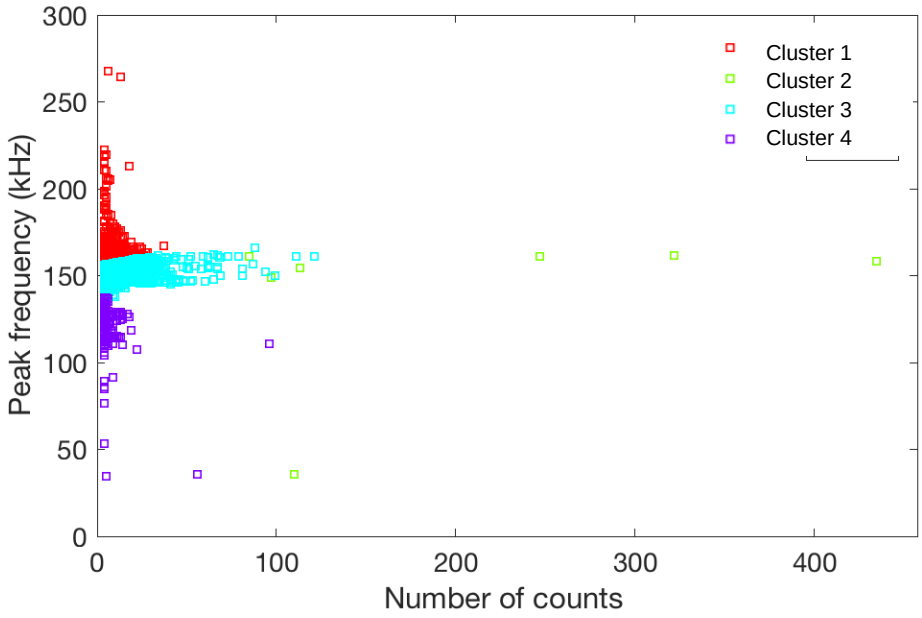

Figure 5-16 Clustering results: the partition of AE signals on number of counts - peak frequency

In comparison with clustering results on the signals obtained from sensor 1, it can be seen that the majority of the signals are in cluster 3, with the peak frequency range from 140 – 175 kHz. This is similar to the results from sensor 1, as for the cluster with the most number of events, the peak frequency range is from 125 kHz to 170 kHz. The high peak frequency range is now clustered from 170 kHz to 250 kHz instead of 200 kHz – 250 kHz. **Error! Reference s ource not found.** shows the number of events for each cluster.

Table 5-8 Clustering results : the number of events for four clusters

Cluster	Peak frequency range (kHz)	Number of events
1	170 – 250	1517
2	140 – 175	7
3	140 – 175	2802
4	50 – 140	182

As the frequency domain features are not consistent with the results from the results from sensor 1, other approaches have to be investigated for identifying the mechanisms relating to these clusters. Figure 5-17 shows the a few time domain features including peak amplitude, rise time, duration and number of counts distributions as a function of average frequency where the signals belong to each cluster are identified. Signals from cluster 4 with a lower peak

frequency range response are having a lower peak amplitude response, which can prove that this group of signals correspond to matrix cracking. The above results are consistent with the conclusions on the signals from sensor 1. Signals from cluster 1 have a high peak frequency response. It can be seen from Figure 5-17(a) that unlike the signals from cluster 2 and 3, signals from cluster 1 have a high average frequency response (above 150 kHz). Therefore it's concluded that this group of signals correspond to debonding. Signals from cluster 2 and 3 show no significant differences in terms of peak frequency response and they have a higher peak amplitude response in comparison with the events in cluster 4. Therefore, in the author's opinion, signals in cluster 1 and 3 correspond to delamination.

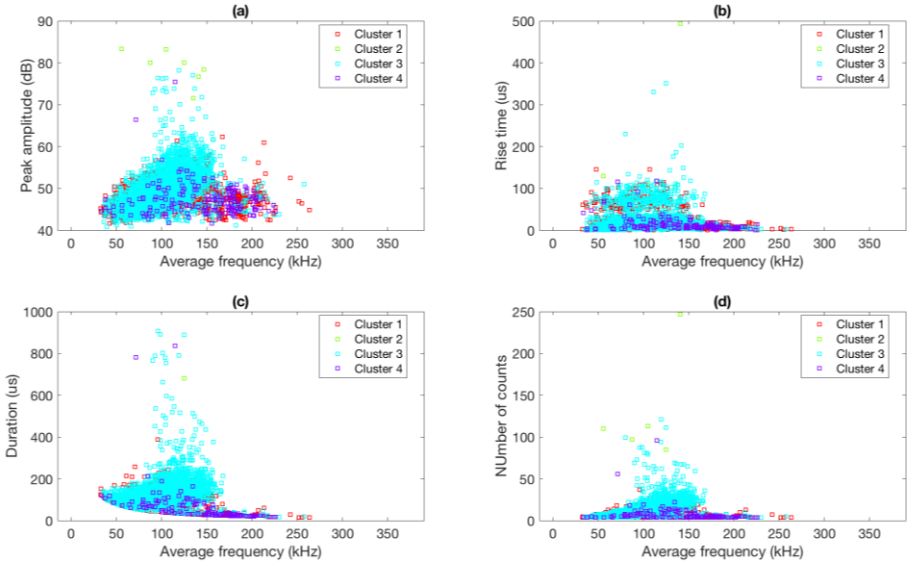

Figure 5-17 Clustering results: the partitions of AE signals on time domain features (a) average frequency vs peak amplitude (b) average frequency vs rise time (c) average frequency vs duration (d) average frequency vs number of counts

It is shown that acoustic emission signals classification by an pattern recognition approach yields four signal clusters which correspond to three different damage mechanisms. The attenuation effects could lead to an effect on the frequency range of the clusters as well as on the number of signals in each cluster.

5.4 Conclusions

Pencil lead break tests and three point bending tests are carried out on a GFRP panel.

For the pencil lead break tests, the attenuation effect of S_0 and A_0 wave mode investigated through the analysis of the signals recorded from the sensors at different distances. It is shown that A_0 mode has a much higher attenuation rate than the S_0 mode in this material. In terms of signal detection distance, it is recommended to place the sensor within a 300 mm radius from the source.

For the three point bending test, it is shown that the attenuation effect has a significant impact on the acoustic emission time domain features, the effect on frequency domain features are not as obvious. The proposed pattern recognition method is then applied to differentiate the damage mechanisms. An optical number of clusters analysis is carried out due to the unknown number of damage mechanisms during the test. The method is applied on signals from sensor 1 and sensor 2 separately. It is shown that acoustic emission signals classification yields four signal clusters which correspond to three different damage mechanisms, matrix cracking, delamination and debonding. The attenuation effects could lead to an effect on the frequency range of the clusters as well as on the number of signals in each cluster.

6 An Experimental Study of Acoustic Emission Methodology for in Service Condition Monitoring of Wind Turbine Blades

6.1 Introduction

Wind turbine blades are manufactured from composite materials using fibreglass and polyester or fibre glass and epoxy, sometimes in combination with wood and carbon [7]. The most commonly used types of composite materials in wind turbine industry are carbon or glass fibre – reinforced plastics (CFRP/GFRP). The micro-damage mechanisms in composites can severely affect the performance of composites therefore correct characterisation of these mechanisms can help avoid catastrophic structural failures.

Advances in acoustic emission testing techniques for condition monitoring of wind turbine blades have been reported in the literature [9], [10], [11]. The main advances include the ability to locate and characterize damage in real time. In determining damage initiation and identifying failure mechanisms, any parameters that affect the acoustic emission signal features will have an impact on results,

In chapter 4 and chapter 5, the two parameters that can affect the acoustic emission signal features including the sensor frequency characteristics and detection distance between the source and the sensor are carefully examined through a series of experiments.

Based on the knowledge obtained through the work above, in this chapter, a laboratory study is reported regarding fatigue damage growth monitoring in a

complete 45.7 m long wind turbine blade. This blade is typically designed for 2MW generator. The main objective of this work is to investigate the feasibility of in-service monitoring of the structural health of blades through damage localization and characterization using acoustic emission technique.

Cyclic loading by compact resonant masses is performed to accurately simulate in-service load conditions and 187 kcs of fatigue were performed over periods which totalled 21 days, during which acoustic emission monitoring is performed with a 4 sensor array. Before the final 8 days of fatigue testing a simulated rectangular defect of dimensions 1 m × 0.05 m × 0.01 m is introduced into the blade material. The growth of fatigue damage from this source defect is successfully detected and localized from acoustic emission monitoring. A pattern recognition method is applied to characterize different acoustic emission activities corresponding to different fracture mechanisms.

6.2 Experimental

6.2.1 Experimental Rig

6.2.1.1 Wind Turbine Blade Support

The blade being tested is a glass-reinforced plastic composite blade, measuring circa 45.7 m in length, with 2 internal supporting webs running the entire length of the blade. An external view of entire blade is shown in Figure 6-1.

(a)

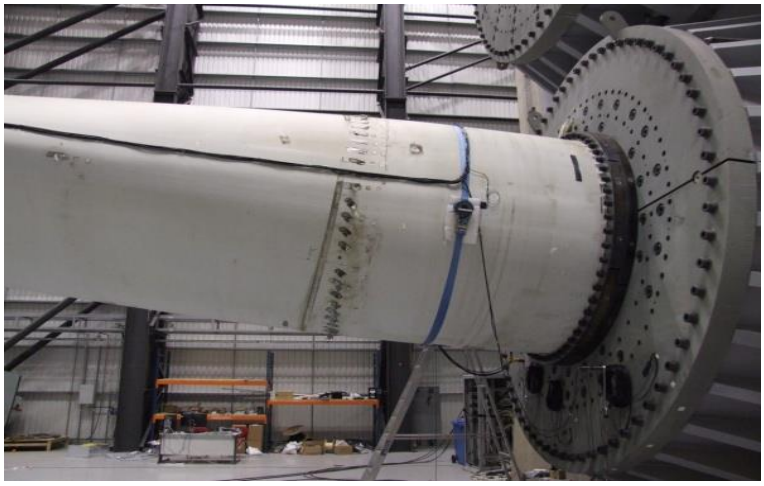

(b)

Figure 6-1 Wind Turbine Blade under Test (a) Full length view of the blade prior to installation (b) Close up view of the blade root on the test stand

6.2.1.2 Cyclic Fatigue Loading

Multiple pairs of Compact Resonant Masses (CRMs) are used to excite vibrations in the blade. The CRM is a common test methodology used throughout the industry, to excite blade to the desired natural frequency. The CRM system consists of a moving mass, mounted on a carriage that slides on tracks. The carriage and tracks ate mounted on a frame, which is fixed to a loading saddle addles at initial distances of 30m and 35m measured from the root of the blade, as shown in Figure 6-2. Within the CRM system, the variables include:

- Position of CRM along the blade length;
- Size of the moving mass;
- Frequency of the moving mass;
- Amplitude of the moving mass.

A combination of actuator position and mass, and strain ranges are used in the control of the test. As the natural frequency is fixed for a particular blade and mass combination, by controlling the above parameters will make sure its frequency of movement matches the natural frequency of the blade-mass system. Strain gauges provide feedback to ensure the blade is being tested as the correct strain/bending moment level. A MOOG Hydraulic Test Controller

and bespoke software is used to apply a sinusoidal excitation profile which is operated at the first resonant mode of the blade, such that the hydraulic power consumed by the actuators is almost entirely coupled into the blade.

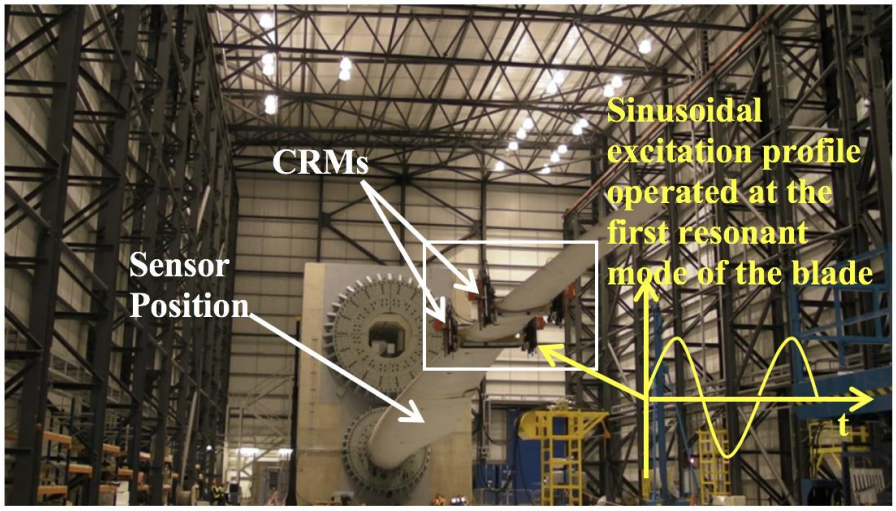

Figure 6-2 Compact resonant masses installed on the wind turbine blade

6.2.2 Acoustic Emission Monitoring Set Up

Acoustic emission signals generated during the test are recorded and analysed using a data acquisition system based on the National Instruments PXIe-1071 card embedded in a bespoke enclosure which provide environmental and impact protection. The sampling rate is 500 kHz. A LabVIEW programme is used to control the data acquisition.

The wind turbine blade under test is large in size and wind turbine designers often employ an increased thickness section of GRP to increase strength. This creates challenges for acoustic emission monitoring in wave propagation because of wave attenuation. Attenuation will reduce the measured signal amplitude and this can cause lack of damage observability. By analysing the two primary wave modes which exist in the wind turbine blade, the extensional and flexural wave modes, Van Dam et.al determined the dispersion curves, their results showing that the sensor spacing should be limited to a maximum value of 1m [123]. In this study an attenuation test using pencil lead break is performed initially on the surface of the blade, in order to determine the

required number and spacing of the sensors. Four sensors are used and the locations of the sensors are shown in Figure 6-3 and Table 6-1.

Acoustic emission can be detected in a wide frequency range from 1 kHz to 1 MHz. Based on the reported frequency range of the failure modes, when the structure reaches a critical condition, fibre fracture-generated acoustic emission signals generally have frequency increments between 300 kHz and 600 kHz. In this paper, we aim to provide an early warning sign of failure, therefore acoustic emission signals generated from matrix cracking, delamination, and debonding are to be discriminated from signals generated from noise. Studies showed that the frequency content of the signals generated from matrix cracking corresponds to the low frequency range (up to 180 kHz), while delamination and debonding usually have a frequency range in between (200–300 kHz). Thus, the minimal sampling rate needed to avoid aliasing is between 400–600 kHz. Four acoustic emission sensors with resonant 150 kHz frequency and a frequency response over the range of 100–450 kHz are used in the experiment. The sensors are connected to an external amplifier with a gain of 34 dB. The sensors are mounted on the blade internally in magnetic holders which engaged with steel collars adhesively bonded to the blade surfaces to ensure constant acoustic coupling, facilitated by the use of a gel couplant. Acoustic emission signals are recorded and analysed using a data acquisition system based on a National Instruments PXIe-1071 card. The sampling rate for this test is 500 kHz to save storage and to improve computational speed. The sensors are mounted internal to the blade, as illustrated in Figure 1. A band pass filter of 5 kHz–250 kHz (Nyquist frequency) is added before the sampler to limit the frequency content of the input filter. Acoustic emission data acquisition can be affected by numerous factors associated with the electronic instruments, cables, sensors, background noise, and threshold. In this study, to verify the response of our acoustic emission system performance, a ‘Hsu pencil source (pencil lead break source)’ is used as the verification source. The calibration followed the ASTM E2374-15 standard. An attenuation test using the pencil lead break method is performed initially on the surface of the blade in order to determine the required number and spacing of the sensors.

(a)

(b)

Figure 6-3 Acoustic Emission sensors mounted internally on the blade (a) sensors mounted between the two webs (b) sensors mounted the trailing edge side

Table 6-1 Sensor locations

sensor number	Location
AE1	In between webs, 9.8 m from root
AE2	In between webs, 8.2 m from root
AE3	Trailing edge side of web, 8.4 m from root
AE4	Trailing edge side of web, 9.6 m from root

6.2.3 Experimental Procedure

6.2.3.1 Fatigue Testing

An evaluation of the vibration characteristics of the blade is carried out in a modal test prior to the fatigue test. The blade in service is most likely to be

excited below the first natural frequency due to the observed frequency spectrum of the wind loads. Therefore, the first natural frequency is selected as the frequency of cyclic loading during the fatigue test. The fatigue test equipment adding mass to the blade is shifting the natural frequencies of the system and the mode frequencies are determined as a function of the static mass loading when the CRMs are attached. A set of 5g accelerometers bonded to the surface of the blade at predefined locations allowed the response measurement during the modal test.

The effective loads applied to the blade are increased in stages during the fatigue test in order to promote the crack propagation. The cyclic loading test is performed in three stages over 6 weeks and details are presented in Table 6-2 and Figure 6-4. A nominal root bending moment for fatigue loading is selected based on prior experience blades with blades of similar length.

Table 6-2 Schedule of experiments

Stage	Duration	Days	Experimental information	Load
1	6 days	Day 1- Day 6	Fatigue test with 0 m defect induced	25% / 50%
	3 days	Day 7 – Day 9	Crack enlarge and modal tests	
2	7 days	Day 10 – Day 17	Fatigue test with 0.2 m defect induced	50% / 70%
	3 days	Day 18 – Day 20	Crack enlarge and modal tests	
3	8 days	Day 21 – Day 29	Fatigue test with 1m defect induced	70% - 115%

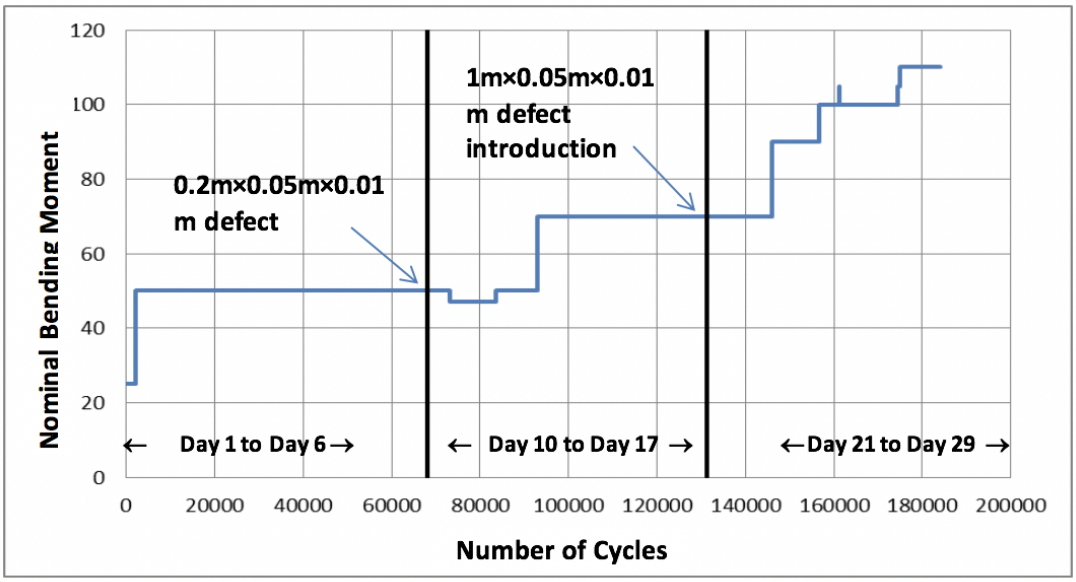

Figure 6-4 Nominal root bending moment of loading used versus number of cycles

After roughly 67,000 fatigue cycles (Day 1- Day 6) at 50% nominal load, a 0.2 m (along the boundary) × 0.05 m (perpendicular to the boundary) × 0.01 m (blade thickness direction) crack is made in one of the shear webs at 30m from the blade tip (Figure 6-5(a)). The acoustic emission sensors are located in this region internally. Testing continued for a further 65,000 cycles (Day 10 – Day 17) at 50% and 70% load without any noticeable changes in the blade structure. It is then decided to increase the size of length of the induced defect to 1 m × 0.05 m × 0.01 m (Figure 6-5 (b)) in order to increase the likelihood of further damage propagation for the purpose of evaluating the proposed acoustic emission damage monitoring technique. However, further testing at 70% load and then 80% yielded no noticeable change in the blade structure. So, a decision is made to further increase the test load to 100% and subsequently this is increased further to 115% on the final day of testing to accelerate the damage growth within a short period of time compared with the normal operation time. This introduced a much more challenging environment for acoustic emission monitoring due to the high 'coherent' noise generated by the movement and friction of the blade. The test environment is optimized to match with the damage level that the blade undergoes in service, where the background noise level is much lower.

6.2.3.2 Visual Inspection Results

Generally, every second day throughout the tests the blade internal (at 9 m from the root) surfaces are inspected for crack initiation or propagation for two reasons: one is to ensure that there is sufficient composite failure during the testing for verification of the acoustic emission system; also for validation of the acoustic emission system, by tracking the time and location of acoustic emission events and correlating them the defect growth history identified by the visual inspections.

(a)

(b)

Figure 6-5 Induced Defect (a) Day 7- Day 9: Defect induced into the internal surface of the blade at a blade-web boundary (b) Day 18- Day 20: Defect extended to 1 m×0.05 m×0.01 m

Typical defect photographs taken during visual inspection are shown in Figure 6-6. The testing focused on the induced internal cracks, which is considered to have a great effect on the blade structural integrity. No significant damage growth occurred until the final three days (Day 27 – Day 29) of testing when delamination and channel cracking initiation and growth are observed on the last day of testing. Figure 6-6 (a-d) shows some of the typical damage initiation and growths in the blade structure that arose in this period. This damage is mostly delamination and channel cracking, but also slight crack propagation which is noticed at the edge of the manually induced cut in the shear web.

(a)

(b)

(c)

(d)

Figure 6-6 Defect growth (a) Day 27: The start of damage propagation (b) Day 28: Further channel cracking arising on (c) Day 29: Delamination reached 0.15 m (d) Further growth in the delamination to 0.3 m

6.3 Acoustic Emission Signal Analysis

6.3.1 Acoustic Emission Signal Detection Threshold

Acoustic emission monitoring is carried out throughout all fatigue tests. Variations and vibrations in the drive chain from the gear teeth and tower caused by wind impact can couple into the blades because of the long wavelengths involved. The steady wind impact will generate standing waves which will be largely time coherent but variable with the wind speeds;

particularly gusts will generate time random components in the standing waves. These sources thus constitute noise which can be both random and coherent, sometimes exceeding by far the crack signals. From the viewpoint of monitoring the progress of damaged mechanisms in blades all of these sources increase the complexity of robust detection. The detection threshold for the recorded events is set at 40 dB to largely eliminate signals from noise; this value is obtained through the pencil lead break testing and is used in similar experiments [124]. In this experiment, the signals are saved for 0.1 s once triggered, an example of which is shown in Figure 6-7.

Whenever the signals generated from noise exceeds a defined threshold, it is called a false alarm. The probability of false alarm $\mathrm{P_{fa}}$ is a number which lies between 0 and 1 which can be calculated as shown

$$\mathrm{P_{fa}} = \frac{1}{2}\left[1 - \mathrm{erf}\left(\frac{\mathrm{TNR}}{\sqrt{2}}\right)\right] \tag{38}$$

where TNR is the threshold of noise ratio, and

$$\mathrm{erf(x)} = \frac{2}{\sqrt{\pi}}\int_0^{\mathrm{x}} \mathrm{e}^{-\mathrm{t}^2}\,\mathrm{dt} \tag{39}$$

As seen in Figure 6-7 the background noise level during this test is 32dB, and with the detection threshold set at 40dB, one obtains

$$\mathrm{TNR} = \frac{40\mathrm{dB}}{32\mathrm{dB}} = 1.25 \tag{40}$$

The resulting probability of false alarm becomes

$$\mathrm{P_{fa}}(4\ \mathrm{sensors}) = \frac{1}{2}\cdot\left[1 - \mathrm{erf}\left(\frac{\mathrm{TNR}}{\sqrt{2}}\right)\right] = 10.57\% \tag{41}$$

Subsequently the probability of false alarm is decreased to 7.9% by choosing a detection threshold of 45 dB, based on preliminary analysis of the measured signals.

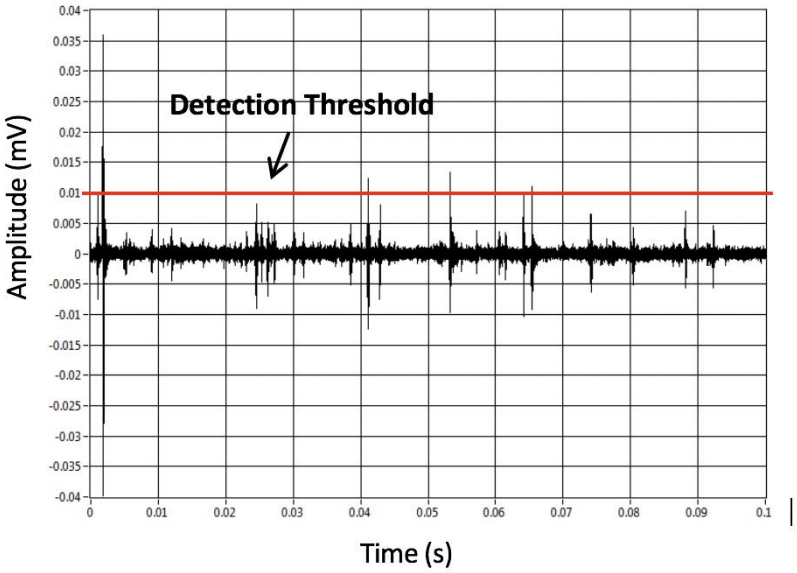

Figure 6-7 A typical AE signal acquired during fatigue tests with the threshold detection level set at 40dB

6.3.2 Acoustic Emission Event Localization

Depending on the crack sources, acoustic emission signals can be roughly divided into three types, burst, continuous and mixed. Burst is a type of emission related to individual events occurring in a material that results in discrete acoustic emission signals. Continuous is a type of emission that related to time overlapping and/or successive emission events from one or several sources that results in sustained signals, it often comes from rubbing and friction. The mixed type signal contains both bursts and continuous and it is the type which is encountered in this test.

When a crack propagation incident occurs this is considered as an ‘acoustic emission event’. This event leads to a wave that can be recorded by different sensors with delays that depend on the distance between the source and the sensors. Due to the visual crack growth prove, the signal analysis is based on the database acquired from day 21 to the end (after the 1 m × 0.05 m × 0.01 m crack is induced).

Initially in the monitoring programme all signals received by any sensor are recorded if they exceeded the threshold. The sum of all events within each day is simply equal to the number of measurements (data acquisition and processing operations) made in that day. Due to the coherent noise and vibrations, the initial data number set number is over 9000. Acoustic emission data for this test is acquired without any restriction, thus there are five different situations concerning the acquired data:

1. None of the sensors acquired an acoustic emission event, implying that the amplitude of all the signals acquired by all sensors is below the threshold.
2. Only one sensor acquired an acoustic emission event.
3. Two sensors acquired an acoustic emission event.
4. Three out of four sensors acquired an acoustic emission event.
5. All four sensors acquired at least one acoustic emission event.

An analysis is conducted to identify the number of files that occurred in each situation and the results are shown in the convenient form of a 3-dimensional histogram, see Figure 6-8.

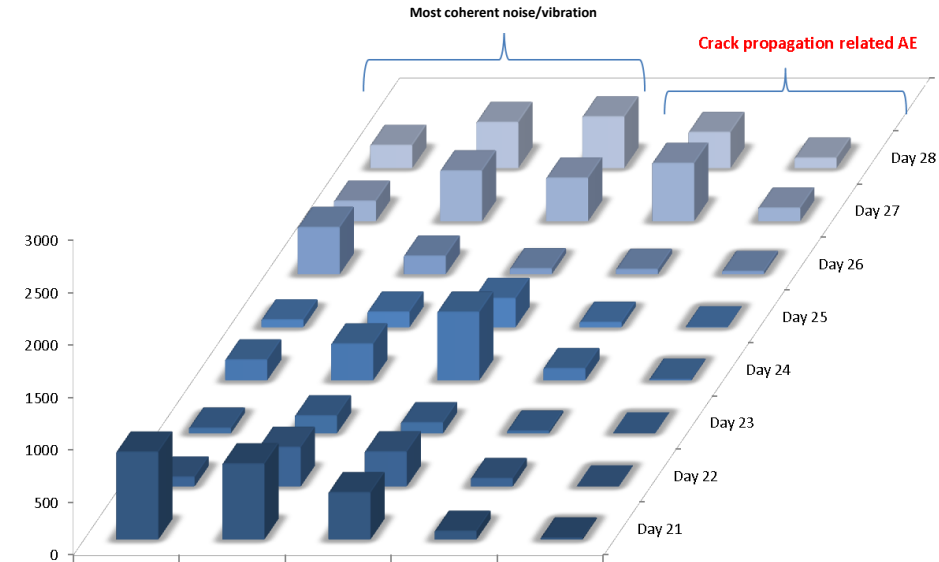

	0	1	2	3	4
Day 21	835	722	448	80	15
Day 22	91	374	331	77	0
Day 23	51	169	103	23	0
Day 24	196	348	651	113	10
Day 25	72	146	276	48	1
Day 26	447	174	54	48	28
Day 27	192	480	412	552	126
Day 28	218	437	490	342	97
Total	2102	2850	2765	1283	277

Figure 6-8 Number of files in which acoustic emission event occurred in none, one, two, three or four sensors

After this step, the data processing focused on the 277 files which are the ones with all the four sensors acquired at least one acoustic emission event at the processing threshold. And then, an acoustic emission event is defined as when all four sensors are hit within the time it would take for an acoustic emission signal to travel from its source through the shortest and longest distances to the four sensors, which is 150-500 µs. This value is calculated by dividing the shortest and longest distance from defect to senor by an average acoustic wave propagation velocity (2100 m/s) in the blade. Depending on the structure of the blade, the acoustic waves will travel in different wave modes. The most common form of wave that travels in finite structure is the Lamb wave [125]. The wave velocity is determined through pencil lead break tests inside the blade [16]. There are 29 acoustic emission events left after this process.

Then localisation is achieved using the triangulation method [126], [127]. On the scale of the wavelength the 4 sensors could be regarded as lying in one

plane. Thus, three circles (rather than spheres) of radius equal to the wave velocity × the travel time from the unknown source point to any of the three sensors, defines a region, approximately triangular in shape, defined by three chords. These chords define the overlap of two circles chosen in the three possible ways out of the set of three circles. This overlap region defines the area in which the acoustic emission source could lie. Then three circles on which this triangulation operation is performed could be selected in 4 different ways out of 4 circles, to increase the accuracy of the localisation. The results are shown in Figure 6-9.

The positions of the 4 acoustic emission sensors are marked. The red rectangular represents the induced planar void defect with the size of 1 m×0.05 m×0.01 m. Defect growths from the 11th, 12th, 13th days of testing are marked with lines in different colours. These 29 acoustic emission events (rectangular blue dots) in total are identified. These located acoustic emission events are around the induced defect which provides evidence of the growth of damage originating from this source. More acoustic emission events were located on the left side where more defect growths were identified, which further proved the results of acoustic emission localization. Some of the acoustic emission events are located far away from the defects, this could be because of the nature of composite materials, in different directions, and the wave velocity is different. In this localization process, a fixed wave velocity is used, which results the inaccuracy. It is recommended for future work to take this effect under consideration when applying localization algorithm.

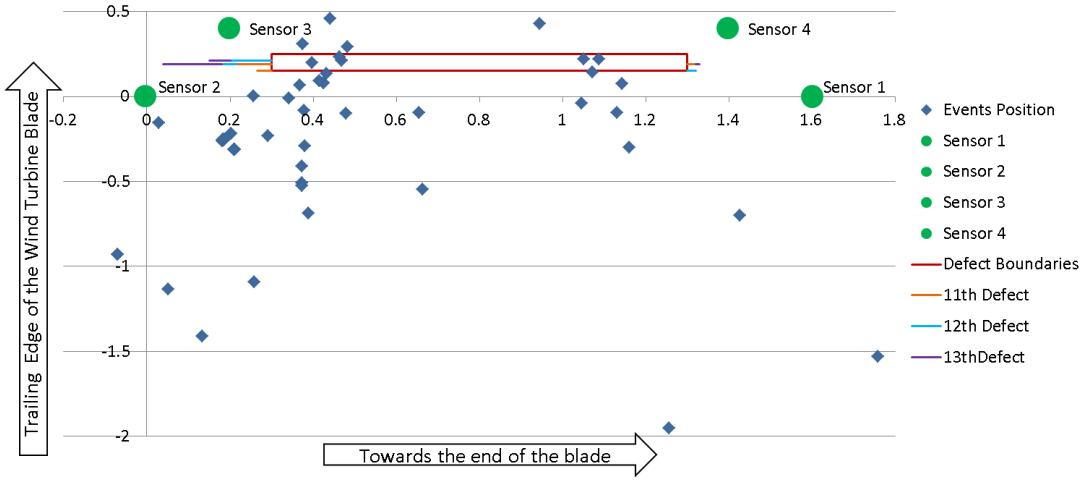

Figure 6-9 Locations of AE event sources obtained by trilateration of data from four sensors situated as indicated

6.3.3 Damage Characterization

The first step of developing an unsupervised pattern recognition process is to classify signals into groups based on similarities. This process involves statistical effects, and the key point of successful feature selection to construct fine classification accuracy.

Based on the above methodology, peak frequency and MARSE are selected as highly correlated features for the clustering process. The signals are classified into four groups by comparing their features and deciding upon their similarity. The assignment of the clustering results to the fracture mechanisms is achieved by a detailed analysis of the physical meaning of the data. The positions of these clusters in time domain features are also presented, and average frequency, MARSE, and peak amplitude are found to be promising to be useful parameters to represent failure modes. This is the first time that the PR technique has been applied to a database acquired from such a complex structure in a fatigue testing environment. The applied feature selection algorithm proves to be a powerful tool providing relevant clustering when used together with a k-means algorithm.

6.3.3.1 Data Pre-processing

Both burst and continuous types of signals are stored for 0.1 s once triggered. For many years, researchers have concentrated on extracting useful information from acoustic emission signals by identifying the transient waves in the signal and extracting features. These transient signals, known as acoustic emission hits, are commonly determined by a selected detection threshold. Acoustic emission hit duration is determined by HDT, selected as 200 µs in this experiment. Once the hit has been determined, acoustic emission hit-based features can be calculated. Time domain features including peak amplitude, duration, MARSE, rise time, average frequency, as well as frequency domain features including peak frequency and frequency centroid are extracted. Signals with fewer than 3 counts and of duration less than 3 µs

are regarded as unwanted signals [41]. The original number of hits is 100,855, which is reduced to 74, 852 after the above filter is applied.

Figure 6-10 shows the peak amplitude versus MARSE distribution for signals generated from noise and signals generated from real damage. The signals generated from noise present with low peak amplitude and MARSE values. After feature extraction, feature normalization is an important part of classifier design and of pattern recognition in general. In this paper, each parameter is normalized over the range [0, 1].

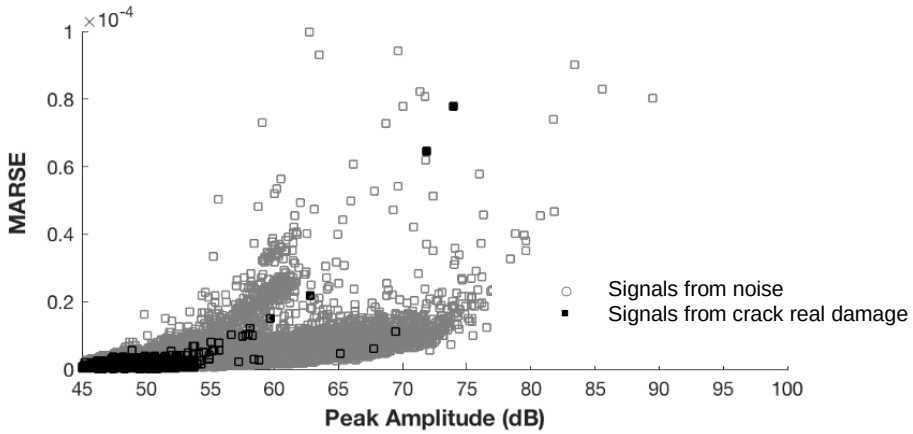

Figure 6-10 Peak amplitude vs. MARSE distribution for signals generated from noise and signals generated from real damage, respectively

6.3.3.2 Pattern Recognition

Feature selection

In this paper, the principle of feature selection processing is achieved by minimizing the value of the Davies-Bouldin (DB) index partitioned by the k-means algorithm as explained in 0.

The selection algorithm is applied with 2, 3, and 4 clusters. Peak frequency has been proven to be an effective parameter to represent different damage mechanisms, and is therefore selected to initiate the feature selection process. At the first interaction, the lowest DB index is given by the combination with MARSE for all three cases, see Figure 6-11 and Table 6-3. No more improvement of the DB criterion occurs at the next criterion. Therefore, peak frequency and MARSE are selected for the clustering algorithm.

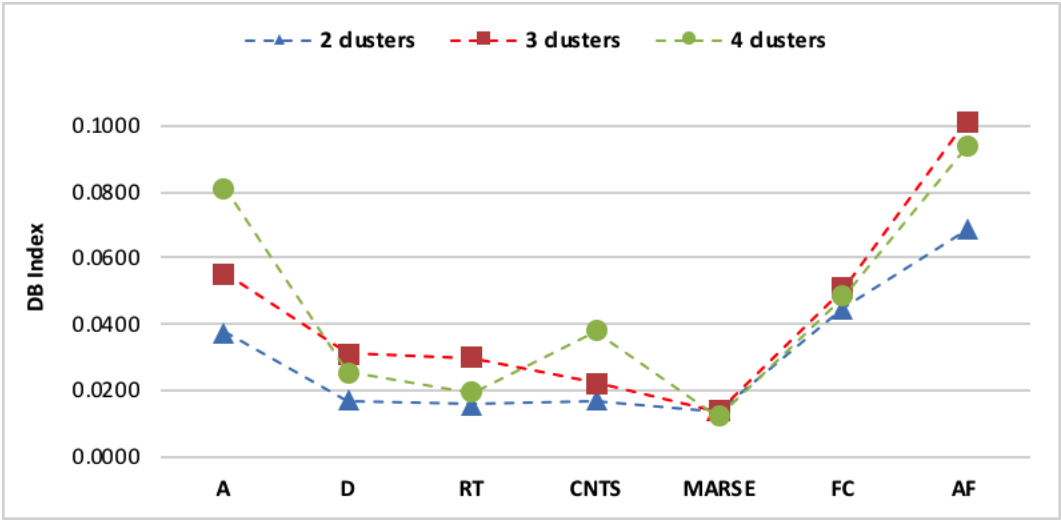

Figure 6-11 First interaction giving MARSE as the best feature of 2, 3, and 4 clusters

Table 6-3 DB index value at the first interaction for 2, 3, and 4 clusters

Features	DB Index		
	2 Clusters	3 Clusters	4 Clusters
Peak Amplitude (A)	0.0373	0.0553	0.0812
Duration (D)	0.0168	0.0312	0.0256
Rise Time (RT)	0.0158	0.0299	0.0194
Counts (CNTS)	0.0171	0.0220	0.0378
MARSE (E)	0.0138	0.0138	0.0122
Frequency Centroid (FC)	0.0446	0.0510	0.0485
Average Frequency (AF)	0.0686	0.1013	0.0937

Optimal number of clusters

A widely used method to choose an optimal value for the number of clusters is Silhouette analysis. A Silhouette coefficient is defined to study the separation distance between the resulting clusters with a higher value, indicating better cluster quality. A Silhouette value greater than 0.6 generally assures that the clustering is sufficient. R. Gutkin et al. [64] investigated failure in CFRP using three different pattern recognition techniques including k-means, self-organising maps combined with k-means, and competitive neural networks on acoustic emission signals. The number of clusters, k, is chosen between 0 and 2 so that the Silhouette coefficient is maximized. The results from the clustering analysis follow the pattern found in peak frequencies distributions. Li Li et al. [117] identified a framework for the analysis of a link between the damage mode and acoustic emission signals originating from the

damage initiation and development of 2D and 3D glass/epoxy woven composites loaded in tension. The number of clusters for k-means ++ analysis is evaluated using both Silhouette coefficients and the Davies-Bouldin index. Aacoustic emission signals are divided into four groups which correspond to matrix cracking, fibre/matrix debonding, delamination, and fibre breakage, respectively. Crivelli, D. et al. [128] developed a technique based on Self-Organizing Mapping in conjunction with the k-means algorithm to separate the acoustic emission signals from tensile tests of pultruded glass-fiber specimens. The optimal number of clusters is evaluated using three performance indexes including Davies-Bouldin, Silhouette, and Calinski-Harabasz. The result is selected depending on the most voted number of clusters. In this paper, the optimal number of clusters is chosen by taking into account both Calinski-Harabasz and Silhouette quality indices [87], see Figure 6-12The calculation is based on the selected feature database.

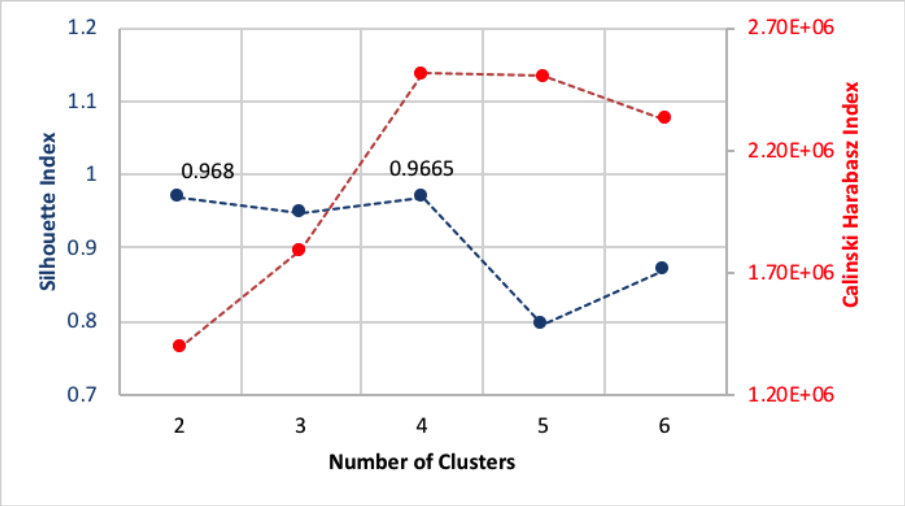

Figure 6-12 Number of clusters evaluated by the Silhouette index and Calinski-Harabasz index

The Silhouette index identifies 2 as the best performing clustering number, followed closely by 4, while for the Calinski-Harabasz index the best clustering is 4. Based on the above calculations, 4 is the most voted number of clusters, and is therefore selected as the optimal number of clusters.

6.3.3.3 Clustering Results

Figure 6-13 shows the partition of acoustic emission signals obtained by the above pattern recognition method. Frequency features including peak frequency and frequency centroid are used to visualize the position of the signal clusters. It can be observed that the acoustic emission signals are well-separated into four clusters in the peak frequency–frequency centroid space. Acoustic emission signals originating from cluster 1 are related to the high peak frequency. The events with a peak frequency ranging from 0–30 kHz is grouped as cluster 2. Cluster 3 and 4 are identified with a group of signals of peak frequency ranging from 30–70 kHz and 70–120 kHz, respectively.

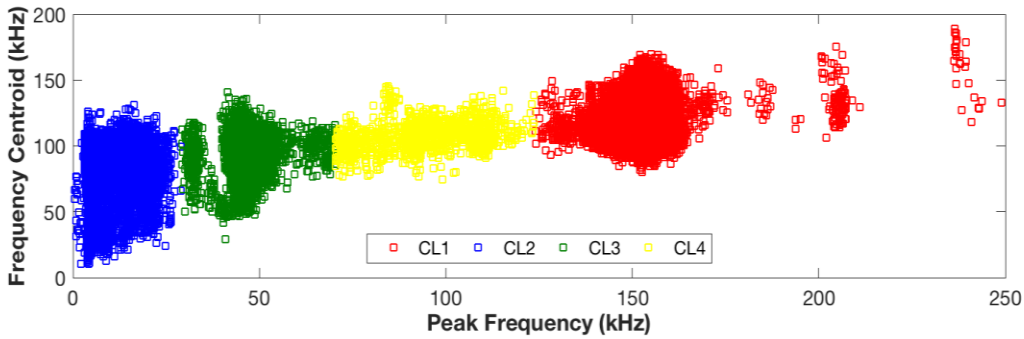

Figure 6-13 Clustering results: the partition of AE signals on peak frequency-frequency centroid

Table 6-4 shows the number of events of four clusters based on the clustering results obtained with the selected features using the k-means clustering algorithm.

Table 6-4 Clustering results: the number of events for four clusters

Cluster	Number of Events
1	44,542
2	8083
3	19,531
4	1577

6.3.3.4 Acoustic Emission Source Characterization

Acoustic emission signals are well-separated into four clusters in the peak frequency–frequency centroid space through the above unsupervised pattern recognition methodology. In this section, the characteristic frequency range of

each failure mode signals are identified based on the detailed review on the frequency response of the acoustic emission signals from composite materials, see Table 5-7. Based on the clustering results, acoustic emission events are classified into four groups of peak frequency ranges from 0–30 kHz, 30–70 kHz, 70–120 kHz, and 120–250 kHz, respectively. The literature review stated that signals generated from matrix cracking and delamination range from 0–150 kHz; therefore, signals from clusters 2, 3, and 4 can be cauterized into these two fracture mechanisms. As for cluster 1, which corresponds to a higher peak frequency range, signals in this cluster are associated with debonding. The positions of these clusters in time domain features including average frequency, MARSE, and peak amplitude are presented in Figure 6-14. The objective of analysing the time domain features is to further discriminate the clusters 2, 3, and 4 into different damage mechanisms by looking into the physical meaning of the signals.

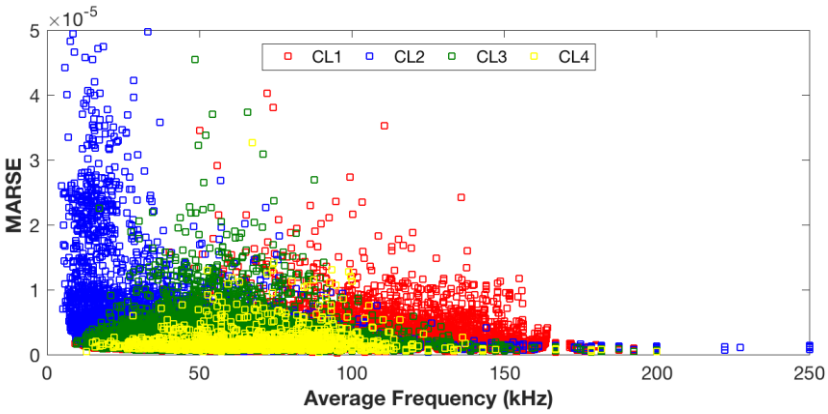

(a)

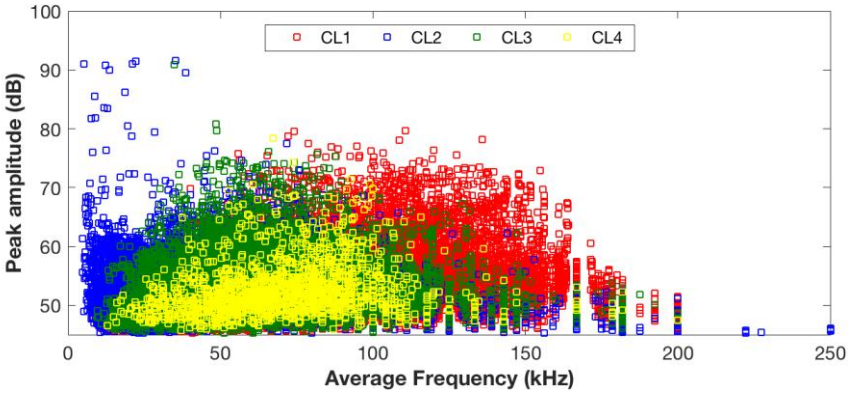

(b)

Figure 6-14 Clustering results: the partition of AE signals on time domain features: (a) Clustering results on average frequency vs. MARSE (b) Clustering results on average frequency vs. peak amplitude

Events in clusters 3 and 4 exhibit a very similar response on time domain features; cluster 2 features a lower average frequency but higher MARSE, see Figure 6-14 (a). It is believed that clusters 3 and 4 correspond to the same fracture mechanism and cluster 2 corresponds to a different one. Events in cluster 2 feature a lower peak amplitude (45–60 dB) in comparison with the events in clusters 3 and 4, see Figure 6-14 (b). It is concluded that matrix cracking generally has a lower peak amplitude response than delamination. Therefore, events in cluster 2 correspond to matrix cracking, while events in clusters 3 and 4 are generated by delamination.

A representative signal from each class is shown in Figure 6-15: the (a) type signal is from cluster 2, with a peak frequency less than 30 kHz, lower peak amplitude, and longer duration (which is the reason for a higher MARSE value); the (b) type signal is related to delamination with a higher peak frequency and higher amplitude, but shorter duration; and the (c) type signal shows a much higher peak frequency and the shortest duration.

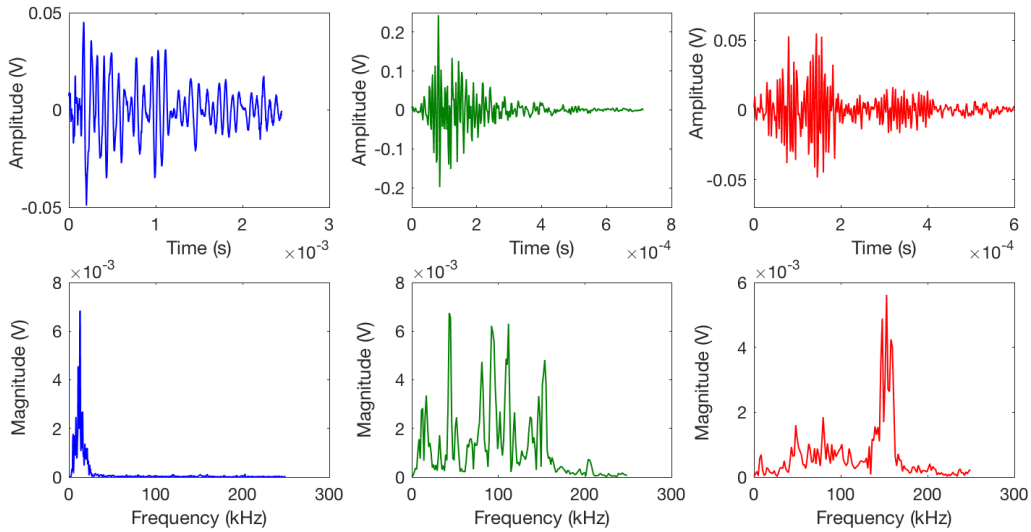

Figure 6-15 A representative signal in the time domain and frequency domain due to: (a) matrix cracking (b) delamination (c) debonding

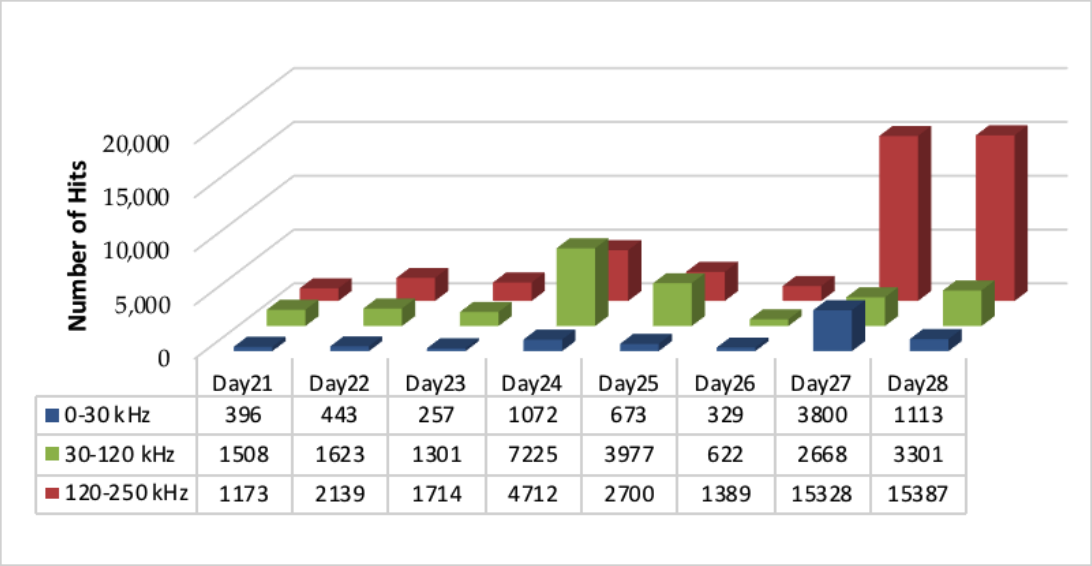

	Day21	Day22	Day23	Day24	Day25	Day26	Day27	Day28
0-30 kHz	396	443	257	1072	673	329	3800	1113
30-120 kHz	1508	1623	1301	7225	3977	622	2668	3301
120-250 kHz	1173	2139	1714	4712	2700	1389	15328	15387

Figure 6-16 Number of events with peak frequency range from 0-30 kHz, 30-120 kHz, and 120-250 kHz.

It can be observed that various damage mechanisms occur at different speeds, and a large amount of acoustic emission activity happened in the peak frequency range from 120 to 250 kHz on days 27 and 28, which is the period when the visual inspection confirmed a severe damage growth.

6.4 Conclusions

Starting from a simulated hole defect of 1 m × 0.05 m × 0.01 m dimensions in the GFRP composite materials of a 45.7 m wind turbine blade the growth of real damage has been detected by continuous acoustic emission monitoring over 21 days of cyclic loading which simulated realistic loading conditions in service.

Damage grew to 0.3 m in length in the final two days of fatigue tests. The detection was achieved through correlations in the arrival times of burst signals from 4 sensors in the array. The developed acoustic emission signal treatment technique employed, involving pulsed signal arrival time correlations, shows promise for on line blade monitoring. The threshold level for signal acceptance in the analysis is set at 45 dB.

Using triangulation techniques applied to the relative arrival times of signals received by all 4 sensors damage growth locations were determined and found to be clustered round the defect. This is confirmed by the photographic evidence.

The effectiveness of the developed unsupervised pattern recognition methodology is proved by being applied on the collected acoustic emission signals. Through the presented methodology, the optimal number of clusters and the best features for clustering are specified. The clustering results are assigned to the fracture mechanisms through a detailed analysis of the physical meaning of the data. Three damage mechanisms have been identified: acoustic emission hits with a peak frequency range from 0 to 30 kHz, a relatively higher MARSE, and lower average frequency and peak amplitude values were found to be indicative of matrix cracking. The second group of signals with a peak frequency range from 30 kHz to 120 kHz occurred with a low average frequency and low MARSE signature in the average frequency–MARSE distribution plot, but with a higher peak amplitude. It is believed that this group of signals identifies delamination activities. Signals with a higher peak frequency range and lower MARSE, but with high average frequency values formed a cluster that was considered to indicate higher energetic sources such as debonding.

This is the first time that an unsupervised pattern recognition technique is applied successfully to a database acquired from such a complex structure in a fatigue testing environment. The developed acoustic emission monitoring methodology shows excellent promise as an in-service blade integrity monitoring technique capable of providing early warnings of developing damage.

7 Conclusions and Recommended Future Work

7.1 Conclusions

This thesis explored the use of an advanced acoustic emission data processing technique for composite structures with the intention of providing an early warning of developing damage. Finite element modelling study as well as experimental studies were undertaken to demonstrate acoustic emission's capability as an inspection technique to detect, locate and characterize damage occurring in the tested specimens. Each of the experimental studies investigated the challenging aspects of applying source characterization methods including the sensor sensitivity and attenuation effects on the obtained acoustic emission signal features. The outcome of the experimental results helped develop a successful acoustic emission damage detection and characterization technique which was demonstrated during a fatigue test in a complete 45.7 m long wind turbine blade.

Direct acoustic emission waves were reproduced using finite element modelling to interpret the acoustic emission signals' relevance to failure mechanisms. The effect of the sensor's sensitivity on the simulated acoustic emission signals was exhibited and the effect on the signal features was investigated. The results were then compared with the acoustic emission signals obtained from different sensors during tensile tests. Characteristics of the acoustic emission signals from plastic deformation were quantified through a novel pattern recognition approach.
The key findings are:

- The amplitude of the generated signals increases as the crack grows for both Mode I and Mode II cracks.
- Different acoustic emission sensors results in different amplitudes of the acoustic emission signals, which thus has an impact on the values of the signal features.
- The quantitative analysis on the sensor effect on the acoustic emission signals shows that the high resonant frequency sensors

are not ideal to use to detect damages growth in both metal and composite materials.

- High peak frequency signals can indicate plastic deformation if the signals are from the broadband sensor and lower resonant frequency sensor (resonant frequency around 150 kHz).
- An advanced unsupervised PR approach is applied on the acoustic emission signals acquired during a tensile test on carbon steel specimen, results show that for broadband sensors, plastic deformation is identified by high MARSE and duration signals; for low resonant frequency sensor, plastic deformation is identified by high MARSE and high peak amplitude signals; for high resonant frequency sensor, plastic deformation is identified by high MARSE and high signal strength signals.
- The frequency analysis of the acoustic emission signals acquired during a tensile test on CFRP specimen shows that defects in composite materials generated acoustic emission signals with the frequency range from 100 kHz to 450 kHz.

The effects of attenuation on the signals and source characterization of acoustic emission signals were investigated during a three-point bending test on a GFRP panel. Before the test, pencil lead break tests were carried out.

Results show that:

- The propagating acoustic emission signal is dominated by different wave modes from different source types.
- A_0 mode has a much higher rate of attenuation than the S_0 mode in GFRP.
- A frequency of more than 200 kHz is difficult to be detected within a 300 mm radius for an in-plane displacement.
- The applied PR technique successfully characterizes the acoustic emission signals into four different groups, which correspond to three different matrix cracking, delamination and debonding.

- Attenuation effects can alter the frequency range of the clusters used for pattern recognition as well as on the number of signals in each cluster.

A laboratory study was performed investigating fatigue damage growth in a complete 45.7 m long wind turbine blade.

The following are concluded:

- An acoustic emission is defined as when four sensors are hit within the time it would take for an acoustic emission signal to travel from its source through the shortest and longest distances to the four sensors. This has been proved to be a very effective way to filter out the non-damage-growth generated acoustic emission signals.
- The triangulation method is then applied on the above acoustic emission events to calculate their localizations. Results have shown that these localized acoustic emission events are clustered around the real damage growth.
- The applied PR approach applied on the acoustic emission signals successfully characterizes three damage types including matrix cracking, delamination and debonding.
- The applied acoustic emission signal treatment technique employed, involving pulsed signal arrival time correlations, shows promise for on line blade monitoring.
- The effectiveness of the developed pattern recognition methodology is proven by being applied on the collected acoustic emission signals. The identified damage has been confirmed by the photographic evidence.

As final remarks, the developed acoustic emission monitoring methodology in this work shows excellent promise as an in-service blade integrity monitoring technique capable of providing early warnings of developing damage.

7.2 Recommended Future Work

Acoustic emission signal features can provide valuable information about source characterisation. This thesis explores mainly two aspects which will influence this process which is the sensor frequency effects and attenuation effects on source characterization results. There is additional work to improve and develop the technique further.

- *Dispersion effect* **–** Acoustic emission waves are subjected to attenuation as well as dispersion. Dispersion is characterised by different frequency waves propagating at different velocities. As a result the sensor that is closer to the source will receive a considerably different signal to a sensor that is located further away. Therefore, the measured signal features "carry" the effect of dispersion. This effect can be quite prominent where the distance between the source and the sensor increases. This is especially true for large structures such as wind turbine blades. Therefore investigation on dispersion effects on acoustic emission signals is recommended to be carried out for large scale structures. This investigation can be performed by means of a numerical study as well as experimental work. Understanding the dispersive nature of the wave modes can lead to significantly improved acoustic emission source location and characterization accuracy.

- *Wave Propagation in Anisotropic materials* – Due to the inhomogeneous and anisotropic nature of composite materials, acoustic emission wave propagation in these materials is much more complex. Analysis of wave propagation in multi-layered anisotropic structures has been extensively studied using finite the element modelling approach. Experimentally, acoustic emission measurements can be performed at angles of propagation of varying degrees with respect to the plate coordinate axes. This can significantly help in the interpretation of acoustic emission signals in anisotropic materials.

- *Fatigue* - Fatigue crack tests should also be carried out as they represent a crack growth scenario closer to real life loading conditions. Environmental noise can bring added challenges during the fatigue testing. It is therefore recommended to investigate an effective algorithm to discriminate acoustic emission signals generated from environmental noise.

8 References

[1] European Wind Energy Association, “Wind in power 2017,” *2017 Eur. Stat.*, no. February, pp. 1–12, 2018.

[2] W. Yang and S. W. Tian, “Research on a power quality monitoring technique for individual wind turbines,” *Renew. Energy*, 2015.

[3] C. A. Walford, “Wind turbine reliability: understanding and minimizing wind turbine operation and maintenance costs,” *Energy*, no. March, pp. SAND2006-1100, 2006.

[4] R.M. Mayer, “Design of Composite Structures Against Fatigue Applications to Wind Turbine Blades,” *Proc. Inst. Mech. Eng. Part A J. Power Energy*, vol. 210, no. 4, pp. 329–330, Aug. 1996.

[5] F. Moeller Larsen and T. Soerensen, *New lightning qualification test procedure for large wind turbine blades*, vol. 36. 2003.

[6] D. Le Gourieres, *Wind power plants: theory and design*. Elsevier, 2014.

[7] B. Eker, A. Akdogan, and A. Vardar, “Using of composite material in wind turbine blades,” *J. Appl. Sci*, vol. 6, no. 14, pp. 2917–2921, 2006.

[8] HBM, “Optical vs. Electrical Which type of strain gauge is the right choice for infrastructure monitoring?” [Online]. Available: https://www.hbm.com/en/6483/optical-fiber-sensors-vs-conventional-electrical-strain-gauges/.

[9] B.-H. Han, D.-J. Yoon, Y.-H. Huh, and Y.-S. Lee, “Damage assessment of wind turbine blade under static loading test using acoustic emission,” *J. Intell. Mater. Syst. Struct.*, vol. 25, no. 5, pp. 621–630, 2014.

[10] P. J. Schubel, R. J. Crossley, E. K. G. Boateng, and J. R. Hutchinson, “Review of structural health and cure monitoring techniques for large wind turbine blades,” *Renew. Energy*, vol. 51, pp. 113–123, 2013.

[11] F. P. G. Márquez, A. M. Tobias, J. M. P. Pérez, and M. Papaelias, “Condition monitoring of wind turbines: Techniques and methods,” *Renew. Energy*, vol. 46, pp. 169–178, 2012.

[12] “ASTM E-1316 Standard Terminology for Non-destructive Examinations.”

[13] F. Dahmene, S. Yaacoubi, and M. El Mountassir, “Acoustic emission of composites structures: Story, success, and challenges,” in *Physics Procedia*, 2015.

[14] J. T. Tou and R. C. Gonzalez, “Pattern recognition principles,” *Image*

Rochester NY, 1974.

[15] M. R. Kaphle, “Analysis of acoustic emission data for accurate damage assessment for structural health monitoring applications.” Queensland University of Technology, 2012.

[16] M. G. R. Sause, “Investigation of pencil-lead breaks as acoustic emission sources,” *J. Acoust. Emiss.*, vol. 29, pp. 184–196, 2011.

[17] G. C. McLaskey, D. A. Lockner, B. D. Kilgore, and N. M. Beeler, “A robust calibration technique for acoustic emission systems based on momentum transfer from a ball drop,” *Bull. Seismol. Soc. Am.*, vol. 105, no. 1, pp. 257–271, 2015.

[18] C. U. Grosse, *Acoustic Emission Testing*. 2008.

[19] E. Tsangouri and D. G. Aggelis, “The Influence of sensor size on acoustic emission waveforms—A numerical study,” *Appl. Sci.*, vol. 8, no. 2, p. 168, 2018.

[20] K. Aid and P. G. Richards, “Quantitative seismology: Theory and methods,” *San Fr.*, 1980.

[21] M. Ohtsu and K. Ono, “The generalized theory and source representations of acoustic emission,” *J. Acoust. Emiss.*, vol. 5, no. 4, pp. 124–133, 1986.

[22] K. Ono and M. Ohtsu, “A generalized theory of acoustic emission and Green’s functions in a half space,” *J. Acoust. Emiss.*, vol. 3, pp. 27–40, 1984.

[23] T. L. Anderson, *Fracture Mechanics: Fundamentals and Applications*. 2012.

[24] K. J. Mach, D. V Nelson, and M. W. Denny, “Techniques for predicting the lifetimes of wave-swept macroalgae: a primer on fracture mechanics and crack growth,” *J. Exp. Biol.*, vol. 210, no. 13, pp. 2213–2230, 2007.

[25] M. I. Rocha-Gaso, C. March-Iborra, Á. Montoya-Baides, and A. Arnau-Vives, “Surface generated acoustic wave biosensors for the detection of pathogens: A review,” *Sensors*, 2009.

[26] R. Marks, A. Clarke, C. Featherston, C. Paget, and R. Pullin, “Lamb Wave Interaction with Adhesively Bonded Stiffeners and Disbonds Using 3D Vibrometry,” *Appl. Sci.*, 2016.

[27] S. Yang and F. G. Yuan, “Transient wave propagation of isotropic plates using a higher-order plate theory,” *Int. J. Solids Struct.*, 2005.

[28] NDT Resource Centre, “Introduction to Acoustic Emission Testing -

Equipment.” .

[29] R. E. Green Jr, “Non-contact ultrasonic techniques,” *Ultrasonics*, vol. 42, no. 1–9, pp. 9–16, 2004.

[30] F. Yu, Y. Okabe, Q. Wu, and N. Shigeta, “Fiber-optic sensor-based remote acoustic emission measurement of composites,” *Smart Mater. Struct.*, vol. 25, no. 10, p. 105033, 2016.

[31] D. Ozevin, D. W. Greve, I. J. Oppenheim, and S. P. Pessiki, “Resonant capacitive MEMS acoustic emission transducers,” *Smart Mater. Struct.*, vol. 15, no. 6, p. 1863, 2006.

[32] S. Masmoudi, A. El Mahi, and S. Turki, “Use of piezoelectric as acoustic emission sensor for in situ monitoring of composite structures,” *Compos. Part B Eng.*, vol. 80, pp. 307–320, 2015.

[33] Y. Zhang, *Real-time weld process monitoring*. Elsevier, 2008.

[34] P. Wei, X. Han, D. Xia, T. Liu, and H. Lang, “Novel Fiber-Optic Ring Acoustic Emission Sensor,” *Sensors*, vol. 18, no. 1, p. 215, 2018.

[35] R. Unnþórsson, “Hit detection and determination in AE bursts,” in *Acoustic Emission-Research and Applications*, InTech, 2013.

[36] Vallen Systeme GmbH, “Acoustic Emission Sensors - Specification.”

[37] Vallen system, “Acoustic emission sensors, specifications.”

[38] D. G. Aggelis and T. E. Matikas, “Effect of plate wave dispersion on the acoustic emission parameters in metals,” *Comput. Struct.*, vol. 98, pp. 17–22, 2012.

[39] J. M. Park and H. C. Kim, “The effects of attenuation and dispersion on the waveform analysis of acoustic emission,” *J. Phys. D. Appl. Phys.*, 1989.

[40] F. Li, H. Murayama, K. Kageyama, and T. Shirai, “Guided wave and damage detection in composite laminates using different fiber optic sensors,” *Sensors*, 2009.

[41] H. Vallen, “AE testing fundamentals, equipment, applications,” *J. Nondestruct. Testing(Germany)*, vol. 7, no. 9, pp. 1–30, 2002.

[42] B. Muravin, “Acoustic emission science and technology,” *J. Build. Infrastruct. Eng. Isr. Assoc. Eng. Archit.*, 2009.

[43] H. Vallen, *Acoustic Emission Testing: Fundamentals, Equipment, Applications*. Castell, 2006.

[44] Z. Zhou, J. Zhou, L. Dong, X. Cai, Y. Rui, and C. Ke, “Experimental study

on the location of an acoustic emission source considering refraction in different media," *Sci. Rep.*, vol. 7, no. 1, p. 7472, 2017.

[45] "AE Source Location Techniques," *NDT resource centre*. .

[46] M. J. Eaton, R. Pullin, and K. M. Holford, "Towards improved damage location using acoustic emission," *Proc. Inst. Mech. Eng. Part C J. Mech. Eng. Sci.*, 2012.

[47] A. Kundu, M. J. Eaton, S. Al-Jumali, S. Sikdar, and R. Pullin, "Acoustic emission based damage localization in composites structures using Bayesian identification," in *Journal of Physics: Conference Series*, 2017.

[48] S. K. Al-Jumaili, M. R. Pearson, K. M. Holford, M. J. Eaton, and R. Pullin, "Acoustic emission source location in complex structures using full automatic delta T mapping technique," *Mech. Syst. Signal Process.*, 2016.

[49] S. M. Ziola and M. R. Gorman, "Source location in thin plates using cross-correlation," *J. Acoust. Soc. Am.*, 1991.

[50] H. Jeong and Y.-S. Jang, "Wavelet analysis of plate wave propagation in composite laminates," *Compos. Struct.*, 2000.

[51] H. Jeong, "Analysis of plate wave propagation in anisotropic laminates using a wavelet transform," *NDT E Int.*, 2001.

[52] M. Shehadeh, J. A. Steel, and R. L. Reuben, "Acoustic emission source location for steel pipe and pipeline applications: The role of arrival time estimation," *Proc. Inst. Mech. Eng. Part E J. Process Mech. Eng.*, 2006.

[53] T. Lokajíek and K. Klíma, "A first arrival identification system of acoustic emission (AE) signals by means of a high-order statistics approach," *Meas. Sci. Technol.*, 2006.

[54] F. M. Jensen, A. S. Puri, J. P. Dear, K. Branner, and A. Morris, "Investigating the impact of non-linear geometrical effects on wind turbine blades-Part 1: Current status of design and test methods and future challenges in design optimization," *Wind Energy*, vol. 14, no. 2, pp. 239–254, 2011.

[55] V. Srinivasa, V. Shivakumar, V. Nayaka, and S. Jagadeeshaiaih, "Fracture Morphology of Carbon Fiber Reinforced Plastic Composite Laminates," *Mater. Res.*, vol. 13, no. 3, pp. 417–424, 2010.

[56] A. J. Brunner, "Identification of damage mechanisms in fiber-reinforced polymer-matrix composites with Acoustic Emission and the challenge of assessing structural integrity and service-life," *Constr. Build. Mater.*, vol. 173, pp. 629–637, 2018.

[57] J. M. Berthelot, “Relation between amplitudes and rupture mechanisms in composite materials,” *J. Reinf. Plast. Compos.*, vol. 7, no. 3, pp. 284–299, 1988.

[58] S. C. Woo and T. W. Kim, “High strain-rate failure in carbon/Kevlar hybrid woven composites via a novel SHPB-AE coupled test,” *Compos. Part B Eng.*, vol. 97, pp. 317–328, 2016.

[59] P. Nimdum and J. Renard, “Use of acoustic emission to discriminate damage modes in carbon fibre reinforced epoxy laminate during tensile and buckling loading,” in *ECCM 15-15th European Conference on Composite Materials*, 2012, p. 8–p.

[60] I. M. De Rosa, C. Santulli, and F. Sarasini, “Acoustic emission for monitoring the mechanical behaviour of natural fibre composites: A literature review,” *Composites Part A: Applied Science and Manufacturing*. 2009.

[61] J. M. Park, D. S. Kim, and S. R. Kim, “Interfacial properties and microfailure degradation mechanisms of bioabsorbable fibers/poly-L-lactide composites using micromechanical test and nondestructive acoustic emission,” *Compos. Sci. Technol.*, vol. 63, no. 3–4, pp. 403–419, 2003.

[62] Q. Q. Ni and M. Iwamoto, “Wavelet transform of acoustic emission signals in failure of model composites,” *Eng. Fract. Mech.*, 2002.

[63] C. R. Ramirez-Jimenez, N. Papadakis, N. Reynolds, T. H. Gan, P. Purnell, and M. Pharaoh, “Identification of failure modes in glass/polypropylene composites by means of the primary frequency content of the acoustic emission event,” *Compos. Sci. Technol.*, vol. 64, no. 12, pp. 1819–1827, 2004.

[64] R. Gutkin, C. J. Green, S. Vangrattanachai, S. T. Pinho, P. Robinson, and P. T. Curtis, “On acoustic emission for failure investigation in CFRP: Pattern recognition and peak frequency analyses,” *Mech. Syst. Signal Process.*, vol. 25, no. 4, pp. 1393–1407, 2011.

[65] M. Eaton, K. Holford, C. Featherston, and R. Pullin, “Damage in carbon fibre composites: the discrimination of acoustic emission signals using frequency,” *J. Acoust. Emiss.*, vol. 25, no. 1, p. 140, 2007.

[66] A. Anastasopoulos, “Pattern Recognition Techniques for Acoustic Emission Based Condition Assessment of unfired Pressure Vessels,” *J. Acoust. Emiss.*, 2005.

[67] A. A. Anastassopoulos and T. P. Philippidis, “Clustering methodology for the evaluation of acoustic emission from composites,” *J. Acoust.*

Emiss., 1995.

[68] T. P. Philippidis, V. N. Nikolaidis, and A. A. Anastassopoulos, “Damage characterization of carbon/carbon laminates using neural network techniques on AE signals,” *NDT E Int.*, 1998.

[69] T. Warren Liao, “Feature extraction and selection from acoustic emission signals with an application in grinding wheel condition monitoring,” *Eng. Appl. Artif. Intell.*, 2010.

[70] X. He, D. Cai, and P. Niyogi, “Laplacian Score for Feature Selection,” *Adv. Neural Inf. Process. Syst. 18*, 2005.

[71] L. Zhu, L. Miao, and D. Zhang, “Iterative Laplacian score for feature selection,” in *Communications in Computer and Information Science*, 2012.

[72] M. G. R. Sause, A. Gribov, A. R. Unwin, and S. Horn, “Pattern recognition approach to identify natural clusters of acoustic emission signals,” *Pattern Recognit. Lett.*, 2012.

[73] M. M. M. Islam, M. R. Islam, and J.-M. Kim, “A hybrid feature selection scheme based on local compactness and global separability for improving roller bearing diagnostic performance,” in *Australasian Conference on Artificial Life and Computational Intelligence*, 2017, pp. 180–192.

[74] D. D. Doan, E. Ramasso, V. Placet, S. Zhang, L. Boubakar, and N. Zerhouni, “An unsupervised pattern recognition approach for AE data originating from fatigue tests on polymer-composite materials,” *Mech. Syst. Signal Process.*, vol. 64–65, pp. 465–478, 2015.

[75] M. R. Islam, M. M. M. Islam, and J.-M. Kim, “Feature selection techniques for increasing reliability of fault diagnosis of bearings,” in *Electrical and Computer Engineering (ICECE), 2016 9th International Conference on*, 2016, pp. 396–399.

[76] Y.-H. Kim, M. M. M. Islam, R. Islam, and J.-M. Kim, “Genetic Algorithm Based Discriminant Feature Selection for Improved Fault Diagnosis of Induction Motor.”

[77] L. Lu, J. Yan, and Y. Meng, “Dynamic genetic algorithm-based feature selection scheme for machine health prognostics,” *Procedia Cirp*, vol. 56, pp. 316–320, 2016.

[78] N. El Aboudi and L. Benhlima, “Review on wrapper feature selection approaches,” in *Engineering & MIS (ICEMIS), International Conference on*, 2016, pp. 1–5.

[79] P. N. Tan, M. Steinbach, and V. Kumar, *Cluster Analysis: Basic Concepts and Algorithms*. 2005.

[80] S. N. Omkar, S. Suresh, T. R. Raghavendra, and V. Mani, “Acoustic emission signal classification using fuzzy c-means clustering,” in *Neural Information Processing, 2002. ICONIP ’02. Proceedings of the 9th International Conference on*, 2002, vol. 4, pp. 1827–1831 vol.4.

[81] C. Leone, G. Caprino, and I. de Iorio, “Interpreting acoustic emission signals by artificial neural networks to predict the residual strength of pre-fatigued GFRP laminates,” *Compos. Sci. Technol.*, vol. 66, no. 2, pp. 233–239, 2006.

[82] A. A. Anastassopoulos, T. P. Philippidis, and S. A. Paipetis, “Failure mechanism identification in composite materials by means of acoustic emission: Is it possible,” *Non Destr. Test.*, pp. 143–149, 1996.

[83] V. Kostopoulos, T. H. Loutas, A. Kontsos, G. Sotiriadis, and Y. Z. Pappas, “On the identification of the failure mechanisms in oxide/oxide composites using acoustic emission,” *NDT E Int.*, vol. 36, no. 8, pp. 571–580, 2003.

[84] M. Moevus *et al.*, “Analysis of damage mechanisms and associated acoustic emission in two SiCf/[Si–B–C] composites exhibiting different tensile behaviours. Part II: Unsupervised acoustic emission data clustering,” *Compos. Sci. Technol.*, vol. 68, no. 6, pp. 1258–1265, 2008.

[85] M. Bora, D. Jyoti, D. Gupta, and A. Kumar, “Effect of different distance measures on the performance of K-means algorithm: an experimental study in Matlab,” *arXiv Prepr. arXiv1405.7471*, 2014.

[86] D. L. Davies and D. W. Bouldin, “A cluster separation measure,” *IEEE Trans. Pattern Anal. Mach. Intell.*, no. 2, pp. 224–227, 1979.

[87] B. Desgraupes, “Clustering indices,” *Univ. Paris Ouest-Lab Modal’X*, vol. 1, p. 34, 2013.

[88] A. Sibil, N. Godin, M. R’Mili, E. Maillet, and G. Fantozzi, “Optimization of acoustic emission data clustering by a genetic algorithm method,” *J. Nondestruct. Eval.*, vol. 31, no. 2, pp. 169–180, 2012.

[89] R. A. Nordstrom, “Acoustic emission characterization of microstructural failure in the single fiber fragmentation test.” ETH Zurich, 1996.

[90] M. G. R. Sause and S. Richler, “Finite Element Modelling of Cracks as Acoustic Emission Sources,” *J. Nondestruct. Eval.*, 2015.

[91] M. Surgeon and M. Wevers, “Modal analysis of acoustic emission signals from CFRP laminates,” *NDT E Int.*, 1999.

[92] M. Eaton, M. May, C. Featherston, K. Holford, S. Hallet, and R. Pullin, “Characterisation of damage in composite structures using acoustic emission,” in *Journal of Physics: Conference Series*, 2011.

[93] N. N. Hsu and F. R. Breckenridge, “Characterization and calibration of acoustic emission sensors,” *Mater. Eval.*, 1981.

[94] W. H. Prosser, “The propagation characteristics of the plate modes of acoustic emission waves in thin aluminum plates and thin graphite/epoxy composite plates and tubes,” *J. Acoust. Soc. Am.*, vol. 92, no. 6, pp. 3441–3442, 1992.

[95] J. P. McCrory *et al.*, “Damage classification in carbon fibre composites using acoustic emission: A comparison of three techniques,” *Compos. Part B Eng.*, 2015.

[96] J. McCrory, “Advanced Acoustic Emission (AE) monitoring techniques for aerospace structures.” Cardiff University, 2016.

[97] M. Zhang, Q. Meng, S. Liu, D. Qian, and N. Zhang, “Impacts of Cyclic Loading and Unloading Rates on Acoustic Emission Evolution and Felicity Effect of Instable Rock Mass,” *Adv. Mater. Sci. Eng.*, vol. 2018, 2018.

[98] N.-S. Choi, T.-W. Kim, and K. Y. Rhee, “Kaiser effects in acoustic emission from composites during thermal cyclic-loading,” *NDT E Int.*, vol. 38, no. 4, pp. 268–274, 2005.

[99] C. Speech, “The Origin of CARP and the Term ‘Felicity Effect.’”

[100] W. Hufenbach, H. Richter, A. Langkamp, and R. Böhm, “Application of acoustic emission analysis for damage investigations in fibre and textile reinforced composites,” in *Conference on Damage in Composite Materials: Non Destructive Testing and Simulation (CDCM06), Stuttgart*, 2006, vol. 18, no. 19.9.

[101] I. Stavrakas, “Acoustic emissions and pressure stimulated currents experimental techniques used to verify Kaiser effect during compression tests of Dionysos marble,” *Frat. ed Integrità Strutt.*, vol. 11, no. 40, pp. 32–40, 2017.

[102] D. I. H. Vallen, “AE Testing Fundamentals,Equipment, Applications,” *NDT.net*, 2002. .

[103] J. M. Waller, E. Andrade, and R. L. Saulsberry, “Use of acoustic emission to monitor progressive damage accumulation in Kevlar® 49 composites,” in *AIP Conference Proceedings*, 2010, vol. 1211, no. 1, pp. 1111–1118.

[104] M. Kotoul and Z. Bilek, “Acoustic emission during deformation and crack loading in structural steels,” *Int. J. Press. Vessel. Pip.*, 1990.

[105] M. Akbari and M. Ahmadi, “The application of acoustic emission technique to plastic deformation of low carbon steel,” in *Physics Procedia*, 2010.

[106] S. Schnabel, P. Marklund, R. Larsson, and S. Golling, “The detection of plastic deformation in rolling element bearings by acoustic emission,” *Tribol. Int.*, vol. 110, pp. 209–215, 2017.

[107] R. Kocich, M. Cagala, J. Crha, and P. Kozelsky, “Character of acoustic emission signal generated during plastic deformation,” in *Proc. 30th European Conf. on ‘Acoustic emission testing’and 7th Int. Conf. on ‘Acoustic emission’, Granada, Spain*, 2012.

[108] A. K. Rao, “Acoustic emission and signal analysis,” *Def. Sci. J.*, vol. 40, no. 1, p. 55, 1990.

[109] M. A. Hamstad, “Testing fiber composites with acoustic emission monitoring,” *J. Acoust. Emiss.*, vol. 1, no. 3, pp. 151–164, 1982.

[110] A. Rotem and J. Baruch, “Determining the load-time history of fibre composite materials by acoustic emission,” *J. Mater. Sci.*, vol. 9, no. 11, pp. 1789–1796, 1974.

[111] M. Suzuki, H. Nakanishi, M. Iwamoto, and E. Jinen, “Application of static fracture mechanisms to fatigue fracture behavior of class A-SMC composite,” in *Japan-U. S. Conference on Composite Materials, 4 th, Washington, DC*, 1989, pp. 297–306.

[112] M. A. Hamstad, A. O‘GALLAGHER, and J. Gary, “A wavelet transform applied to acoustic emission,” *J. Acoust. Emiss*, vol. 20, pp. 39–61, 2002.

[113] Z. M. Hafizi, J. Epaarachchi, and K. T. Laul, “An investigation of acoustic emission signal attenuation for monitoring of progressive failure in fiberglass reinforced composite laminates,” *Int. J. Automot. Mech. Eng.*, 2013.

[114] J. Bohse, “Acoustic emission characteristics of micro-failure processes in polymer blends and composites,” *Compos. Sci. Technol.*, vol. 60, no. 8, pp. 1213–1226, 2000.

[115] P. J. De Groot, P. A. M. Wijnen, and R. B. F. Janssen, “Real-time frequency determination of acoustic emission for different fracture mechanisms in carbon/epoxy composites,” *Compos. Sci. Technol.*, vol. 55, no. 4, pp. 405–412, 1995.

[116] R. Gutkin, C. J. Green, S. Vangrattanachai, S. T. Pinho, P. Robinson,

and P. T. Curtis, “On acoustic emission for failure investigation in CFRP: Pattern recognition and peak frequency analyses,” *Mech. Syst. Signal Process.*, 2011.

[117] L. Li, S. V. Lomov, X. Yan, and V. Carvelli, “Cluster analysis of acoustic emission signals for 2D and 3D woven glass/epoxy composites,” *Compos. Struct.*, vol. 116, no. 1, pp. 286–299, 2014.

[118] D. Crivelli, M. Guagliano, and A. Monici, “Development of an artificial neural network processing technique for the analysis of damage evolution in pultruded composites with acoustic emission,” *Compos. Part B Eng.*, 2014.

[119] B. Desgraupes, “Clustering indices. University Paris Ouest, Lab Modal ‘X.” Tech. Rep., April, 2013.

[120] L. F. Li, W. L. Zhang, Z. Q. Chen, L. J. Wen, F. Wang, and G. T. Shen, “Application of Pattern Recognition to the Acoustic Emission Signals of Carbon Steel,” *Proc. 2009 2nd Int. Congr. Image Signal Process. Vols 1-9*, pp. 4536–4539, 2009.

[121] Q. Q. Ni and M. Iwamoto, “Wavelet transform of acoustic emission signals in failure of model composites,” *Eng. Fract. Mech.*, vol. 69, no. 6, pp. 717–728, 2002.

[122] D. J. Collins, “Damage detection in composite materials using acoustic emission and self-sensing fibres.” University of Birmingham, 2010.

[123] J. Van Dam and L. J. Bond, “Acoustic emission monitoring of wind turbine blades,” 2015.

[124] M. Kharrat, E. Ramasso, V. Placet, and M. L. Boubakar, “A signal processing approach for enhanced Acoustic Emission data analysis in high activity systems: Application to organic matrix composites,” *Mech. Syst. Signal Process.*, vol. 70–71, pp. 1038–1055, 2016.

[125] H. Lamb, “On Waves in an Elastic Plate,” *Proc. R. Soc. A Math. Phys. Eng. Sci.*, vol. 93, no. 648, pp. 114–128, 1917.

[126] A. Manikas, Y. Kamil, and M. Willerton, “Source Localization Using Sparse Large Aperture Arrays,” *IEEE Trans. Signal Process.*, vol. 60, no. 12, pp. 6617–6629, 2012.

[127] R. J. Kozick and B. M. Sadler, “Source Localization With Distributed Sensor Arrays and Partial Spatial Coherence,” *IEEE Trans. Signal Process.*, vol. 52, no. 3, pp. 601–616, 2004.

[128] D. Crivelli, M. Guagliano, and A. Monici, “Development of an artificial neural network processing technique for the analysis of damage

evolution in pultruded composites with acoustic emission," *Compos. Part B Eng.*, vol. 56, pp. 948–959, 2014.

Appendix A

For fracture assessments, the following equation applies:

$$Y\sigma = (Y\sigma)_P + (Y\sigma)_S$$

where:

$(Y\sigma)_P$ is the contribution from primary stress;

$(Y\sigma)_S$ is the contribution from secondary stress.

They are calculated as follows:

$$(Y\sigma)_p = Mf_w\{k_{tm}M_{km}M_mP_m + k_{tb}M_{kb}M_b[P_b + (k_m - 1)P_m]\}$$

$$(Y\sigma)_s = M_mQ_m + M_bQ_b$$

In this work,

$a = 0.375, 0.75, 1.125, \text{and } 1.5;$

$W = 3;$

With the stress intensity factor equations above, for $a/W \leq 0.6$:

$M = 1;$

$f_w = 1;$

$$M_m = M_b = 1.12 - 0.23(a/W) + 10.6(a/W)^2 - 21.7(a/W)^3 + 30.4(a/W)^3$$

Therefore,

$$K_I = Mf_wM_m\sigma\sqrt{\pi a}$$

$F = 150 \text{ kN};$

$A = 3\text{mm} \times 1.2 \text{ m} = 0.0036\text{m}^2;$

Appendix B

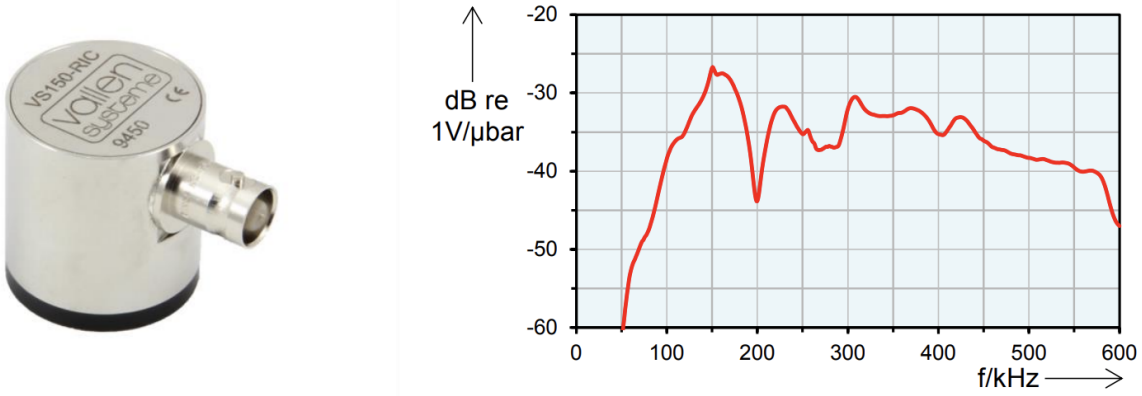

Figure 0-1 VS150-RIC sensor and calibration sheet

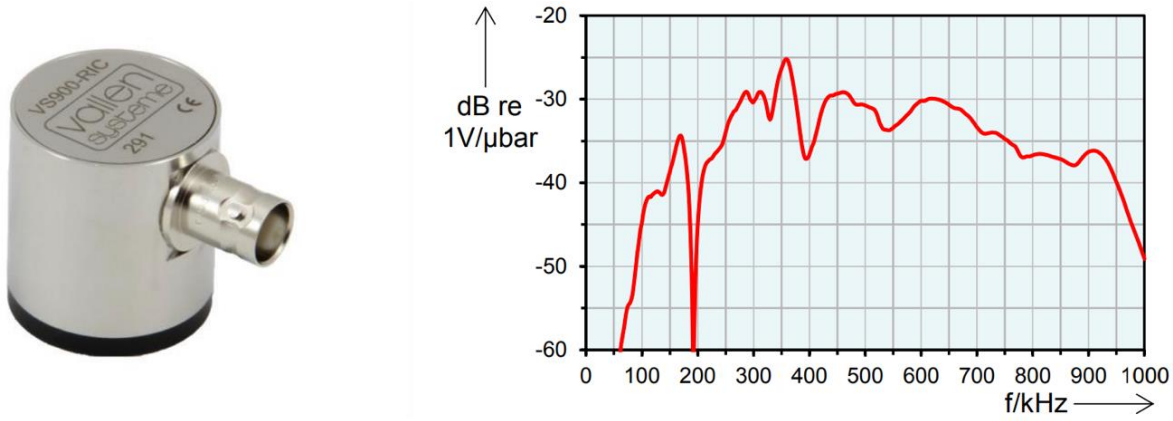

Figure 0-2 VS900-RIC sensor and calibration sheet

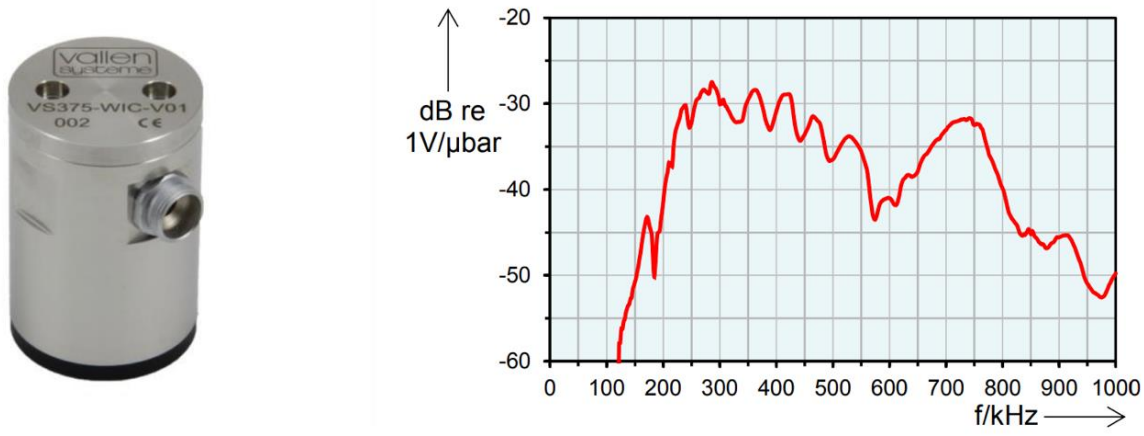

Figure 0-3 VS375-WIC sensor and calibration sheet

Appendix C

The K-means algorithm is a clustering method that attempts to find a user-specified number of clusters, which are represented by their centroids. It aims at partitioning an *N* × *n* input dimensional dataset into *c* clusters to minimize the within-cluster sum of squares:

$$\sum_{i=1}^{c} \sum_{k \in A_i} \| x_k - v_i \|^2$$

where A_i is a set of data points in the i-th cluster and v_i is the mean for that points over cluster i. The above equation actually denotes a distance norm. v_i is the cluster centre:

$$v_i = \frac{\sum_{k=1}^{N_i} x_k}{N_i}, x_k \in A_i$$

where N_i is the number of objectives in A_i.

K-means clustering has been applied in a wide range of applications due to its high processing speed and simplicity. On the other hand, the requirement for a definite number of clusters as input is often an issue due to the fact that in most tests it is almost impossible to know the number of damage modes in advance.